KEM-24b
Preliminary assessment of beneficial effects of nitrogen injection in depleted reservoirs

Energy & Materials Transition
www.tno.nl
+31 88 866 42 56
info@tno.nl

TNO 2024 R11366 – 10 October 2024

KEM-24b
Preliminary assessment of beneficial effects of nitrogen injection in depleted reservoirs

Author(s)	Osinga, S., Leeuwenburgh, O., Vogelaar, B., Pena Clavijo, S., Bottero, S.
Classification report	TNO Public
Title	KEM-24b: Preliminary assessment of beneficial effects of nitrogen injection in depleted reservoirs
Report text	TNO
Number of pages	92 (excl. front and back cover)
Number of appendices	2
Sponsor	The Dutch Ministry of Economic Affairs and Climate
Programme name	Kennisprogramma Effecten van Mijnbouw - KEM program
Project name	KEM-24b
Project number	060.58402

Executive summary

This report documents the results of the KEM-24b project conducted by TNO as part of the "Kennisprogramma Effecten van Mijnbouw" (KEM programme), which was initiated by The Dutch Ministry of Economic Affairs and Climate.

The KEM-24b project is a scientific study into effects that are associated with re-pressurization of the Groningen gas field by large-scale post-production injection of nitrogen. This has previously been identified as a possible means to decrease the number of earthquakes, and consequently the seismic hazard and risk. In particular nitrogen gas (N_2) has been identified as a suitable fluid since it is largely inert, readily available, and does not show complex phase behaviour. The project has focussed on beneficial effects on seismicity only and has not considered economic, practical and societal aspects of such an injection campaign, nor the potential negative effects on seismicity due to cooling-induced reservoir compaction.

A literature review highlighted the unique character of the Groningen case and re-confirmed the need for a dedicated approach. The study was therefore conducted with the existing model chain Groningen (used for the Seismic Hazard and Risk Analysis by TNO), into which a recently developed publicly available reservoir simulation model of the Groningen field was included. It was first verified and confirmed that the reservoir model produces results that are largely consistent with historic gas production data. Different scenarios for availability and injection of gas were subsequently evaluated with the model chain and compared to a scenario where no nitrogen is injected (the base case). Two scenarios were considered for gas availability, one based on an estimate of the current national nitrogen generation capacity, and one hypothetical scenario meant to investigate the theoretical potential of gas injection. Since the effect of cold gas injection on reservoir cooling and associated compaction and stresses is currently not included in the model chain an investigation was additionally performed on how such effects can be included in the future. Including these cooling effects will lead to a seismic source model where N_2 injection has both beneficial effects on seismicity (by reducing or reverting compaction through increasing pore pressures) and negative effects on seismicity (by increasing reservoir compaction through cooling). The updated seismic source model has not been implemented as part of this study and therefore the relative magnitude of these competing positive and negative effects has not been investigated here.

The results of KEM-24b are as follows:

Model chain:
- Basic notions about the expected pressure equilibration and gas flow after the cessation of production without any injection of gas are reproduced by the new reservoir simulation model that has been adopted for this study to replace the previously used proprietary NAM model.
- The model chain incorporating the new reservoir model is able to produce base case reference seismicity predictions that are consistent with observed seismicity as well as with earlier results obtained with the previously used reservoir model.
- A relatively simple way was outlined to include the potentially adverse effects of reservoir cooling and compaction (leading to more seismicity) in a possible update of the seismic source model.

Expected impact of nitrogen injection:
- The potential reduction in number of earthquakes, seismic hazard, and seismic risk compared to the 'no injection' base case, can be considerable, mostly depending on the amount of nitrogen injected. For example, our model results show that the number of buildings exposed to a risk level above the Meijdam norm goes down from approximately 500 to 200 after 1 year of N_2 injection (amounting to a total volume of 1.58 bcm of nitrogen) in the Loppersum well cluster.
- The potential positive effects of injection increase with the amount of injected nitrogen and is dependent on the spatial and temporal distribution of nitrogen over the field.
- Under the modelling assumptions used in this study, these positive effects could disappear again, depending on when injection is stopped.

While the effects of gas injection on pressure as simulated with the model chain can be considered realistic, possible effects of composition and temperature of the injected gas were not explicitly considered in the scenario evaluation. Furthermore, several simple assumptions were made about availability and distribution of nitrogen across the field. A follow-up study could be conceived in which potential negative effects are quantified, and possibly minimized, while optimizing beneficial effects.

Contents

1 Introduction

1.1 Background

The production of gas from the Groningen gas field has caused seismic events whose impact have ultimately led to the decision to cease production in October 2023. It is generally accepted that the seismicity is largely the consequence of compaction at reservoir level, caused by lowering of the gas pressure in the reservoir, in turn leading to critically stressed faults.

It is expected that this form of induced seismicity will continue for some time also after production has stopped, because of the existing pressure gradients in the field and the time that it will take for gas to re-distribute and pressure to equilibrate. Such equilibration implies pressure increases in some parts of the field and pressure decreases in other parts of the field. These decreases in pressure could cause further compaction and therefore potentially new seismic events. A more favourable pressure state that could lead to a reduction in seismicity could be actively created by strategic injection of gas. The objective of injection would be to reduce or prevent pressure decline in crucial parts of the field, leading to a more stable stress state and less seismicity. Pressure maintenance by fluid injection is therefore considered as a possible safety measure to the Groningen field, along with the ongoing reinforcement of buildings after the recent cessation of gas production.

As part of the initial KEM-24 project (2022), research was performed into the effectivity of nitrogen gas injection for reduction of seismicity in the Groningen field following the end of production. It was concluded that nitrogen gas injection is the most promising option. Conclusions about the effectiveness of such injection were difficult to judge with confidence due to characteristics of the model available for that study.

1.2 Objectives

The current study aims to deliver useful insights into the potential to reduce the number of seismic events in the Groningen field post production by injection of nitrogen gas. In particular, it aims to answer the following questions:

1. What can be learned from examples of fluid injection in reservoirs similar to the Groningen reservoir?

2. Which injection scenarios for mitigating seismicity could be applied after production has stopped?

3. How can the existing SHRA (Seismic Hazard and Risk Assessment, https://www.nlog.nl/publieke-sdra-groningen) model chain be adapted to include fluid injection?

4. What is the potential beneficial effect of fluid injection on the overall seismic risk?

1.3 Scope and approach

Learnings from gas injection operations are collected and discussed in a literature review (Chapter 2) that will consider both national and international projects. Special attention is given to gas storage projects in the Netherlands as these are most similar to the Groningen case in terms of geology and injected gas.

Scenarios for injection of nitrogen are designed with reference to currently available nitrogen generation capacity in the Zuidbroek II facility, and to the distribution of well clusters in the Groningen field. We will simulate these scenarios with the reservoir simulation model developed and released for public use by NAM. Since the model does not support simulation of different gas compositions, we will consider injection of gas with the same properties as the Groningen gas. These simulations will therefore show the effect of re-pressurization of the reservoir. The volumetric effects of gas composition will be investigated in a separate box model experiment with a compositional simulator. Furthermore, we will assume that nitrogen is available to be injected at all wells that are potentially operational in the field. That is, the availability and/or suitability of the surface infrastructure and the sourcing and distribution of the nitrogen are not explicitly considered and studied. The results of the reservoir simulations are presented in Chapter 3.

The reservoir flow simulations produce snapshots over time of the pressure conditions in the reservoir. These pressure states can be used as input to a hazard calculation involving the quantification of expected seismicity. In this study, the modelling of seismicity will be performed using the current seismic source model that is available in the Groningen model chain (TNO, 2022). This model considers the relation between pressure decrease and compaction to be elastic and immediate, and the relation between compaction and seismicity to be immediate as well. The source model can also capture the reverse process, in which pressure increases lead to decompaction, stabilization of faults and a reduction of seismicity. The projected seismicity, seismic hazard and risk can be calculated for all injection scenarios with the TNO model chain. The impact on seismicity will be reported both in terms of total seismicity rate through time (number of events per year) and the spatial distribution of seismicity through time. The impact on hazard will be reported as spatial difference maps for ground motions at 475 and 2475 year return period for a range of spectral periods. The impact on risk will be quantified using an aggregated risk metric: the mean LPR of the total building stock of the exposure database. The number of buildings exceeding the Meijdam norm through time will be reported for each case. Results from application of the model chain to different injection scenarios will be described in Chapter 4.

The seismic source model does not account for potentially destabilizing (seismicity enhancing) effects related to pressure increase, or temperature decrease. Since the injection of nitrogen will primarily lead to pressure increases, in the seismic source model, nitrogen injection is expected to lead to a reduction in overall seismicity. Potentially adverse (seismicity enhancing) effects of nitrogen injection are not quantified in this study. However, this study will investigate possible future adjustments that can be made to the current seismic source model to include the potentially destabilizing (seismicity enhancing) effects related to pressure increase, or temperature decrease. A proposal for such adjustment is provided in Chapter 5.

We end the report with Conclusions and Recommendations.

2 Literature review

2.1 Introduction

The aim of current literature study is threefold: 1) summarize the available knowledge on injection-induced seismicity and risk mitigation strategies. 2) provide analogous cases (e.g., gas storage), provide lessons learned and determine its relevance for the Groningen case. 3) comment on differences with other injection techniques (e.g., wastewater disposal) and what those differences imply for mitigation strategies.

This literature review covers a brief overview of the Groningen Pressure Maintenance (GPM) study program by NAM (2016), including research by TNO (2015a, 2015b, 2015c) and Shell Global Solutions. We summarize induced seismicity by geomechanical stress changes by water injection in geothermal fields (Buijze et al., 2019) and the mechanism-based assessment of induced seismicity related to fluid injection (and gas production). Next, several examples of possible injection-induced seismicity in the Netherlands are presented as lessons learned. Field cases of cyclic injection in Underground Gas Storage (UGS) facilities, production water injection in depleted gas fields and aquifers, and geothermal operations may serve as possible analogues to fluid injection in the Groningen gas field. Where possible, example field cases of injection and/or fluid circulation with a geological setting comparable to the Groningen field have been chosen. In addition, differences with fluid-injection operations outside the Netherlands are given.

2.2 Previous injection studies Groningen

2.2.1 The Groningen Pressure Maintenance study

NAM (2016) has assessed possibilities for pressure maintenance in the Groningen gas field by injection through the Groningen Pressure Maintenance (GPM) study program since early 2013. Pressure maintenance was considered as a possible safety measure with regard to the Groningen gas field, along with reducing (and ceasing) of gas production and reinforcing buildings. The GPM program includes research by Shell Global Solutions as well as research by external academics and consultants (NAM, 2016). TNO (2014, 2015a, 2015b, 2015c) did a generic study on injection-induced seismicity by means of literature studies and the modelling of geomechanical effects of nitrogen injection on fault stability. Shell Global Solutions did research into the technical feasibility of gas injection into the Groningen field with the objective to reduce seismicity and subsidence by sustaining the reservoir pressure. The local group 'Groningen 2.0' did research into alternative options and potential synergies between GPM and local economic or industrial developments in the Groningen area (NAM, 2016).

The study (NAM, 2016) showed that injection of nitrogen into the Groningen field is technically feasible and can reduce the rate of pressure decline or stabilize pressures. However, the seismic hazard for GPM could not be calculated (back in 2016) and it remained uncertain whether large scale injection will have a significant positive or negative effect on seismicity. Finally, NAM (2016) indicated that a field test in Groningen and additional research would be required to establish whether GPM is effective in reducing seismicity.

2.2.2 Initial KEM-24 study

The initial KEM-24 study by Fugro (2022a, 2022b) investigated the effect of fluid injection on seismicity using the Groningen reservoir as an example. The main conclusions on induced seismicity of the KEM-24 study by Fugro were that N_2 injection appeared to be much more effective than CO_2 injection and that injection should be avoided near the critically-stressed Loppersum fault system (Fugro, 2022a). Therefore, Fugro (2022b) concluded that, from the seismic hazard point of view the "best action" for induced seismicity is to allow the Groningen reservoir system to re-equilibrate pressures in a natural way. In addition, Fugro (2022b) concluded that fluid injection would lead to an increase in the seismicity rate and to an increase of the seismic hazard.

The KEM-panel evaluated the results from the initial KEM-24 study by Fugro. KEM (2022) found that the conclusions and recommendations by Fugro were based on somewhat incomplete results, since the Fugro model was incapable to simultaneously mimic historic changes in the reservoir pressure and observed seismicity. As such, the forecasting potential of the Fugro model could not be validated.

As part of the original KEM-24 project, it was concluded that nitrogen gas injection is the most promising option (KEM, 2022). The KEM-panel has suggested a follow-up that resulted in issuing this study.

2.3 Reviews of fluid injection-related induced seismicity

Following McGarr et al. (2015), fluid injection-related induced seismicity from human operations can be classified in five different broad classes. Injection activities that are distinguished are (1) disposal of wastewater into deep formations, (2) injection of water or CO_2 into depleted reservoirs for enhanced oil recovery, (3) hydraulic fracturing to enable production of oil and gas from low-permeability rock, (4) injection of CO_2 for permanent carbon capture and storage, and (5) development of (enhanced) geothermal systems (Zang et al., 2019).

Review articles are available for the different classes of fluid injection-related induced seismicity (Zang et al., 2019). For example, Suckale (2009) and Davies et al. (2013) reviewed induced seismicity in hydrocarbon fields. Warpinski et al. (2012) elaborated on induced seismicity related to hydraulic fracture operations in shale-gas extraction. At European scale, Evans et al. (2012) separated crystalline from sedimentary environments, and reviewed induced seismicity from fluid-injection into geothermal reservoirs and CO_2 storage sites. For the US, Ellsworth (2013) focused on injection-induced earthquakes caused by wastewater disposal. Zang et al. (2014) gave an overview of induced seismicity in geothermal operations with emphasis on Enhanced Geothermal Systems (EGS), where fluid is injected to re-open pre-existing fractures, but also in comparison to other classes of fluid-induced seismicity. Rubinstein and Mahani (2015) discussed fluid-induced seismicity related to wastewater injection, hydraulic fracturing, and enhanced oil recovery.

All reviews above, including the recent one by Foulger et al. (2018), beside from monitoring strategies and traffic light systems, do not discuss innovative technologies how to actually reduce fluid injection-related induced seismicity, e.g., by advanced injection schemes (Zang et al., 2019). Better knowledge of the stress and pressure conditions at depth; the hydrogeologic framework, including the presence and geometry of faults; and the location and mechanisms of natural seismicity will be needed to develop a predictive understanding of the hazard posed by induced earthquakes (Zang et al., 2019). We will first discuss the stress and pressure mechanisms that may cause induced seismicity.

2.4 Mechanisms of induced seismicity

Buijze et al. (2019) point at stress changes as the key mechanisms causing induced seismicity in geothermal fields by e.g., fluid injection: stress changes due to 1) pore pressure increase; 2) poro-elastic stressing; and 3) thermoelastic stressing. First, an increase in pressure on a fault due to e.g. fluid injection reduces the effective normal stress on the fault and brings the fault closer to failure. The elevated pressure diffuses away from the injection well as a function of time, raising pressures and inducing seismic events further away from the source (e.g., Shapiro and Dinske, 2009). Second, a change in pore pressure also causes a volumetric strain (volume change) of the rock mass experiencing a pressure change. This volume change causes a change in stress within the rock mass itself controlled by pore pressure changes, and in the surrounding rock formations, i.e., poro-elastic stressing. Third, analogous to poro-elasticity, changes in temperature cause volumetric strain of the rock mass, which leads to stress changes within and around the volume experiencing a temperature change. The thermoelastic stress changes are opposite to those resulting from a pressure increase, because cooling leads to a decrease in total stresses (Buijze et al., 2019). NAM (2023a) identified five different mechanisms that may lead to induced seismicity:

2.4.1 Increase of shear stress during depletion

Gas production causes a decrease of pore pressure and a possible increase of shear stress on existing faults in the reservoir leading to fault reactivation and induced seismicity. Depletion induced earthquakes are for example observed in Groningen, Roswinkel and Bergermeer. These earthquakes demonstrate that some of the faults in and bounding the reservoir reached a critical state, where small stress perturbations may lead to seismic activity. The shear stress increase by depletion is dictated by the amount of depletion, the fault geometry, and the mechanical properties of the reservoir rock. Although gas production from the Groningen field is ceased since October 2023, it is foreseen that autonomous fieldwide pore pressure equilibration (i.e., without fluid injection) will continue to lead to local pore pressure decrease in some areas, which can therefore continue to cause future earthquakes in the field.

2.4.2 Fieldwide pressure increase by fluid injection

As described by mechanism 2.4.1, fieldwide pore pressure equilibration decreases the local pore pressure leading to an increase of shear stress along existing faults. However, in the case of pore pressure restoration by fieldwide equilibration by local fluid injections, the stress path would revert to its initial condition with a decrease of the shear stress as a state that is less critical for fault reactivation. As noted by NAM (2023a), it is however, likely that reservoirs deform during depletion with partial plastic behavior, with permanent deformation and stress change as a result (stress hysteresis). This could lead to the development of higher shear stresses when compared to the fully elastic response.

2.4.3 Near-wellbore contraction due to thermal cooling

Studies into geothermic systems have shown that the injection of relatively cold fluids into a relatively warm reservoir may trigger seismicity. Injection of a cold fluid causes a portion of the reservoir to cool down. This temperature reduction is accompanied by thermal contraction of the reservoir rock, potentially activating nearby faults changing the local stress state.

Besides pressure increase by fluid injection as described by mechanism 2.4.2, the stress state in the reservoir near the well bore can be changed by rock contraction due to the injection of relatively cold fluid. During cold fluid injection, both the pore pressure increase (mechanism 2.4.2) and temperature decrease (mechanism 2.4.3) are largest in magnitude in the near-wellbore area. Consequently, in this near-wellbore area cold fluid injection has the largest impact on the stress state and on possible fault reactivation. However, the volume of cooled rock near the well bore (temperature front) is significantly smaller than the volume of reservoir rock exhibiting an increased pore pressure value (pressure front) due to cold fluid injection (NAM, 2023a).

2.4.4 Near-wellbore pressure increase in a fault

As described by mechanism 2.4.2, fieldwide pore pressure increase would (partially) revert the stress path compared to depletion and decrease the shear stress to a state that is less critical for fault reactivation. However, if the fluid pressure inside a fault increases more than the pressure in the host rock, this situation might cause a direct decrease of the effective normal stresses on the fault (NAM, 2023a). This situation occurs when the permeability in the fault is relatively high compared to the host rock and when a conductive path from the injection well to the fault exists. Fluid injection directly into the fault rock should be avoided by not using candidate injection wells that penetrate faults in the reservoir.

2.4.5 Chemical weakening of the fault strength

Chemical weakening is translated to a decrease of the friction in a fault. Chemical weakening is, however, relatively uncommon (NAM, 2023a).

2.4.6 Aseismic slip

Aseismic slip is also known to affect seismicity, but its exact contribution remains elusive. To address this, Mandal and Lui (2022) performed numerical modelling to understand the effects of injection volume and rate on long-term seismic and aseismic fault slip behavior. Their results suggest that both parameters can affect fault behavior, and, in some cases, their roles are interdependent, thus they should be examined simultaneously in order to fully characterize their effects on triggered fault responses.

2.5 Examples of possible injection-induced seismicity in the Netherlands

Below we list examples of *possible* injection-induced events in the Netherlands for underground gas storage (UGS), production water injection, and geothermal operations.

2.5.1 UGS in the northern Netherlands

In the Netherlands, four former natural gas reservoirs are used for underground gas storage: Norg, Grijpskerk, Bergermeer and Alkmaar. Only UGS Alkmaar has never registered any seismic activity.

The Dutch UGS sites in the Rotliegend sandstone are of interest as an analogue to GPM in the Groningen field (NAM, 2016). Although these fields are much smaller in size than the Groningen field, the reservoir rocks have the same geologic age (Permian Rotliegend sandstone) and are also cut by faults. Most importantly, the pore pressure changes during UGS are >100 bar and should thus bring about similar or even higher compaction and dilation (volume decrease and increase, respectively) and stress changes to faults and reservoir rock as during pressure maintenance in the Groningen field. Notably, injection at UGS sites in the north of the Netherlands did not give rise to large earthquakes (TNO, 2014). An injection-induced earthquake (M1.1) during UGS in the Netherlands was an recorded in 1999 at Norg at a pore pressure of 309 bar, after it was increased by about 125 bar above the pore pressure of the depleted field (about 185 bar) to values just 20 bar below the virgin pore pressure of 328 bar.

Of interest is also UGS Bergermeer in the province of Noord-Holland. In 1994 and 2001, during primary depletion of this reservoir, four seismic events were recorded with magnitudes varying between M3.0 and 3.5. The largest seismic event recorded during injection of gas was the 2013 M0.7 Bergermeer event, interpreted to be located close to the central fault (TNO, 2015b). At UGS Grijpskerk, an 1997 M1.3 event was observed during production. Fifteen years after conversion and start of UGS Grijpskerk operation, a second 2015 M1.5 event was recorded by the KNMI network during cyclic operation (Muntendam-Bos et al., 2022).

In summary, UGS data from three Dutch storage fields do not indicate large (e.g. M > 1.5) earthquakes during gas injection, although the pore pressure was increased by 90 to 129 bar after depletion of 150 to 200 bar (TNO, 2015b).

2.5.2 Water injection Borgsweer, Groningen

State Supervision of the Mines (SodM, 2023) has no indications that water injection in Borgsweer poses a danger to people and the environment or that water injection increases the risk of earthquakes in this specific case. Since 1972 production water is injected in the eastern flank of the Groningen gas field at the NAM location Borgsweer. The total injected volume through several injectors accumulates to 20-25 million m^3 to date. Injection target is the deeper Lower Slochteren aquifer, which is separated from the overlaying Ameland Claystone and the Upper Slochteren Sandstone gas bearing reservoir. The Groningen gas field around the Borgsweer injection site is in eastern direction connected to the Rysum aquifer (NAM, 2023b). A fault system in western direction restricts fluid flow from the Borgsweer site to the former production locations. As a result, the reservoir pressure at the Borgsweer injection site is several tens of bar higher than the adjacent Groningen gas field. Due to the flow-restricting presence of the fault system and the overlying Ameland Claystone, injection of production water at Borgsweer has no or limited impact on the reservoir pressure of the Groningen gas field. This interpretation is supported by measurements of the nearby Delfzijl-1 observation well (DLZ-1), situated west of the fault system. Since the pressure development in the Groningen reservoir is not or very limited influenced by Borgsweer water injection, it is expected that seismic activity due to water injection is limited.

2.5.3 Water injection in Weststellingwerf gas field, Friesland

Bois et al. (2013) tested five triggering mechanisms in a study to identify whether water injection in a relative distant well could have caused the so-called Weststellingwerf fault to slip leading to the 2009 M2.8 De Hoeve earthquake in southwestern Friesland, the Netherlands. These mechanisms include: 1) Pressure depletion during gas production; 2) Re-pressurization due to water injection; 3) Thermal stresses due to cold water injection; 4) Salt dissolution; and 5) Fault weakening due to water injection (chemical alteration).

The 2009 M2.8 De Hoeve earthquake occurred during injection of production water in the depleted gas field of Weststellingwerf, about 1 to 1.5 km to the north. At the time of the event, the De Hoeve gas field was not yet discovered and so no gas had been produced. Bois et al. (2013) connected the 2009 De Hoeve earthquake to fault lubrication by the water-weakening effect and/or a decrease in capillary pressure in the fault gouge material upon first contact with water. Since the rates of injected water were very low, both pressure increase (mechanism 2) and temperature decrease of the host rock (mechanism 3) resulted in low values, leaving the authors to conclude that strength weakening of the fault (fault lubrication) as the most plausible failure mechanism.

2.5.4 Water injection the Schoonebeek–Zechstein gas field

Recently, NAM (2023a) presented a mechanism-based assessment of induced seismicity related to gas production and water injection in the Schoonebeek-Zechstein gas field using a Mohr-Coulomb analysis. The 2017 M1.2 and 2018 M1.1 Schoonebeek events coincide with a period of injection of produced water in the SCH-597 injector. Since the epicenter of the 2017 M1.2 event is much closer to multiple gas production wells, this event is most likely associated with ongoing gas production in the field. The epicenter of the 2018 M1.1 Schoonebeek event is located close to ongoing gas production in the German part of the Schoonebeek field. The relatively nearby injection well ENZ-7 did not inject in 2018, but a possible relation between the 2018 event and transient pressure and temperature effects related to this injection cannot be completely ruled out (NAM, 2023a).

The 2000 M1.3 Dalen event coincided with a period of injection and gas production (NAM, 2023a). Since the epicenter is 5 km distant from the injector and at proximity to a gas production well, this event is not expected to be related to water injection activities but rather to the gas production.

2.5.5 Geothermal operation at Kwintsheul, South–Holland

In 2018, a geothermal doublet began operations in Kwintsheul, the Netherlands, aiming to supply heat to 64 hectares of greenhouses (Draganov et al., 2023). The reservoir used for the geothermal operation allows the extraction, circulation and reinjection of the fluid at a depth of 2.4 km. A case study review (Buijze et al., 2019) concluded that this kind of geothermal operations in the West Netherlands Basin (Lower Cretaceous and Upper Jurassic sandstones) are unlikely to generate felt seismicity.

Muntendam-Bos et al. (2022) reported on the 2019 M0.0 Kwintsheul event soon after a temporary special dense seismic monitoring array had been installed at the geothermal site in South-Holland. Despite the significant level of background noise in this highly populated part of the Netherlands, the signal was recorded by all 30 seismometers in the array.

A preliminary analysis of the event yielded a hypocenter relatively close to the tip of the injector at a depth estimate of 2.46 km. Muntendam-Bos et al. (2022) noted that the depth estimate is subject to a large uncertainty of more than a kilometer. Consequently, the event cannot unambiguously be attributed to the geothermal operation, since it cannot be excluded that the event is of tectonic origin.

2.5.6 Geothermal doublets in North-Limburg

Although the tectonic activity of the Ruhr Valley Graben and reservoir formation (Carboniferous Limestone Group) are not comparable to Groningen stress and gas field, two geothermal doublets in North-Limburg, the Netherlands, experienced seismicity, when fluid was produced and injected near the Tegelen fault zone, which intersects the reservoir formation. The largest hazard was inferred to result from thermo-elastic stresses, originating from cold water injection close to the Tegelen fault. Natural earthquake activity was observed in the vicinity of the geothermal systems. The hypocenter of the main M1.7 event was estimated to be in the depth interval of 4 to 6 km (Muntendam-Bos et al., 2022), well below the geothermal reservoir (located at 2–2.5 km depth). However, the uncertainty in the depth estimate is large and an occurrence at 2.5– 3.0 km (just below reservoir level) cannot be excluded, which led to the conclusion that the geothermal operations are a possible cause of the events. However, again it cannot be excluded that the event is of tectonic origin. Furthermore, a plausible explanation for the physical mechanism is hampered by the limited available geological information. Validation and refinement of the poorly constraint seismic velocity model and subsequent reassessment of the hypocenter locations as well as improved imaging of the geological structure in the area could provide important information towards a causal explanation (Muntendam-Bos et al., 2022). Vörös and Baisch (2022) relocated the hypocenters aligned along the Tegelen fault close to the CWG wells approximately at reservoir depth. At the moment, operations in both systems remain suspended.

Just south of the Dutch border, the same carbonates, but significantly deeper buried, are targeted at Balmatt geothermal site, near Mol, Belgium. Here, seismic events up to M2.2 occurred and were attributed to water injection/production (Buijze et al., 2023). The events led to suspension of operations.

2.6 Lessons learned from injection-induced seismicity in the Netherlands

2.6.1 Geothermal fields in the West Netherlands Basin

Most geothermal doublets in the Netherlands are located in relatively shallow, porous, sedimentary aquifers at 2–2.7 km depth with fluid temperatures of 60–100 °C (Mijnlieff, 2020). A case study review (Buijze et al., 2019) concluded that these systems are unlikely to generate felt seismic events (M > 2.0). The study suggested that especially geothermal operations in the shallow porous sandstones of the West Netherlands Basin (Lower Cretaceous and Upper Jurassic sandstones) are unlikely to generate seismicity. The study investigated 85 cases in various geothermal plays world-wide to assess the seismogenic potential of these systems.

Their assessment showed no cases of geothermal doublet projects in shallow, porous sandstone formations with reported seismicity of M > 2.0. Buijze et al., (2019) related this absence to the fact that these systems are 1) far away from a seismogenic basement, which is more prone to seismicity, 2) the pore pressure changes are very limited spatially as no stimulation is required. In addition, the intercalation of the sandstone formations with clay and shale layers would hydraulically isolate these formations from deeper layers (Muntendam-Bos et al., 2022).

2.6.2 Underground Gas Storage (UGS)

The relation between induced seismicity and underground gas storage (UGS) operations in Dutch gas reservoirs has been studied extensively. The general consensus of the studies of Dutch field cases of UGS (e.g., Muntendam-Bos et al., 2022) is that induced seismicity in the Rotliegend sandstone reservoirs is possible during the (re-)injection of cushion gas and the cyclic storage phase in which only the volume of working gas is produced and reinjected. Magnitudes are expected to remain well below those observed during depletion.

2.7 Differences with injection-induced seismicity outside the Netherlands

Ongoing interest in developing (deep) geothermal systems, hydraulic stimulation, and the sequestration of large quantities of CO_2 underground has prompted the need to identify factors that influence the different seismogenic responses to fluid injection. Recently, Kivi et al. (2023) collected worldwide data for 158 cases of injection-induced seismicity from 7 geologic gas storage projects (two natural gas and five carbon storage sites), 15 research projects, 54 tight and shale gas hydraulic fracturing projects, 58 deep geothermal programs, and 24 wastewater disposal activities. Their numbers show that geothermal operations contribute the most to their induced seismicity database (36.5 %), closely followed by hydraulic fracturing operations (34.6 %), wastewater disposal (15.1 %), research projects (9.4 %) and underground gas storage (4.4 %). Factors identified by Kivi et al. (2023) are, among others, host rock properties (e.g., porosity, Young's modulus, etc.), site characterization (e.g., depth of basement, temperature, etc.), fault properties (dip, type, etc.) and operational data (e.g., injection rate, maximum bottom-hole pressure, etc.).

Recently, Cheng et al. (2023) made an inventory of induced seismicity related to CO_2 injection. Compared with wastewater injection, shale gas hydraulic fracturing and EGS, the CGS (CO_2 Geological Storage) usually operates in high permeability reservoirs. For long-term CO_2 migration and storage, the injection pressure is easier to dissipate and the increase of injection pressure is always smaller under the same injection volume. CO_2 in CGS migrates further due to high reservoir permeability and the spatial distribution of the induced seismicity in CGS is usually wider. Although most seismic events related to CO_2 injection are M < 3, large magnitude events are occasionally recorded (Cheng et al., 2023).

Evans et al. (2012) document a study at various sites that seeks to determine where fluid injection has taken place without generating seismic events that were felt by the local population, as well as cases where it has. Evans et al. (2012) document 41 European case histories that describe the seismogenic response of crystalline and sedimentary rocks to fluid injection. The data generally support the view that injection in sedimentary rocks tends to be less seismogenic than in crystalline rocks. Examples of injection in crystalline rock, e.g., performed during Enhanced Geothermal System (EGS) projects are omitted in this literature review because of the lack of relecance to the Groningen case. Evans et al. (2012) acknowledge that the coverage of injection into sedimentary rocks is not complete, especially

for non-geothermal injections that did not produce felt earthquakes. Nevertheless, several sites where CO_2 is injected into sedimentary rock are included here.

2.7.1 CO_2 injection in Ketzin test site, Germany

The Ketzin test site in Germany is designed to monitor the behavior of CO_2 injected into the Triassic Stuttgart formation (Evans et al., 2012). Natural seismicity is very low. The highly heterogeneous reservoir is an 80 m thick fluvial sandstone saline aquifer that has its top at 630 m depth. The CO_2 is a gas under formation P-T conditions. The caprock consists of fine-grained, clay-rich clastic sediments and mudstone, which served as the caprock to a gas storage reservoir that was seasonally operated from 1960s until 2000. There are no observed faults within the CO_2 reservoir.

The reservoir is penetrated by three vertical wells drilled in 2007: one injection well and two monitoring wells. The CO_2 is injected through screens at a depth of 650 m. CO_2 injection commenced in 2008 and the pressure at the formation depth increased steadily to 81 bar after 1 year, which is 17 bar above the formation pressure. A seismic network has been operational at the site since 2009. No seismic events have been felt at the site (Evans et al., 2012).

2.7.2 CO_2 injection in Sleipner, North Sea, Norway

This is a pioneering project of Statoil to remove CO_2 from natural gas produced from the Sleipner-Vest gas reservoir underlying the Sleipner-A platform in the Norwegian part of the North Sea. CO_2 is injected into the extensive, high-permeability, 200 m thick saline aquifer that lies at a depth of 800–1100 m (Evans et al., 2012). Several events of magnitude M2–3 have occurred within 50 km of the platform over the past 20 years. The unconsolidated formation is hydrostatically-pressured. Injection began in 1996. The CO_2 is injected at a wellhead temperature of 25 C and a pressure 62–64 bar, and is thus close to the liquid/gas phase boundary. The downhole injection pressure above hydrostatic is uncertain (Evans et al., 2012). A value of 35 bar above hydrostatic pressure is probably an upper bound: other evidence suggests pressure may be only marginally above hydrostatic (Evans et al., 2012). Possible local seismic activity is not monitored at the site. However, there is no evidence from the regional networks of seismicity associated with the CO_2 injection operations (Evans et al., 2012).

2.7.3 Castor gas storage, Spain

Aforementioned studies of Dutch UGS field cases showed that induced seismicity in the Rotliegend sandstone reservoirs is possible during the (re-)injection of cushion gas and the cyclic storage phase in which gas is produced and reinjected. Magnitudes are expected to remain well below the level observed during depletion of the gas fields.

However, the observations at the Castor project in the old Amposta oil field, Spain, appear to contradict the conclusions from the Dutch field cases, as a cluster of events was observed during gas injection, while no induced seismicity was previously recorded during production (Muntendam-Bos et al., 2022). The Castor project aimed to convert the old, depleted oil field into a gas storage facility. Similar to the observations at Bergermeer, induced seismicity commenced shortly after the onset of cushion gas injection (Cesca et al., 2021). In contrast to Bergermeer, events up to magnitude 2.6 occurred during the injection in the Amposta field, and after 12 days injection was stopped. After the cessation of injection, the earthquakes continued to occur for some time and magnitudes increased up to M4.1.

There are a few important differences to consider between Amposta and the Dutch storage fields. First of all, the Amposta field is located in karstic, fractured and brecciated Lower Cretaceous dolomitic limestone (Cesca et al., 2021). The Dutch seismically active storage sites are located in the Rotliegend sandstone. Secondly, the Amposta field was characterized by a strong water drive during depletion, rendering enhanced oil recovery unnecessary. None of the Dutch storage fields showed substantial water drive during depletion. The lack of a proper seismic monitoring at the Castor site was previously recognized and potential monitoring solutions for offshore industrial operations proposed (Grigoli et al., 2017). Finally, the hypocenter depths of the Amposta earthquakes ranged from the injection depth to several kilometers deeper (Cesca et al., 2021, 2022; Vilarrasa et al., 2022). Considering that the field is located in the active Catalon-Valencian normal faulting extensional region (Muntendam-Bos et al., 2022), this may indicate that these earthquakes also contain an important tectonic component. In the Dutch studies, a non-critical subsurface stress state prior to depletion is assumed.

2.7.4 Injection-induced earthquakes in the U.S.

Ellsworth (2013) reviewed induced seismic activity in the United States (U.S.) that may be associated with industrial activity, with a focus on the disposal of wastewater by injection in deep wells and by hydraulic fracturing ("fracking") to increase permeability. The earthquakes involved can be induced as part of the process to stimulate the production from tight shale formations, or by deep wastewater disposal. These latter operations are not commercialized in the Netherlands.

2.8 Monitoring and mitigating actions of injection-induced seismicity

2.8.1 Monitoring of U.S. regulated wells

Wells used in the U.S. petroleum industry to inject fluids are regulated (Ellsworth, 2013). Approximately 110,000 of these wells are used for enhanced oil recovery. In addition, 30,000 regulated wells in the U.S. are used for wastewater disposal. Of these wells, most have no detected seismicity within tens of kilometers, although a few are correlated with seismicity. However, this can be said with confidence only for earthquakes M ≥ 3, as smaller earthquakes in the U.S. are not routinely reported or below the magnitude of completeness threshold.
Conclusions about the cause of many of the recent earthquakes suspected of being induced by injection are complicated by incomplete information on the hydrogeology, the initial state of stress and pore pressure, the pumping history of the well(s), and where pressure changes are being communicated at depth. Routine earthquake locations with uncertainties of 5 to 10 km and a high magnitude-detection threshold are of limited use. Particularly well-documented cases of injection-induced seismicity through a dedicated monitoring network illustrate what can be learned when more is known about the pre-injection stress state and seismicity, as well as the injection history (Ellsworth, 2013).

2.9 Conclusions

A review of the available knowledge on injection-induced seismicity suggests that the injection of nitrogen in the Groningen field with the aim of reducing seismicity would be unique in the world. The closest analogous cases to the Groningen case (in terms of expected possible geomechanical failure mechanisms, injection depth, and reservoir properties) show that magnitudes of the events observed at underground gas storage, geothermal heat production, and production water disposal projects in the Netherlands have so far been of relatively small (magnitudes ≤ 1.7). The relevance of these cases for the Groningen case is however limited, as their analogy with the Groningen gas field is often limited. The Groningen gas field is a unique case in many ways, for example because of its physical size and its history of seismicity during depletion, which took approximately 30 years after the start of production to initiate in terms of recorded events. Although the mechanical mechanisms at play in the Groningen gas field are likely not different than those in Dutch UGS operations, in the end it is the relative importance of all mechanisms, in combination with the geological and operational history of a field that determines the behavior in terms of seismicity. The Groningen gas field is also a unique case in the sense that it has a calibrated/history-matched model for its induced seismicity that appears to forecast reasonably well. It is therefore believed that application of the existing Groningen Seismic Risk and Hazard Analysis (SHRA) framework is a more suitable way to obtain a first indication of expected effects of gas injection in the Groningen field, rather than relying on similarities with other field cases.

3 Scenarios for nitrogen injection

3.1 Introduction

The estimation of hazard and risk associated with future scenario's for the Groningen field requires the use of predictive models. Hazard and Risk Assessment (HRA) tools established by NAM and TNO connect a series of physical-statistical models that include a reservoir dynamical model, a seismic source model, a ground motion model, and a fragility and consequence model. The first element of this model chain simulates the pressure distribution in the Groningen field resulting from historic production using the proprietary Shell reservoir simulator MoReS. In support of the transition of the Groningen HRA to the public domain, NAM has developed and released an Eclipse 100 simulation model. This chapter describes modifications implemented in the Eclipse model to make it suitable for prediction of the effects of re-pressurization by gas injection, scenarios for available gas injection volumes, and scenarios for the distribution of those volumes over space and time. Results from simulations of some of these scenarios are presented to validate the model. We also investigate the possible impact of the neglect of gas compositional effects in the Eclipse 100 model by separate simulations with the compositional simulator Eclipse 300.

3.2 Model description

An Eclipse 100 (Schlumberger) reservoir simulation model of the Groningen gas field has been developed by NAM, based on the existing MoReS model, and was made publicly available through https://public.yoda.uu.nl/geo/UU01/8JYW40.html together with a Petrel geo-model. The model simulates the gas production from the Groningen gas field and from several neighboring small fields between December 1955 and 1 January 2023. A basic quality check was performed by TNO to assess the suitability of the model for the purpose of this study. A summary of the main findings is provided here.

The main regional characteristics of the MoReS model appear to be reproduced by the model, as discussed in the document accompanying the Eclipse model[1]. Regional differences in pressure behaviour are reported for the Harkstede and Oldorp regions in the western periphery of the field. No extensive comparison was reported for individual wells. Poor well matches appear to be primarily associated with several small fields that are also included in the model. An important difference between the MoReS and Eclipse models is that the latter assumes dry gas, while the former includes water vapour in the gas phase. While this will mean that produced water rates in the Eclipse model are too low, water production in Groningen is known to be low, so the overall impact of reservoir volumes should be limited.

---

[1] Dynamic model (Eclipse version) to predict the formation pressure response to gas extraction in the Groningen gas field, The Netherlands, P. Tummala, NAM, 2023.

In the Eclipse model, wells are operated at combined observed gas and water production targets, presumably to ensure that the correct reservoir volumes are extracted, but this is not discussed in the document provided with the model.

The analytical aquifers implemented in the Eclipse model are different from the proprietary method available in MoReS. No discussion of differences or comparison of e.g. aquifer inflow volumes are available. It could be verified that specified gas rate targets are consistent with production volumes reported under normal conditions (nlog.nl). Pore volumes are explicitly defined by values imported from the Dynamo platform (the Shell proprietary model software framework). While fault transmissibility multipliers have been implemented in the MoReS model, no such multipliers are used in the Eclipse model. The history matching process and the resulting model modifications, e.g. to pore volume values, are not documented.

A few relatively small issues were identified (e.g. some erroneous grid connections in an unconnected aquifer and an incorrect end date, see Figure 8) but overall, the model is deemed appropriate for large-scale studies such as those currently executed as part of the KEM programme. In the following we provide further details of the model.

The Eclipse model made available by NAM contains the complete MoReS (model version GFR2022_HM_vV7_Jan23_clean1) time series of gas and water production data for 335 gas production wells of the Groningen field up to 1 January 2023. Gas production is given in Nm3/day whereas water production is given in bbl/day. It is not clear if water rates are specified for standard or normal conditions but differences in volumes should be very small and therefore have an insignificant impact on the outcome of the simulation.

The model grid is based on the Petrel geo-model that has also been made available by NAM. The model grid is divided into 45 equilibration regions and 20 fluid-in-place regions. Inflow into and outflow out of the modelled domain are determined by conditions specified at the boundaries. 4681 Carter-Tracy type aquifers are defined in the model to represent the connection to the Moewensteert, Rodewolt, and Usquert aquifers to the north and the Rysum aquifer to the east. The Groningen field is connected in the south-west to the Lauwersee aquifer. This aquifer is experiencing pressure decline as a result of both gas production from the Groningen field and from the nearby Roden, Vries, Faan and Pasop gas fields located to the (south)west. The contribution of these small fields is represented in the Groningen model by 10 pseudo production wells positioned along the south-west edge of the model that operate at specified water production rates. 11 wells represent gas and water production from four small gas fields that are included within the confines of the model boundaries: Bedum, Saaksum, Kiel-Windeweer and Warffum. Of these four, only Kiel-Windeweer is no longer in production. The remaining three fields are located to the (north)west of the Groningen field. No history matching has been performed to match history production from the small fields. Finally, 5 water injection wells of the Borgsweer location near the Eems-Dollard estuary are included in the model. The total number of wells in the model is therefore 365.

As part of the HRA workflow, simulated 3D pressure fields are vertically upscaled to 2D grids and interpolated to a regular map. Since earlier maps obtained with MoRes are still available we can compare the Eclipse maps to the MoReS maps (Figure 1). It is noted that the Eclipse-based maps are much smoother, indicative of much stronger pressure dissipation across faults in the model and consistent with the absence of any fault transmissibility multipliers in the NAM Eclipse model.
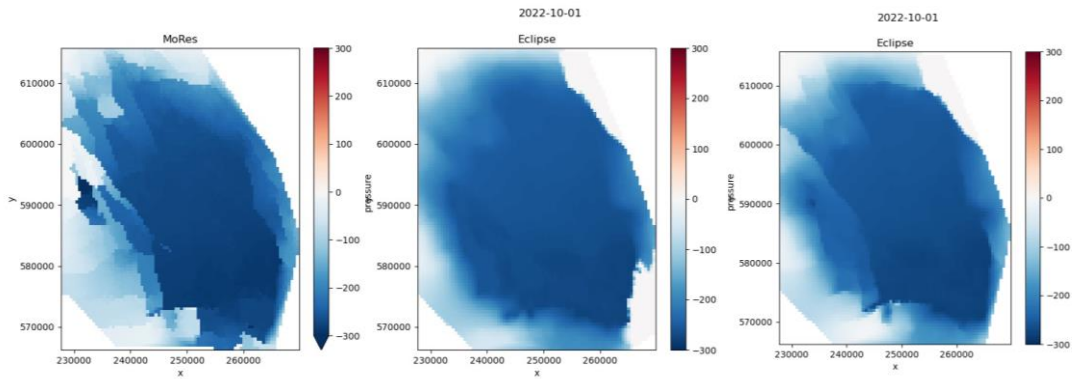
Figure 1 Pressure change at 2022-10-01 relative to initial pressure. Results are shown from simulations with the MoRes model (left) and with the Eclipse model without fault multipliers (middle) and with fault multipliers (right).

In order to obtain simulation results that are closer to the earlier MoReS results, fault multipliers were implemented that were taken from Table 12-1 of the 2016 Groningen model review report (SGS Horizon, 2016). While these multipliers were determined at the time for the MoReS model, and not tuned for use with the new Eclipse model, simulated pressures obtained with the latter model suggest a closer similarity to both the most recent available MoReS results and to pressure data when the multipliers are included (see Figure 2, Figure 3 and Figure 7 below). We therefore include these multipliers in all our simulations.

3.3 Production period

Production data for the period 1 January 2023 to 1 October 2023 were extracted from NLOG (nlog.nl) and used to extend the simulation schedule up to the end-of-production. Figure 2 to Figure 7 illustrate the performance of the simulation model in comparison to historic data obtained over the period of gas production from the Groningen field. Observed gas rates are very well matched on both field scale and for individual wells (we show results for one representative well only) for both versions of the Eclipse model (Figure 2 and Figure 3).

Examples of simulated flowing bottom-hole pressures (BHP) are shown for 4 wells from 4 different production regions in Figure 4 to Figure 7. Production regions and well cluster locations are shown in Figure 9. Simulated BHP values are similar for both versions of the Eclipse model, but the version with fault multipliers appears to produce slightly lower pressures, closer to the results obtained with the extensively history matched MoReS model.
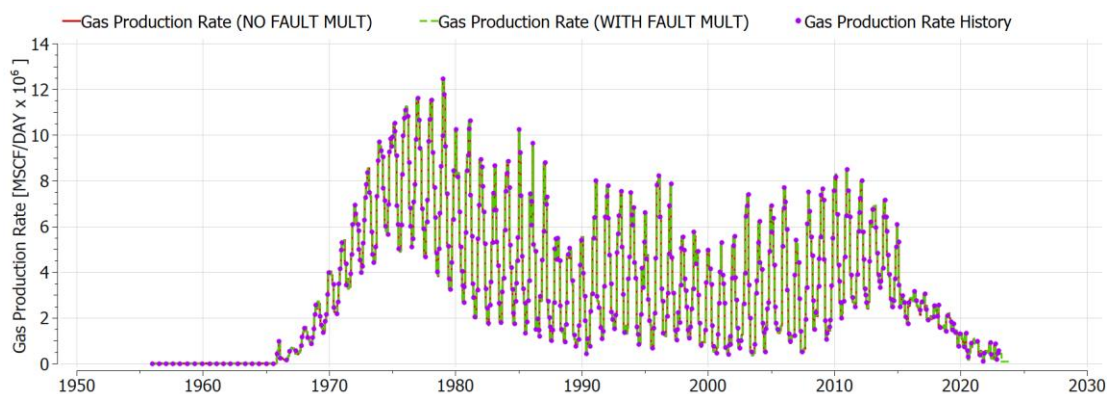
Figure 2 Field gas production rate simulated with the NAM Eclipse model without fault multipliers (red solid line) and the modified version with fault multipliers (green dashed line).

The dots indicate observed values. Note that the simulated rates (red solid and green dashed lines) overlap
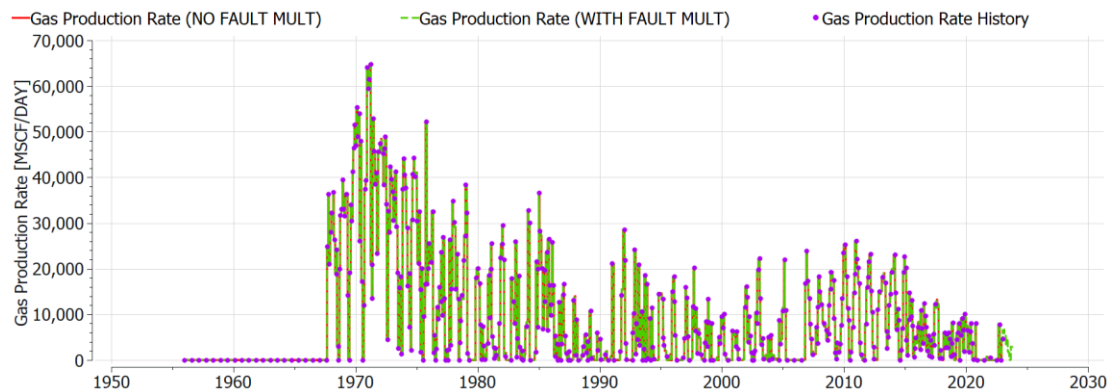
Figure 3 Well gas production rate for the Spitsbergen 3 well. Lines and colours are as in Figure 2.
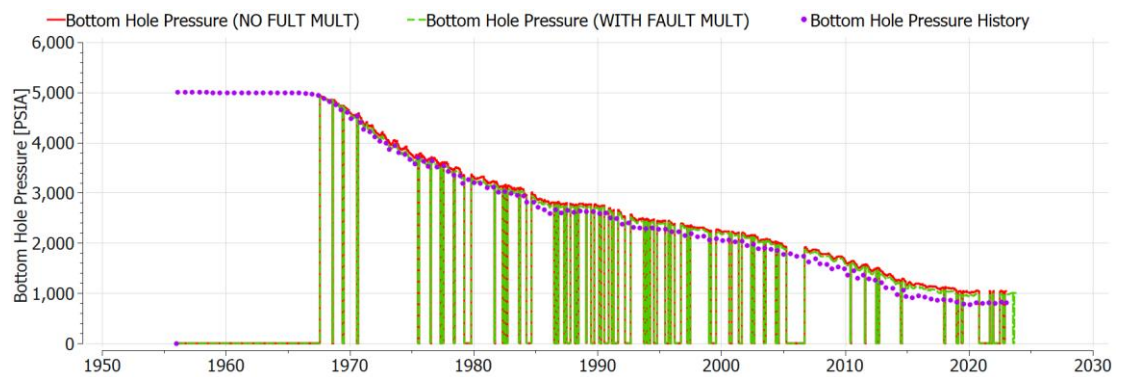
Figure 4 Simulated bottom hole pressures over the gas production period for the Spitsbergen 3 well obtained with the NAM Eclipse model without fault multipliers (red solid line) and the modified version with fault multipliers (green dashed line). The dots (labelled Bottom Hole Pressure History) indicate values simulated with the MoReS model. Vertical lines indicate times as which wells were closed.
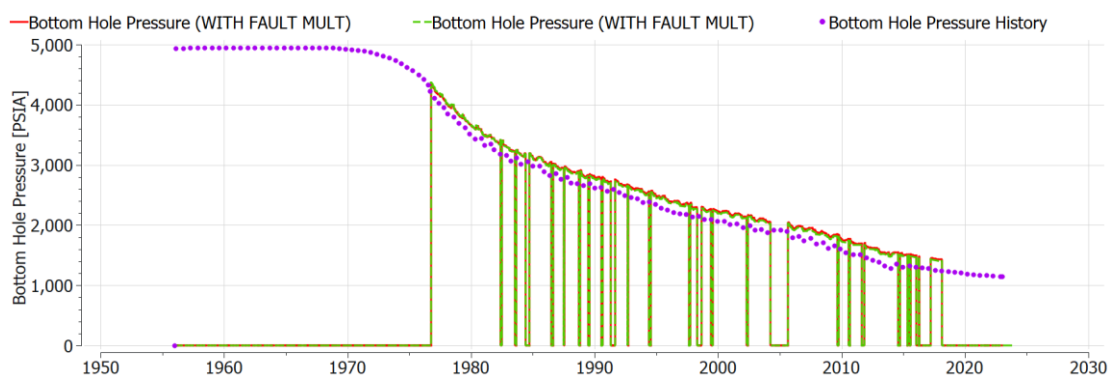
Figure 5 Simulated bottom hole pressures over the gas production period for the 't Zandt 3 well. Colors are as used in Figure 4.
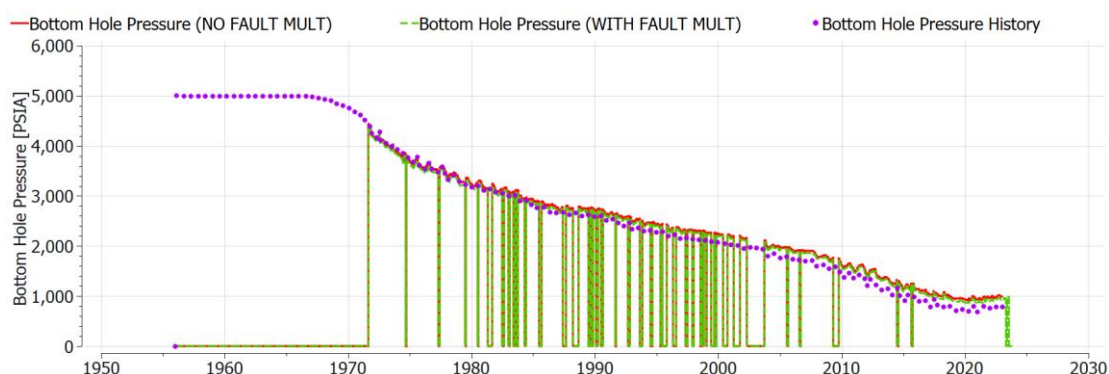
Figure 6 Simulated bottom hole pressures over the gas production period for the Zuidpolder 11 well. Colors are as used in Figure 4.
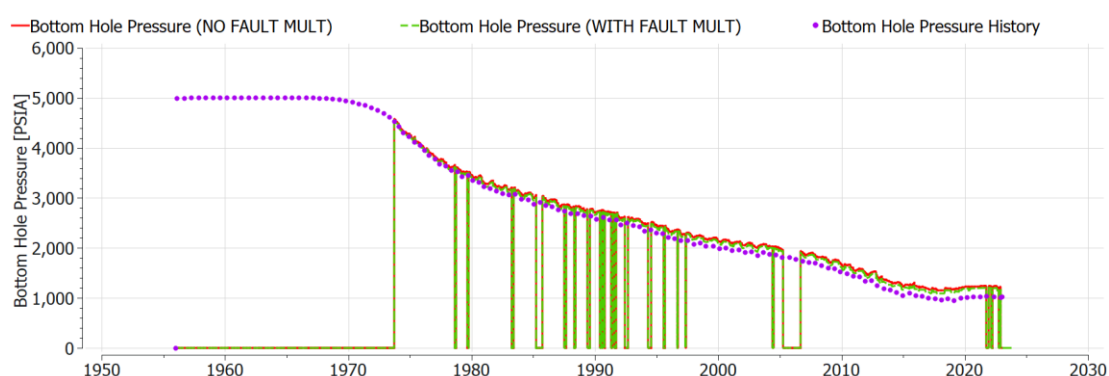
Figure 7 Simulated bottom hole pressures over the gas production period for the Amsweer 1 well. Colors are as used in Figure 4.

Figure 8 shows top views of the model grid and some basic results from simulation of the model over the production period. Clearly visible are the relatively pressure connection to the aquifer towards the south-west of the field, and the large pressure decline in especially the south-east of the field. The pressure in surrounding aquifers that are not dynamically connected with the gas reservoir remain unchanged.

3.4   Injection scenarios

The Eclipse 100 simulator is based on a so-called black-oil formulation in which fluid phases water and (dry) gas are given bulk properties consistent with their composition. Individual molecular components of the gas are not explicitly distinguished, as would be done in a compositional simulator. It is therefore not possible with this model to simulate injection of a gas with properties that are different from the gas that is already present in the reservoir. The focus of this simulation study is therefore primarily on the impacts of re-pressurization, where, for the practical reasons explained, we will assume that injected gas has the same properties as the natural gas present in the Groningen reservoir. The volumetric effects of gas composition will be investigated in a separate box model experiment with a compositional simulator.
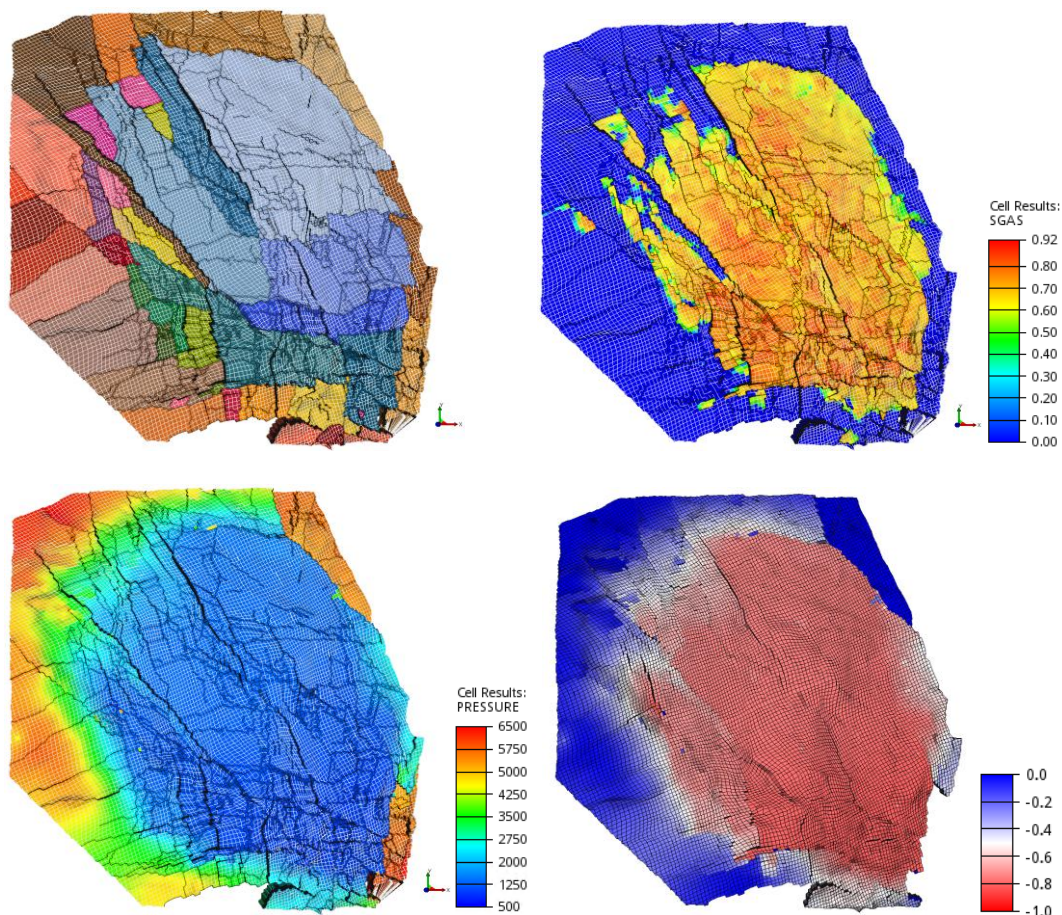
Figure 8 Top views of the NAM Eclipse 100 Groningen model grid. Top left: Fluid-in-place/equilibration regions. Top right: Initial gas saturation. Bottom left: Pressure [psi] in October 2023. Bottom right: Fractional pressure change in October 2023 relative to January 1965 (note that the aquifer region in the bottom-right part of the grid is de-activated).

Different scenarios for gas injection will be considered in which a given total volume rate is distributed in different ways over available clusters of injection wells. This includes not only the geographical distribution associated with the locations of these clusters, but also the distribution over time. The 335 Groningen gas wells are grouped into clusters which are listed in Table 1 and shown in Figure 9. We assume that closed-in wells are directly available, that suspended wells have been temporarily closed, but could be made available again if desired, and that abandoned wells are not available anymore.

Well clusters are themselves grouped according to production regions (Figure 9). Scenarios will be defined that distribute injection gas volumes over all active clusters in one or more production regions by different defined proportions. Individual well injection rates are calculated by the simulator using the well group target functionality of Eclipse and the injection potential of each well. Well rates are limited by historic production rates (e.g. well must have produced more than some minimum to be used as injection wells, and wells cannot inject at a rate higher than the maximum production rate).

We define four base scenarios for spatial distribution of gas injection: No injection, Injection in the Loppersum (LOPPZ) production region, Injection in the South-East production region, and simultaneous injection in the Loppersum and South-East production regions. These scenarios are motivated by the current understanding that seismicity in the field can be associated primarily to pressure decline and the associated reservoir compaction and changes to the stress field. Injection could reduce or even reverse pressure decline and therefore lead to a reduction in seismicity. In the following we discuss the various scenarios in more detail.

Figure 9 Overview of gas well clusters and past production regions in the Groningen field Source: NAM (2020). The status of wells in these clusters is summarized in Table 1.

Table 1 Status of well clusters in the Groningen field in October 2023 (End of Production).

Cluster	Well name abbreviation	Production region	Number of wells	Status (October 2023)
Amsweer	AMR	East-Central	12	Closed-in
Bierum	BIR	North	13	Suspended
Eemskanaal	EKL	Eemskanaal	12	Suspended
Eemskanaal 13	EKL	Eemskanaal	1	Suspended
De Eeker 1	EKR	South-East	11	Closed-in
De Eeker 2	EKR	South-East	10	Closed-in
Froombosch	FRB	South-West	8	Closed-in
Kooipolder	KPD	South-West	12	Closed-in
Leermens	LRM	LOPPZ	11	Suspended
Midwolda	MWD	n.a.	9	Abandoned
Noordbroek	NBR	n.a.	9	Abandoned
Nieuw Scheemda	n.a.	n.a.	9	Abandoned
Overschildt	OVS	LOPPZ	11	Suspended
Oudeweg	OWG	East-Central	11	Closed-in
De Paauwen	PAU	LOPPZ	5	Suspended
Ten Post	POS	LOPPZ	11	Abandoned
Sappemeer	SAP	South-West	9	Closed-in
Schaapbulten	SCB	East-Central	11	Closed-in
Siddeburen	SDB	East-Central	11	Suspended
Slochteren	SLO	South-West	8	Closed-in
Spitsbergen 1	SPI	South-West	10	Closed-in
Spitsbergen 2	SPI	South-West	9	Closed-in
Scheemderzwaag 1	SZW	South-East	10	Closed-in
Scheemderzwaag 2	SZW	South-East	10	Closed-in
Tjuchem	TJM	East-Central	11	Suspended
Tusschenklappen	TUS	South-West	10	Closed-in
Uiterburen	UTB	n.a.	10	Abandoned
't Zandt	ZND	LOPPZ	10	Suspended
Zuiderpolder	ZPD	South-East	12	Closed-in
Zuiderveen	ZVN	South-West	11	Closed-in

In the 'no injection' base case scenario, no gas injection is assumed to take place. However, redistributive flow of gas will still occur due to the existing pressure gradients in the field, that result from uneven production in the past. This scenario provides the baseline expectation for seismicity.

The area around Loppersum has experienced the highest seismic activity, including the largest event registered to date, at Huizinge. While production from this area was stopped already years ago, production continued from the south of the field. The resulting pressure gradient towards the south-east of the field (see Figure 8) will still cause flow of gas away from the Loppersum region, and therefore result in local lowering of the pressure and compaction of the reservoir. Injection in this area could potentially deliver direct beneficial effects on seismicity by, at least temporarily, maintaining pressure. At the same time, this would maintain or even strengthen the existing large-scale pressure gradient and thus cause gas to flow away from the injection area. Retaining any positive impacts would therefore require sustained injection over a long period until large-scale pressure equilibration has been established.

As soon as injection is stopped, local pressure may be expected to start to decline again, but possibly at a slower pace than before.

The south-east region of the field has depleted most strongly (i.e. pressure is lowest here), since gas production in recent years has primarily occurred here, and therefore will be the main driver for redistributive large-scale flow in the field. An increase in pressure in this region should reduce the large-scale pressure gradient across the field and thus permanently reduce the trend towards further pressure decline in regions further north. However, beneficial effects in the Loppersum area can be expected to occur slower and later than if gas were injected there. A compromise scenario that could deliver both short-term direct benefits as well as slower but long-term ones, is therefore to inject in both the Loppersum and South-East regions.

All presented simulations are variations of the above scenario's, where either the total injection volume rate, the distribution over the regions (and thus clusters), or the duration of injection is varied (see Table 2).

The total availability of injection gas used in the scenarios will be based on assumptions about the capacity of factories for nitrogen generation. One of these facilities is the recently completed phase II extension of the Zuidbroek factory, which has a reported capacity of 180.000 m^3/hour (https://zuidbroek.gasunie.nl/het-project). A rough estimate of total volume capacity based on possible contributions from all nitrogen factories in the Netherlands suggests that the Zuidbroek Phase II capacity might be a reasonable basis (from a technical and procedural point of view) for the comparison of various capacity scenarios, as further detailed below. For brevity we will sometimes refer to the Zuidbroek capacity as 1ZB, i.e. 1ZB = 180.000 m^3/hour (or, equivalently, 122 MSCF/day, or 1.58×10^9 Nm^3/year, where 10^9 Nm^3 = 1 BCM). To provide some context, this capacity can be compared to the historic field production rates of natural gas from the Groningen field and corresponds to about one fifth of daily natural gas production in the gas year 2020-2021. Total gas production from Groningen over the past 50 years amounts to more than 75×10^{12} SCF (or 2130×10^9 Nm^3). Complete replacement of that volume at the Zuidbroek nitrogen production rate, would take around 1350 years, which would clearly be infeasible. However, seismicity has not been an issue in the Groningen field from the start, and it may therefore be possible to influence current and future seismic activity by much lower injection volumes. This is the focus of the experiments that we will report here.

The definition of meaningful scenarios will require some assumptions about the future availability of nitrogen generation capacity and the future availability of wells in the Groningen field. Both of these will depend on (geo)political, market and societal developments that must be considered highly uncertain. Rather than speculating on possible outcomes, we will consider scenarios for injection of nitrogen that are based on the currently available nitrogen generation capacity, and on the distribution of available well clusters in the Groningen field at the time of end of production (end of 2023). In addition we will consider a more scientifically motivated set of scenarios that assumes a very high nitrogen generation. We will assume that nitrogen is available to be injected at all wells that are potentially operational in the field. That is, the availability and/or suitability of the surface infrastructure and the sourcing and distribution of the nitrogen are not explicitly considered and studied.

The first set of scenarios that we consider assumes a continuous nitrogen generation capacity of 1 ZB. This is based on a rough estimate of the spare capacity of all combined nitrogen generation facilities in the country (the total capacity is estimated to be roughly 3.2 ZB or 5.1 BCM/year). With spare capacity we mean the capacity not immediately needed to meet the current requirements for conversion of high-caloric imported gas to Groningen-grade gas. For the year 2023 Gasunie Transport Services (GST) reported using 2.84 BCM of nitrogen. This would suggest a spare capacity of about 2.2 BCM/year, or 1.4 ZB. We will consider the scenario that 1 ZB of this capacity is available for continuous injection throughout the year. We stress that the actual value is uncertain and may be even lower.

Since it is likely that injection of gas with this relatively modest volume rate (the reader is reminded of the earlier provided comparison with the historic gas production) does not lead to very significant reduction of seismicity in the short term, we will also consider a more sci-entifically motivated set of scenarios that assume a nitrogen injection capacity of 10 ZB. These scenarios will help to understand and illustrate fundamental mechanisms associated with re-pressurization and its impact on seismicity and also provide an indication of what might be achievable if there were no practical limitations. The 1ZB and 10ZB scenarios represent two cases; one of injection of an amount of N_2 that is currently being produced in the Netherlands (although not necessarily available for this specific purpose), and one case that would require a significant increase in the national N_2 production.

The complete set of scenarios considered in this study is summarized in Table 2.In this table, the abbreviation LO stands for Loppersum and SE stands for South-East. Scenarios 2 to 4 are based on a total nitrogen generation and injection capacity of 1 ZB, while scenarios 5 to 7 are the corresponding scenarios for a capacity of 10 ZB. Scenario's 8 and 9 are informed by results obtained for scenario's 5 and 6 and are meant to investigate the hypothesis of re-bouncing of seismicity after cessation of injection due to pressure equilibration throughout the field. In scenarios 8 and 9, injection is stopped at the time that model-predicted seismicity is reduced to zero in scenario's 5 and 6 respectively.

As an explanation of the Volume factors listed in Table 1, consider e.g. scenario 4. The total injected rate corresponds to 1 ZB, and this volume is divided equally over the LOPPZ and South-East regions. So 0.5 ZB is injected in LOPPZ and 0.5 ZB is injected in the South-East region.

For simplicity we assume that all gas production from nearby small fields ends on 1 October 2023. As a result both the small field wells and the pseudo aquifer wells are shut in at that time. Keeping these wells active during the injection scenarios would require that we include projected production rates for these fields, including expected dates for the end of operations of each of these fields. This would introduce a speculative element into the scenarios. Secondly, the production from the small fields has not been history matched and its impact is most likely not accurately represented anyway. Thirdly, the impact on seismicity in the Groningen field **is** expected to be insignificant.

During the period 1 January 2023 to 1 October 2023 the small fields and pseudo aquifer wells are operated in the model at the targets specified on 1 December 2022. The only pseudo aquifer well open during this period is the one representing production from the Faan field.

Table 2 Overview of injection scenarios. All injection scenarios are simulated until 2054. Injection is started in October 2025 in all cases except scenario 1. Volume factors express the total injected surface volume rate in terms of the of Zuidbroek Phase II nitrogen production capacity (180.000 m³/hour). The time to stop injection in scenario 8 (9) is based on the results from scenario 5 (6) and corresponds to the time that model-predicted seismicity is reduced to zero.

Scenario	Name	Active clusters	Volume factors	Strategy
1	Base Case	None	0	no injection
2	LO	LOPPZ	1	continuous injection until 2054
3	SE	South-East	1	continuous injection until 2054
4	LO_SE	LOPPZ, South-East	0.5, 0.5	continuous injection until 2054
5	LO-10ZB	LOPPZ	10	continuous injection until 2054
6	SE-10ZB	South-East	10	continuous injection until 2054
7	LO_SE-10ZB	LOPPZ, South-East	5, 5	continuous injection until 2054
8	LO-10ZB-7Y	LOPZZ	10	stop injection after 7 years
9	SE-10ZB-11Y	South-East	10	stop injection after 11 years

3.5 Results

Figure 10 shows time series of the near-well pressure (averaged over 9 grid blocks) for all the scenarios listed in Table 2. Pressure curves are provided for the Amsweer 1, Eemskanaal 1, Ten Post 1, and Spitsbergen 1 wells, which are located in the Central-East, Eemskanaal, Loppersum and South-West production regions respectively. All four wells are inactive during the forecast (injection) period.

For the wells WEKL1 and WPOS1, located in the Eemskanaal and Loppersum regions respectively (Figure 10b and Figure 10c), the pressure tends to decline if no gas is injected due to pressure equilibration (see the red lines). Since pressure in these regions is initially higher than in the regions towards the east and south, the resulting pressure gradient will drive a gas flow that would ultimately result in a more or less homogeneous pressure throughout the field. At the Eemskanaal cluster location this tendency is observed for the first 6 to 20 years also when gas is injected in the Loppersum or South-East regions. The pressure decline stops later (around 2044) and at a lower value (about 1280 psi) when the total injected volume is lower.

As may be expected, the pressure increases much faster when gas is injected with a higher volume rate. Considering, for example, the location of the Amsweer 1 well (WAMR1), pressure is increased by up to 90 psi (6 bar) over the 30 year injection period for an injection rate of 1 ZB, while an increase of about 700 psi is observed over that same period for a rate of 10 ZB (Figure 10a). For context, these values compare to a historical pressure decline at this location of about 3800 psi (262 bar) over the production period (compare e.g. the change in BHP for WAMR1 as shown in Figure 7). Since this well is somewhat closer to the Loppersum region than to the South-East region, the pressure increase is somewhat delayed if the gas is injected in the South-East region (compare e.g. the blue and yellow lines).

At the Ten Post 1 (WPOS1) well location (Figure 10c) interesting behaviour is observed for scenario 8 (LO_10ZB_7Y, green line). Pressure decreases during the first few years after the end of production and before the start of injection. Pressure builds up quickly for a period of 7 years when large volumes of gas are injected using wells in the same production region.

When the injected is stopped after 7 years pressure starts to decline again immediately, reaching its lowest value at the end of the forecast period in 2054. If gas is injected in the South-East region (scenario 9, SE_10ZB_11Y, the black line), the initial pressure decline takes somewhat longer to reverse, but no second period of pressure decline is observed in this case, also not after 11 years, when injected is stopped.

Similar behaviour can be observed at the Spitsbergen 1 (WSPI1) well location as shown in (Figure 10d). This location is fairly close to the South-East production region and a clear decline of pressure is observed when injection is stopped after 11 years for scenario 9 (SE_10ZB_11Y, black line). No initial decrease in pressure is expected at this location due to the fact that pressure is already very low in the south of the field at the end of production. Gas will therefore tend to flow towards this location, especially from further north where the pressure is higher, even in the case that no gas is injected.

Several curves are reproduced in Figure 11, which also shows the pressure decline as a result of the production of gas, at two of these four locations. As can be clearly seen, even continuous injection at a rate of 10 ZB will not lead to complete re-pressurization of the Groningen field. However, more relevant for seismicity may be the elimination of spatial pressure gradients within the field.

A spatial impression of the pressure effect of several example injection scenarios is provided in Figure 12. Each panel shows the difference in pressure in 2054 between one injection scenario and the base case (no injection). Injection in the South-East region with a rate corresponding to 1 ZB results in limited pressure increases that are primarily limited to that region (panel b). In contrast, an even distribution of 10 times that rate over the Loppersum and South-East regions (panel e) results in significant increases in pressure throughout the field. Some pressure gradients remain between the two regions (not clearly visible due to the color scale), due to the existing pressure gradient across the field at the end of production, which means that further pressure equilibration would take place if injection is stopped.

(a)

(b)

WPOS1, Nine-point Pressure Average

(c)

WSPI1, Nine-point Pressure Average

(d)
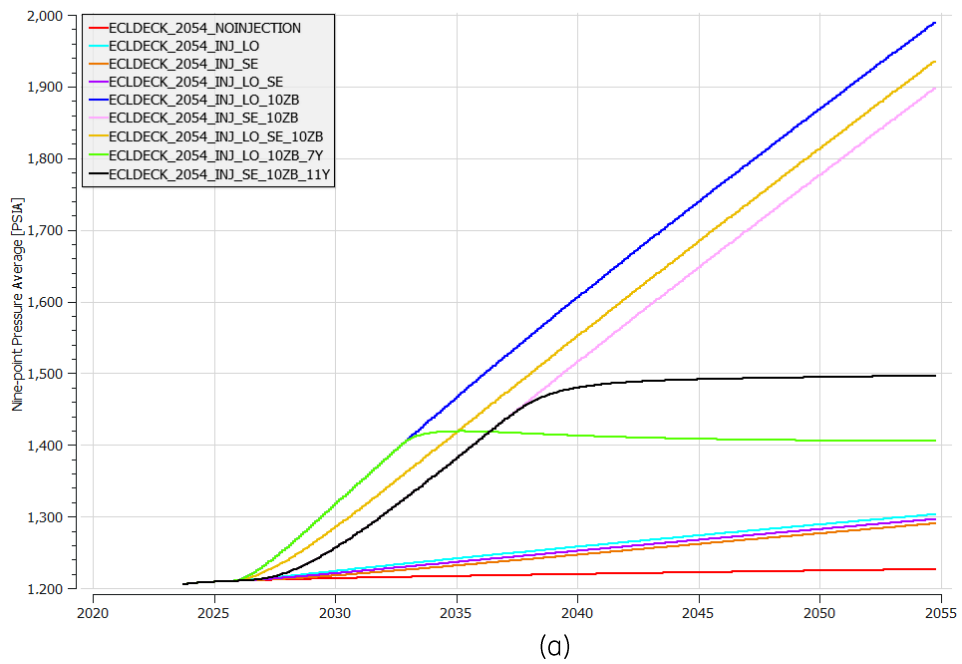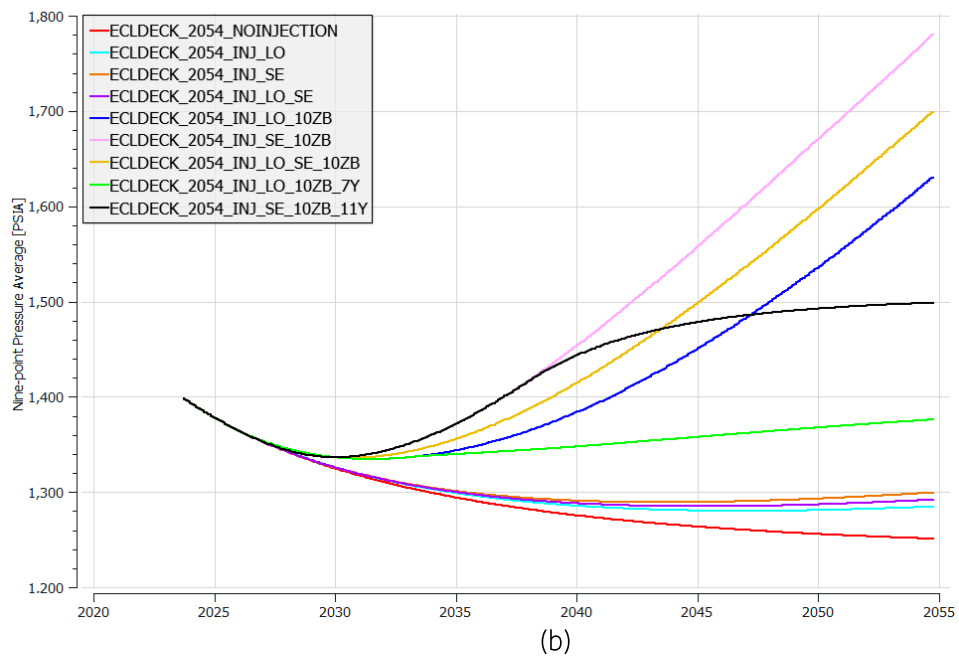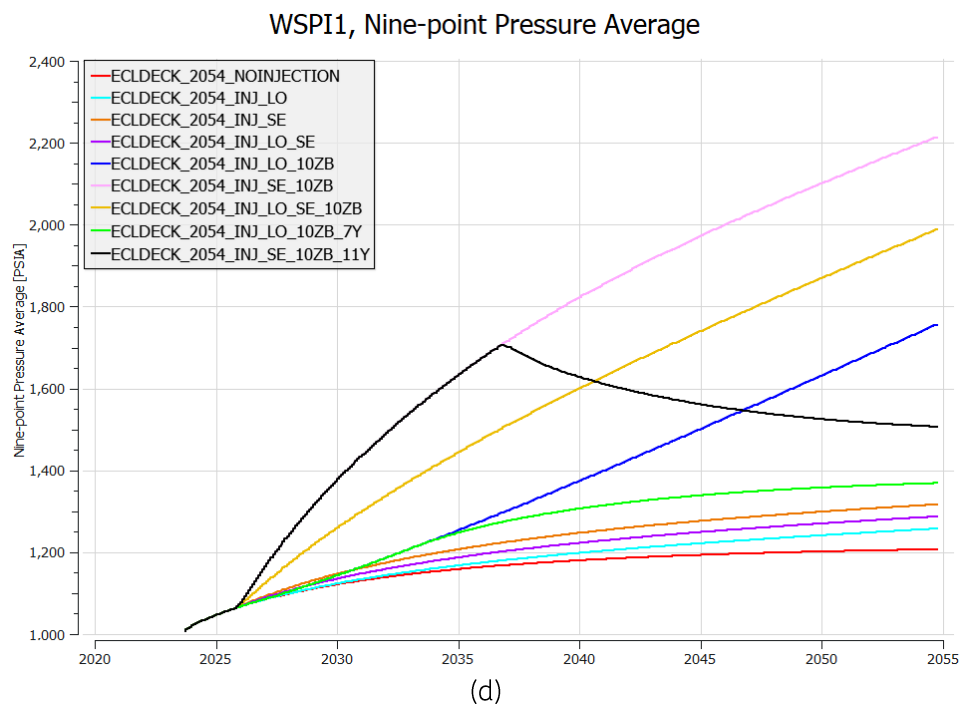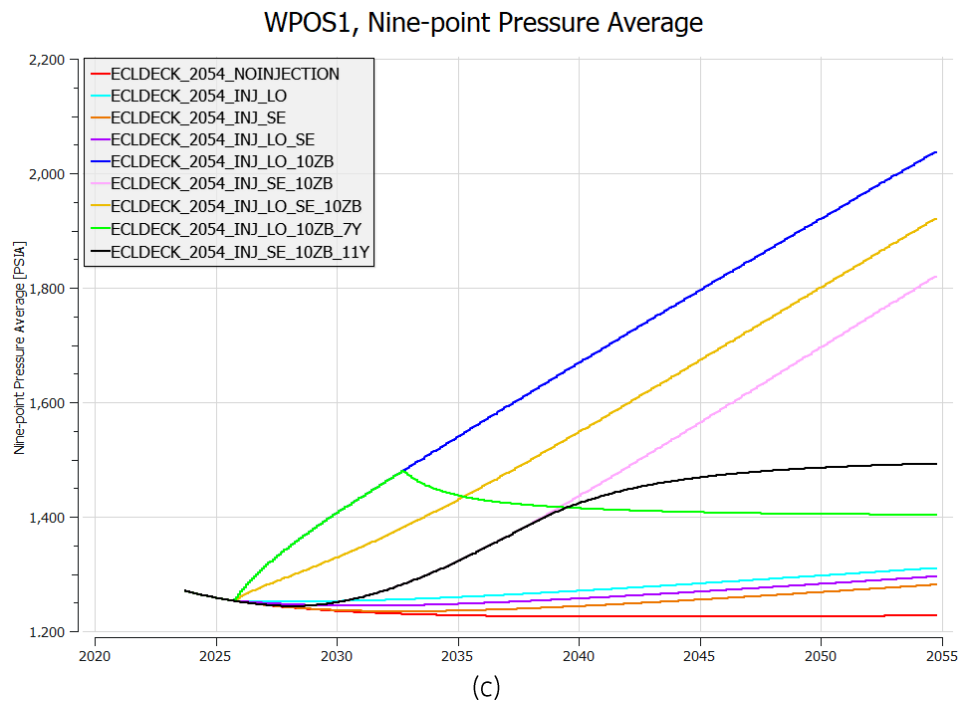
Figure 10 Near-well average simulated reservoir pressure around 4 wells from 4 different production regions that are not used for injection. (a) Amsweer 1, located in the East-Central region, (b) Eemskanaal 1, located in the Eemskanal region, (c) Ten Post 1, located in the Loppersum region, and Spitsbergen 1, located in the South-West region. Results are shown for the base case and all injection scenarios.

(a)

(b)
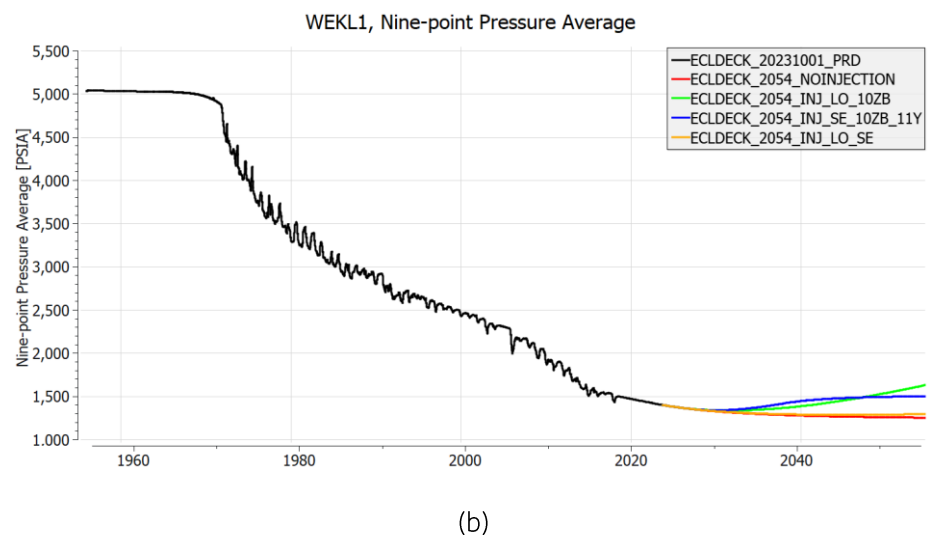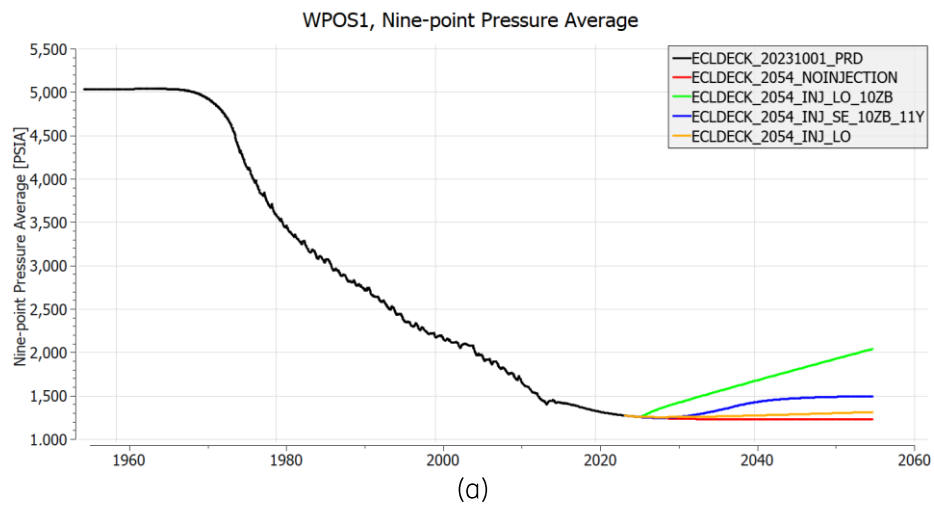
Figure 11 Near-well average simulated reservoir pressure around 2 wells from 2 different production regions that are not used for injection. (a) Ten Post 1, located in the Loppersum region, (b) Eemskanaal 1, located in the Eemskanal region. Results are shown for the production period (black line), the no-injection scenario (red line), two scenarios with 10ZB injection capacity, and one scenario with 1ZB injection capacity.
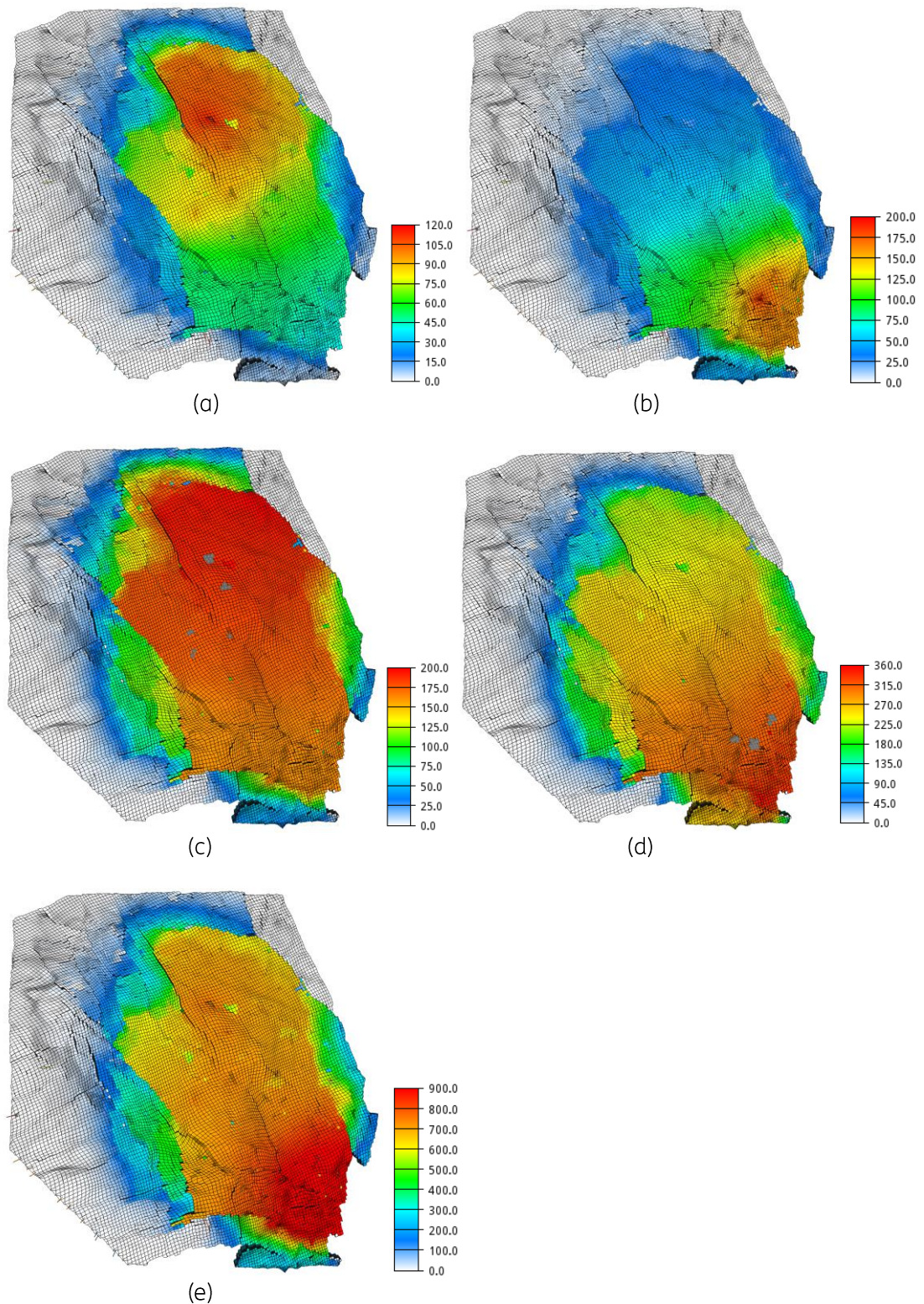
Figure 12 Pressure differences at the end of the simulation period (year 2054) relative to the Base Case (no injection). (a) LO, (b) SE, (c) LO_10ZB_7Y, (d) SE_10ZB_11Y, (e) LO_SE_10ZB. Note the different colour scales. Units are psi (100 psi ≈ 6.9 bar). The locations of active injection wells in the Loppersum and South-East regions are indicated by the clusters of grey dots in panels (c) and (d) respectively.

3.6 Compositional effects

A compositional Eclipse 300 (Schlumberger) model was created to evaluate the effect of gas composition on the expected pressure response. The model can be used to determine the N_2 injection volumes that would be required to achieve the same pressure results as simulated with injection of Groningen gas. A single-cell box model was created that was initialized at a pressure similar to the pressure in the Groningen field at the end of production. The input for the Eclipse 300 compositional simulation model was created using Petrel (Schlumberger) using the built-in components C_1 to C_6, representing methane, ethane, propane, butane, pentane and hexane, N_2 (nitrogen), CO_2 (carbon dioxide), and H_2O (water vapour). Mole fractions were taken from standardized average composition of Groningen natural gas (Gasunie, 1980). The parameters of the compositional model were calculated by Petrel using database values for critical pressure, temperature, Z factor etc. Results for simulations with injection of Groningen gas and injection of N_2 are shown in Figure 13.

The results suggest that injection of the same volume of nitrogen gas will result in a faster increase in pressure. In other words, in order to reach a desired reservoir pressure, a smaller surface volume of nitrogen gas is required than of Groningen gas. The ratio between the two curves increases from 1 at the initial time to 1.06 around 2030 and 1.14 at 2054. The simulation results obtained with Eclipse 100 reported earlier should therefore be interpreted as providing something like an upper bound on the volume of gas required to reach the simulated pressure states, or as providing an upper bound on the time required to reach a desired pressure state (or, more or less equivalently, reduce the seismicity to a desired level). Note that a pressure of around 2000 psi, reached here around simulation time 2030, is similar to the maximum pressure that was obtained in the Groningen injection scenarios, suggesting that errors due to compositional effects are smaller than 6%.
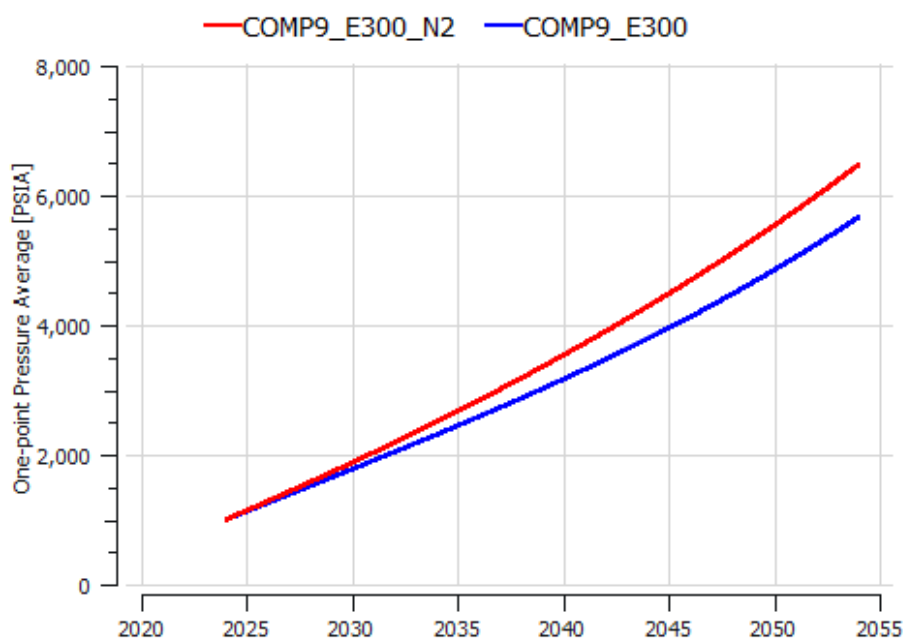
Figure 13 Comparison of single-cell pressure behaviour for a constant surface volume injection rate resulting from simulations with Eclipse 100 (gas properties from the NAM Eclipse model), Eclipse 300 with specification of Groningen gas composition and injection of Groningen gas, and Eclipse 300 with specification of Groningen gas composition and injection of N2.

3.7 Additional comments

In this chapter we have considered relatively simple scenarios for gas injection where we have assumed constant nitrogen generation and injection capacity. Future increases due to changes in gas production and usage, or even the addition of an additional nitrogen facility, could be imagined. Given the low pressures currently present in the field, and the relatively low volume injection rates that we consider here, pressures increases will approximately scale linearly with the average volume injected (as confirmed by the first parts of the curves in Figure 13 for pressures up to 2000 psi, and the last parts of the curves in Figure 10 after transient effects have more or less disappeared). This means that, given an average injection rate of e.g. 2 ZB, pressure increases relative to the no injection case at 2054 can be expected to be higher by approximately a factor 2 than the pressure increase obtained for an average injection rate of 1 ZB.

We have assumed that individual wells cannot inject at rates higher than their maximum historic gas production rates. These maximum production rates range from 0.2 to 1.2 ZB for wells in the LOPPZ region, and from 0.1 to 0.7 ZB for the wells in the South-East region. This means that the wells with the highest productivity (> 1 ZB) could already by themselves inject all nitrogen injected in the LO scenarios (Table 2). Note that nearly 60 wells were used for the scenarios where gas is injected in the South-East region. The high well productivity estimates imply that this number of wells could in principle be strongly reduced.

For completeness we note that a similar simulation as was used to produce Figure 13 but with the Eclipse 100 black-oil formulation results in a curve that does not exactly match the Eclipse 300 result for injection of Groningen gas. An explanation for the difference could lie in the gas formation volume factor, which in the Eclipse 100 deck may have been tuned by NAM to account for the presence of water vapour in the produced gas. However, practical experience has shown that these two simulators always tend to produce different results that require separate tuning of each type of model. It is also not known to the authors how accurate the density calculations of Eclipse 300 are for arbitrary gas compositions.

4 Hazard & Risk Analysis

4.1 Introduction

In this chapter we will investigate the effect of gas injection and the resulting pressure changes on the overall seismicity, seismic hazard and seismic risk. The seismicity, seismic hazard, and seismic risk is modelled by applying the *TNO Model chain for Groningen* (TNO, 2022). In the seismic source model used within the model chain, seismicity is only possible at locations and times in the field where the gas pressure is decreasing. Since nitrogen injection will cause an overall increase in the gas pressure, we expect to observe primarily beneficial effects of fluid injection. Any potentially negative effects (e.g. caused by reservoir cooling, or local development of tensile stresses due to high injection pressures) are currently not modelled and are therefore not considered in this study.

In this chapter we include a number of key figures. A full set of figures related to seismicity, seismic hazard, and seismic risk is included in Appendix A.

4.2 Model description

To calculate seismicity, hazard, and risk, we apply the *TNO Model chain for Groningen* (TNO, 2022, 2023b, 2023c) with the same model versions that were used for the 'analysis according to the most recent scientific insights' in the public Seismic Hazard and Risk Analysis 2023 (TNO, 2023):

〉 Seismic source model V6: Linear elastic reservoir response to pore pressure changes, leading to spatio-temporal Coulomb Stress Change field. This stress field controls the activity rate through an exponential rate model and the earthquake magnitudes though a stress-dependent Gutenberg-Richter b-value.
  The activity rate model and the magnitude model are calibrated over the period 1995-01-01 through 2023-02-28.
〉 Ground Motion Model V7 (Bommer et al., 2022)
〉 Fragility and Consequence model V7 with adjusted parameters to reflect the results of the TNO typology project. (Crowley et al., 2019; TNO, 2023)

For more details on the *TNO Model chain for Groningen* see (TNO, 2022).

The seismic hazard and risk calculation is based on time series of yearly snapshots of pore-volume weighted vertically averaged pressure grids, resulting from the simulations described in Chapter 3. The NAM Eclipse model does not provide the exact same historical gas pressures as the NAM internal reservoir model (MoRes) which has provided the pressure grids for all previous pSHRA model runs. Since the calibration of the source model is conditioned on the historical gas pressures (see TNO 2022 for a description of the source model calibration procedure), the calibrated source model posterior parameter distribution is slightly different compared to the pSHRA '23.

Therefore, the resulting seismicity hindcasts over the production period, as well as the seismicity forecast for the base case scenario (no gas injection) are also different from the pSHRA '23 results (TNO, 2023). For the purposes of this study, which compares different N_2 injection scenarios, this is not a concern, since we're interested in the magnitude of the effect of different N_2 injection scenarios on seismicity/hazard/risk compared to the 'no injection' base case.

4.3 Seismicity

For all scenarios detailed in Chapter 3, Table 2, we forecast the event rate until gas year 2052/2053, and provide a full seismicity forecast (including magnitudes, suitable for hazard and risk assessment) for the gas years 2024/2025 until 2036/2037. Since this study focusses on the impact of different nitrogen injection scenarios, which are clearly visible in the first 13 years of these scenarios, full seismicity forecasts, as well as hazard and risk calculations beyond 2036/2037 are not provided. In Appendix A Figure 14 to Figure 25, the temporal evolution of the forecasted event rate is shown for all modelled cases. A comparison to the reference case (the base case in which no injection occurs) is included. Figure 26 to Figure 27 show the spatio-temporal evolution of the full seismicity forecast used for hazard and risk analyses.

The main effects that can be seen are:
⟩ Injecting more nitrogen leads to a faster reduction of seismicity in the forecasts. In the models where the equivalent of 10 Zuidbroek II facilities worth of N_2 production capacity are injected (10ZB), seismicity rapidly declines to zero expected events per year in 7 to 11 years, depending on the injection location (Figure 14, Figure 18, Figure 19). In contrast, in scenarios where the equivalent of 1 Zuidbroek II facility worth of N_2 production capacity is injected (1ZB), the decline in seismicity is slower and reaches zero expected events close after approximately 25 years of continuous injection (Figure 15, Figure 16, Figure 17).
⟩ When considering the same injection volume, injecting in the Loppersum area leads to a faster reduction in seismicity compared to injecting the South-East. The seismicity reduction for injection of equal volumes in the Loppersum and South-East areas (cases LO_SE and LO_SE-10ZB) falls in between these two end-members (Figure 14, Figure 15, Figure 16, Figure 17, Figure 18, Figure 19).
⟩ Although injection in the Loppersum area leads to a faster decline in seismicity compared to other tested spatial N_2 distribution scenarios, it is also associated with the largest increase in seismicity after injection stops (Figure 20). This is due to the pressure equilibration in the field that continues to occur after cessation of the injection. Injection in the Loppersum area maintains the spatial pressure differences in the field, which leads to gas flow to equilibrate pressures. In the current implementation of the seismic source model, any local gas pressure decrease leads to seismicity, even if that particular location has seen even lower gas pressures in the past. This is potentially a limitation of the current source model, and it is beyond the scope of this project to assess whether this particular feature is a realistic representation of the physics relevant for seismicity.
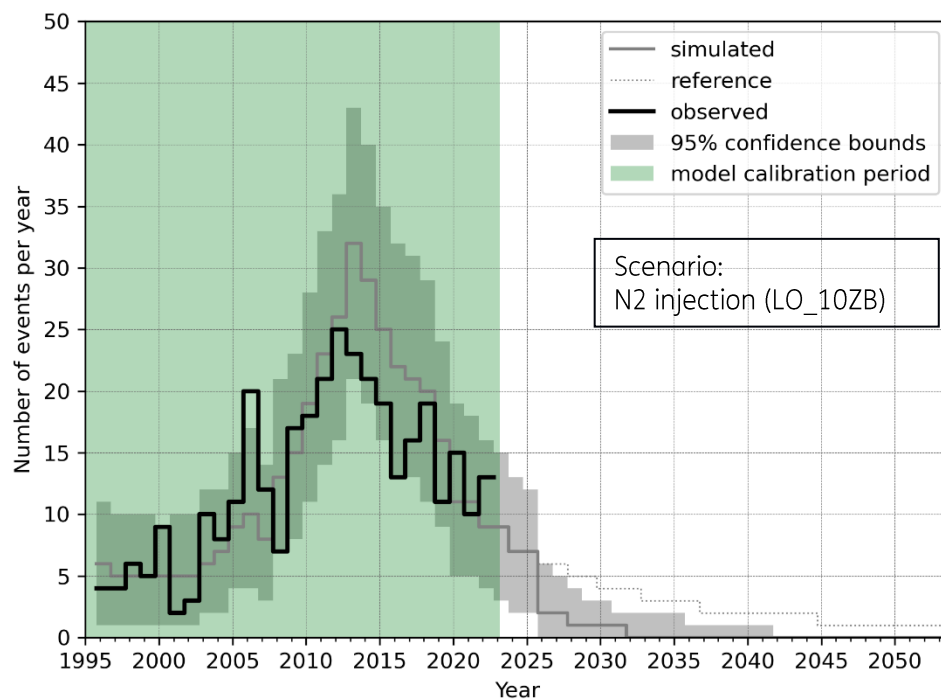
Figure 14: Number of events per year in the Groningen field of M1.5 and above for the LO_10ZB scenario. The solid grey line is the modelled expected number of events, the grey area gives the 95% confidence bounds per year. The solid black line is the data and the green area is the period over which the model is calibrated. The dotted reference line represents the base case for comparison.
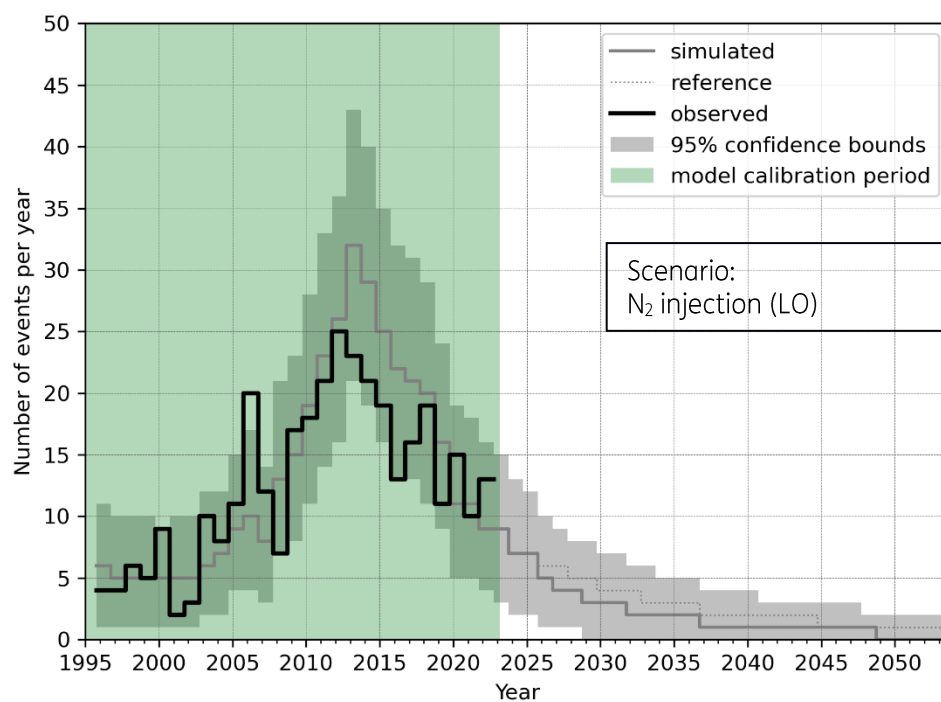
Figure 15: As Figure 14, except for the LO scenario. The dotted reference line represents the base case for comparison.
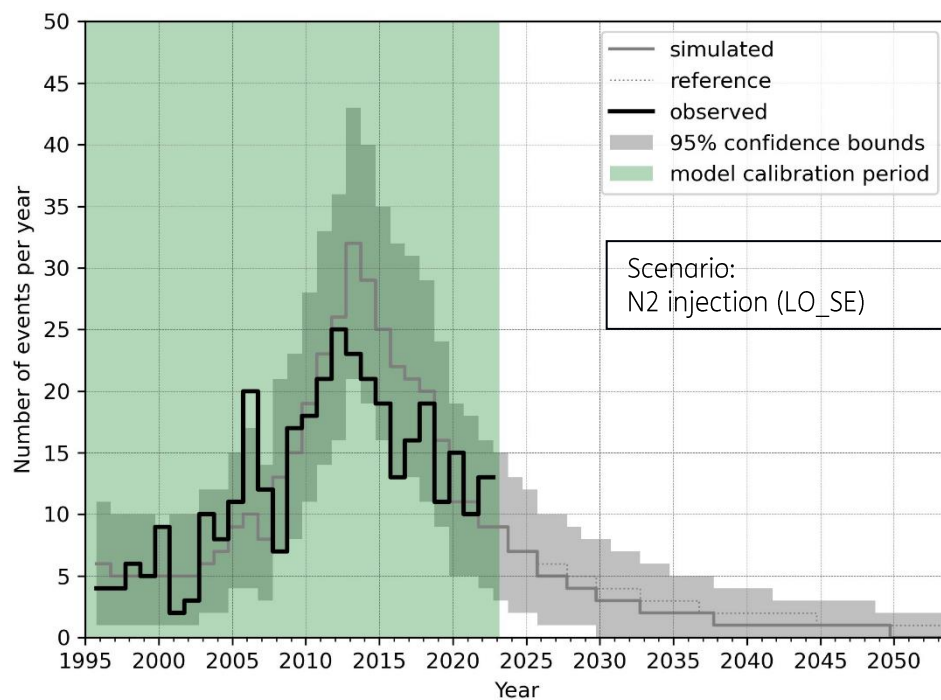
Figure 16: As Figure 14, except for the LO_SE scenario. The dotted reference line represents the base case for comparison.
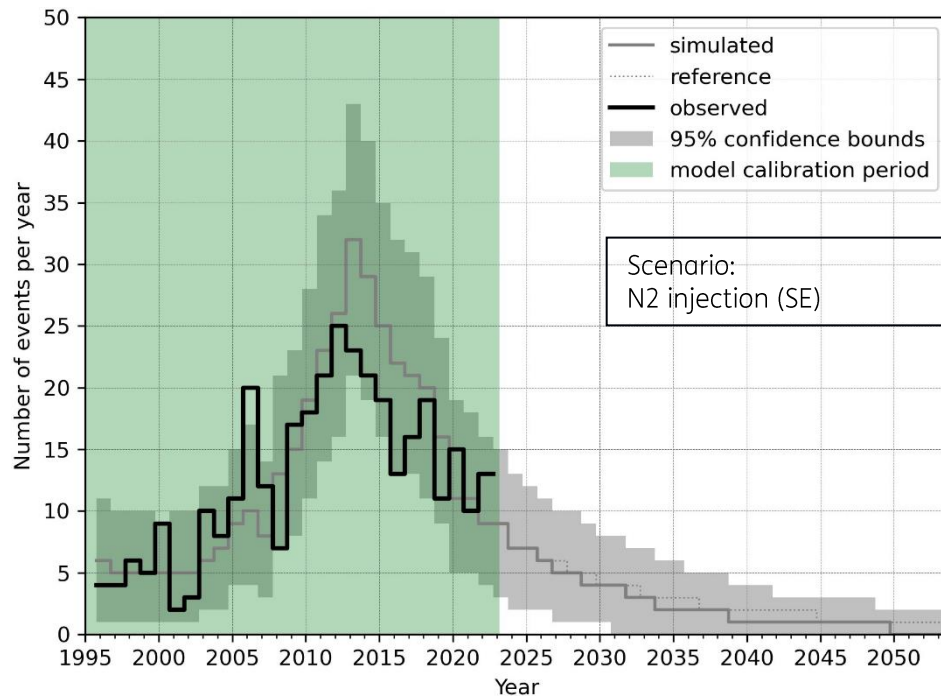
Figure 17: As Figure 14, except for the SE scenario. The dotted reference line represents the base case for comparison.
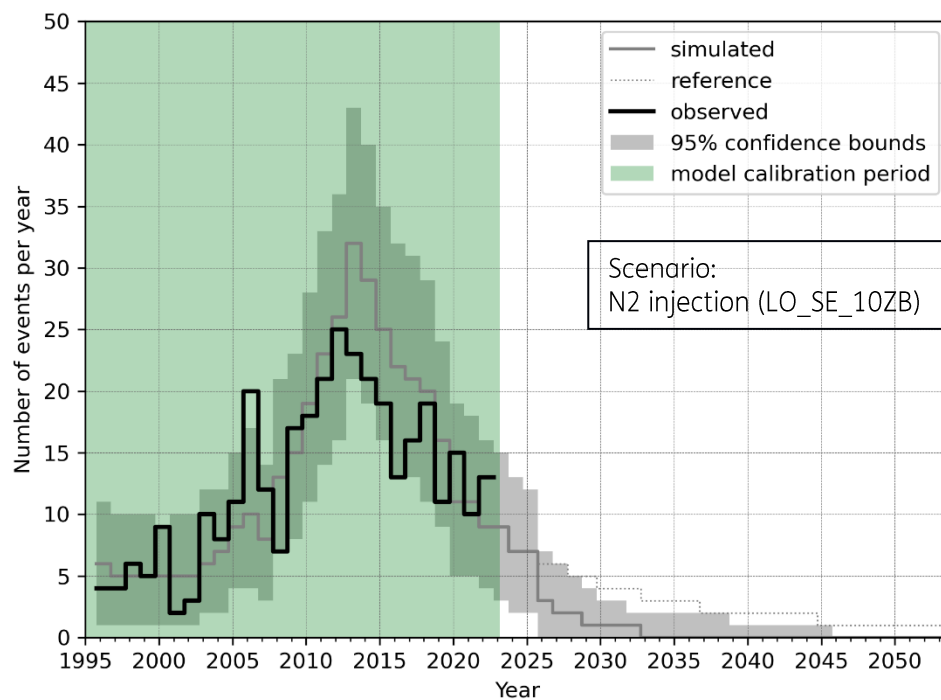
Figure 18: As Figure 14, except for the LO_SE_10ZB scenario. The dotted reference line represents the base case for comparison.
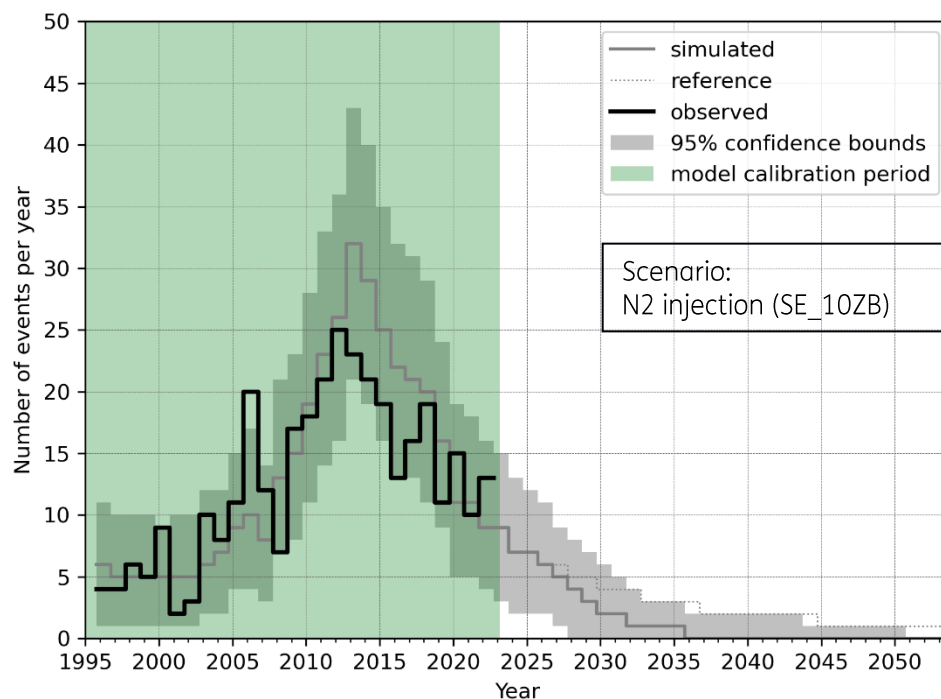
Figure 19: As Figure 14, except for the SE_10ZB scenario. The dotted reference line represents the base case for comparison.
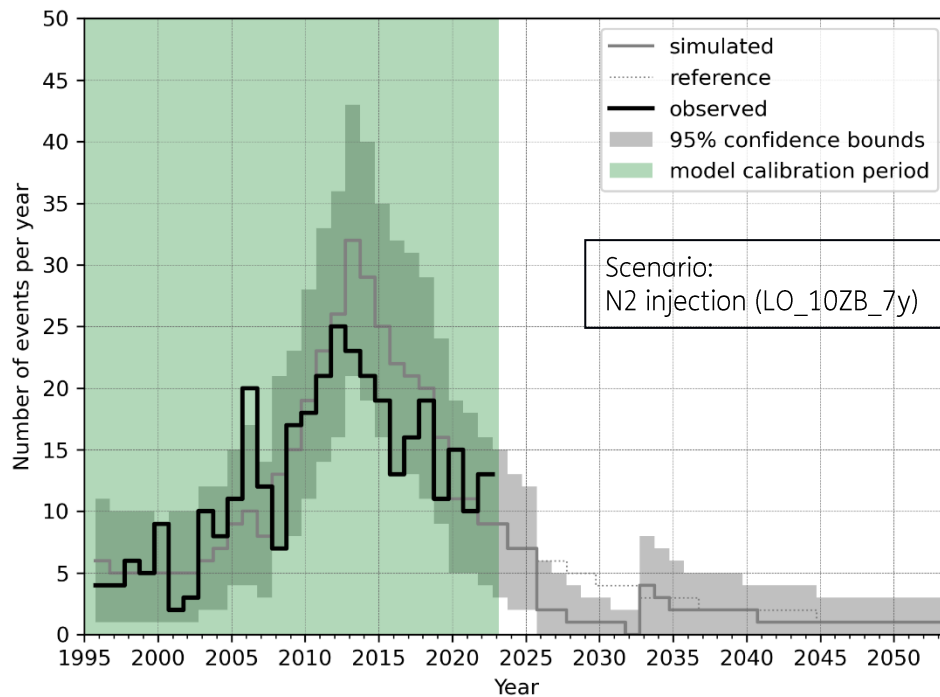
Figure 20: As Figure 14, except for the LO_10ZB_7y scenario. The dotted reference line represents the base case for comparison.

4.4   Hazard and risk

In Appendix A, Figure 46 to Figure 54 show the hazard maps (PGA for 475 year return period) for all cases. Their general pattern is comparable to that of the seismicity maps; the hazard is higher in areas with more expected earthquakes. The hazard maps also show the effects of the shallow subsurface (through the site response model in the Ground Motion Model), which can locally increase/decrease the hazard, depending on the mechanical properties of the shallow subsurface layers. Here, we show the hazard for the base case (Figure 21), the LO case (Figure 22), and the LO_10ZB case (Figure 23).
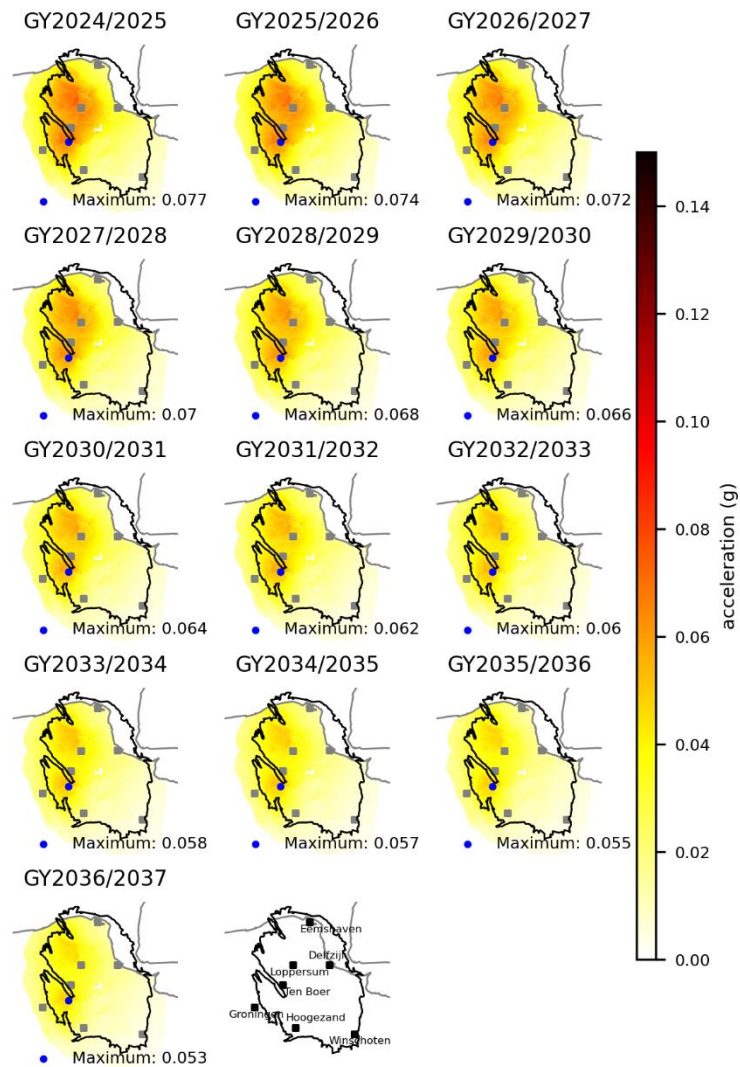
Figure 21: Peak Ground Acceleration (pseudo-spectral acceleration at 0.01 s) hazard map for a 475 return period (10% probability of exceedance in 50 years). The blue dot indicates the position of the largest hazard for each year. Base case (no injection).
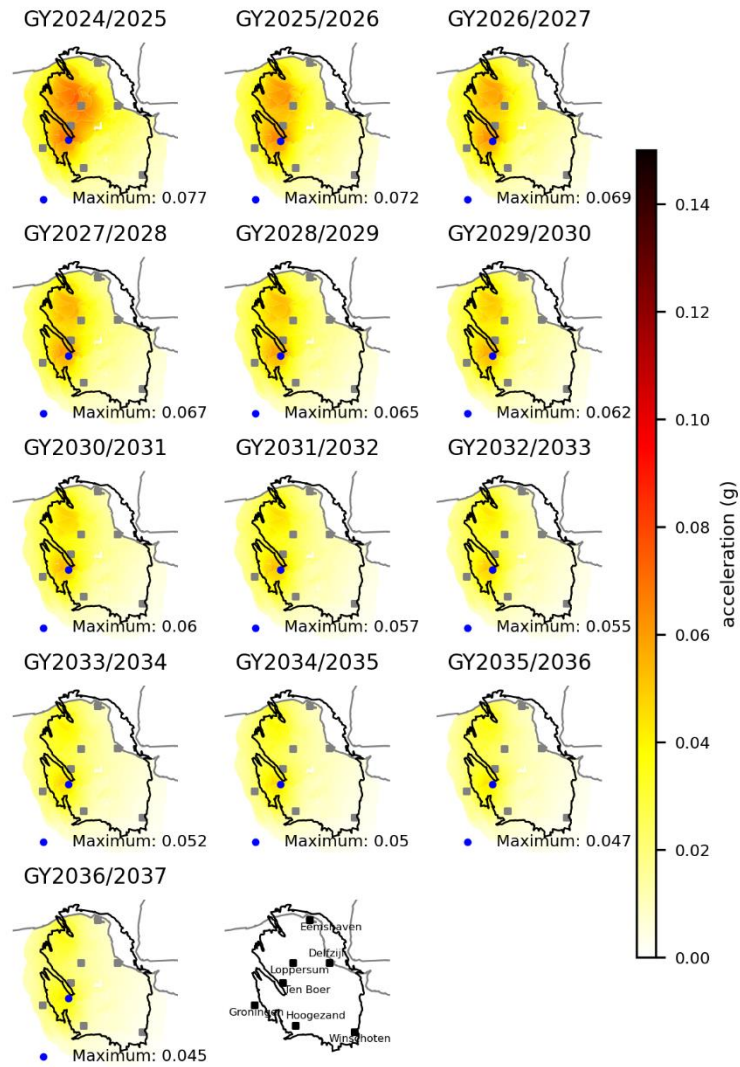
Figure 22: As Figure 21, except for the LO scenario

Sa[0.01] return period: 475 years
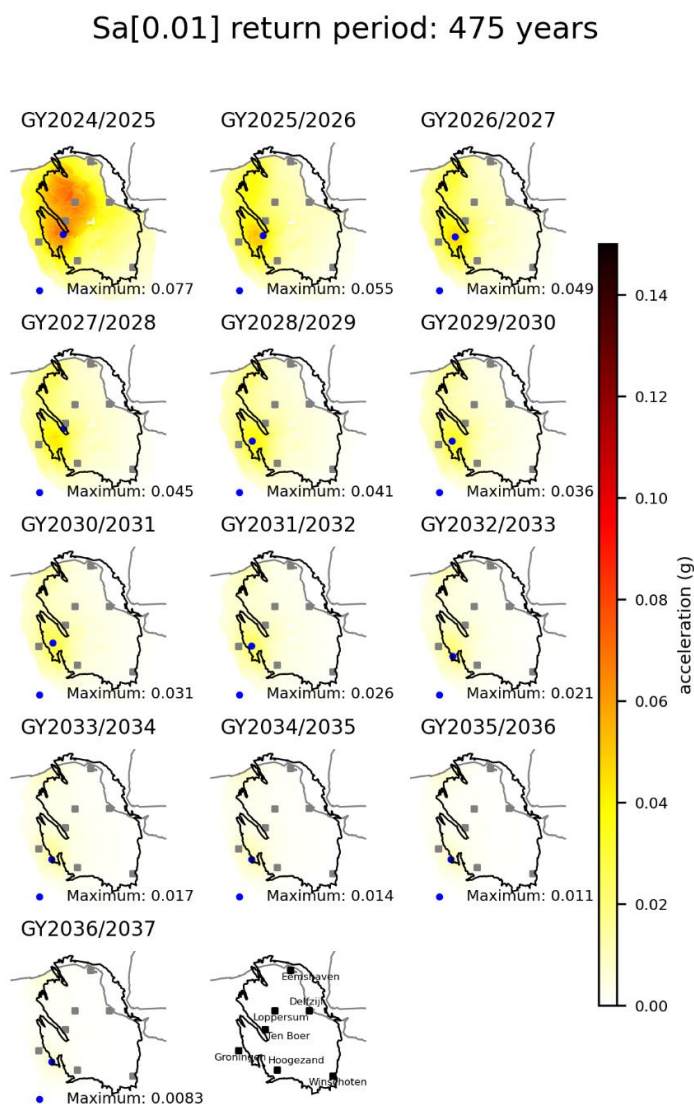
Figure 23: As Figure 21, except for the LO_10ZB scenario

In Appendix A, Figure 55 to Figure 67 show the risk exceedance curves for all gas years 2024/2025 until 2036/2037. Four of these figures are also shown below. Since the N_2 injection for all cases except the base case starts on 1 October 2025 (the first day of gas year 2025/2026), the risk is identical for all scenarios in gas year 2024/2025 (Figure 24). Over the subsequent years, we see a general reduction in the risk for all scenarios when compared to the base case. When N_2 is injected in the Loppersum area at a rate equivalent to the Zuidbroek II production capacity (1ZB), the number of buildings that do not conform to the safety norm (Local Personal Risk of 10^{-5} y^{-1} (Commisie Meijdam, 2015)) goes from ~500 to ~200 after 1 year of injection (Figure 25). The most pronounced reduction occurs when 10ZB is injected in the same area, resulting in a reduction to ~3 after only 1 year. However, if injection in this scenario is stopped after 7 years (when the expected event rate reaches zero), the number of buildings that don't conform to the safety norm goes back up to ~300 (Figure 26), due to the reappearance of seismicity associated with pressure redistribution in the gas reservoir. If the same volume of N_2 is modelled to be injected in the South-East clusters, the decline of seismic risk is less rapid. However, the increase in risk level associated with cessation of the N_2 injection is much less pronounced (Figure 27).
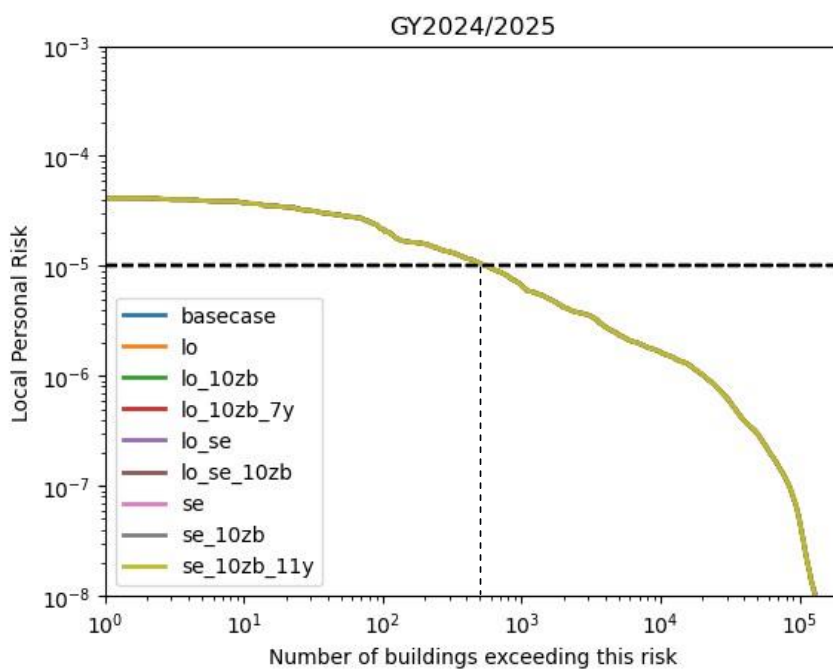
Figure 24: Risk exposure plot. Shows how many buildings (on the x-axis) are exposed to a given local personal risk (y-axis). Shows all scenarios considered for GY 2024/2025. Since N_2 injection starts on the 1st of October 2025 in all scenarios (1st day of gas year 2025/2026), the risk exposure is identical for all scenarios, leading to all the lines being on top of one another. Approximately 500 buildings exceed the Meijdam norm ($10^{-5}\,y^{-1}$) for all scenarios.
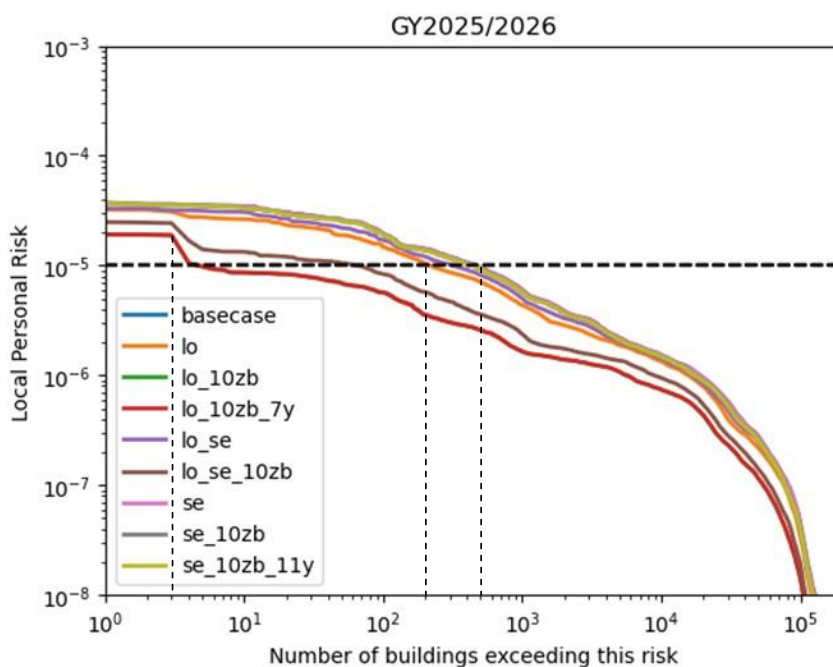
Figure 25: Risk exposure plot for GY 2025/2026. The risk profile decreases compared to previous year for all scenarios (including the base case), but with different amounts. For the scenarios where 10x the Zuidbroek II capacity of N_2 production is injected in the clusters around Loppersum (overlapping green and red curves), the number of buildings not conforming to the safety norm goes down to 3 buildings.
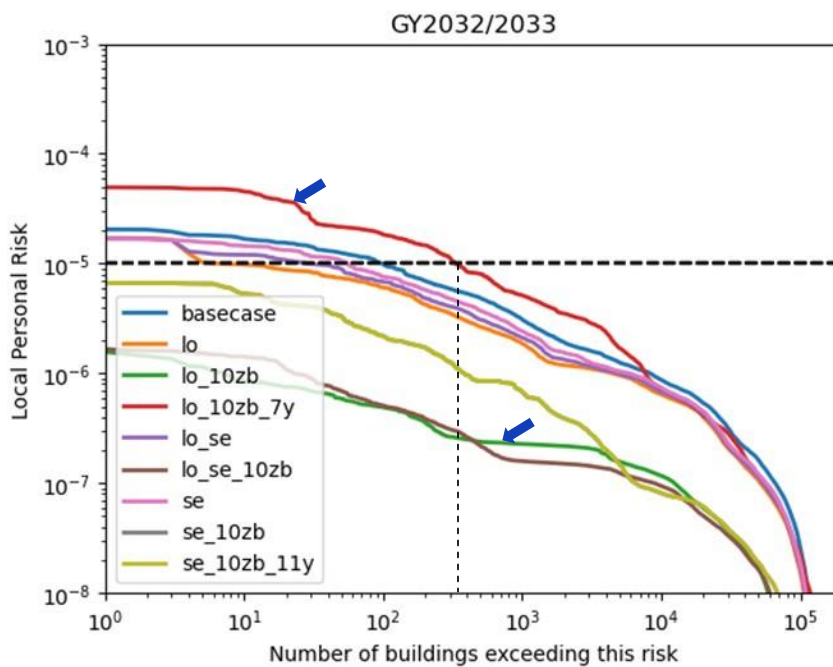
Figure 26: Risk exposure plot for GY 2032/2033. Note the large increase in risk for the lo_10zb_7y case, where nitrogen injection ceases on the 1 October 2032.
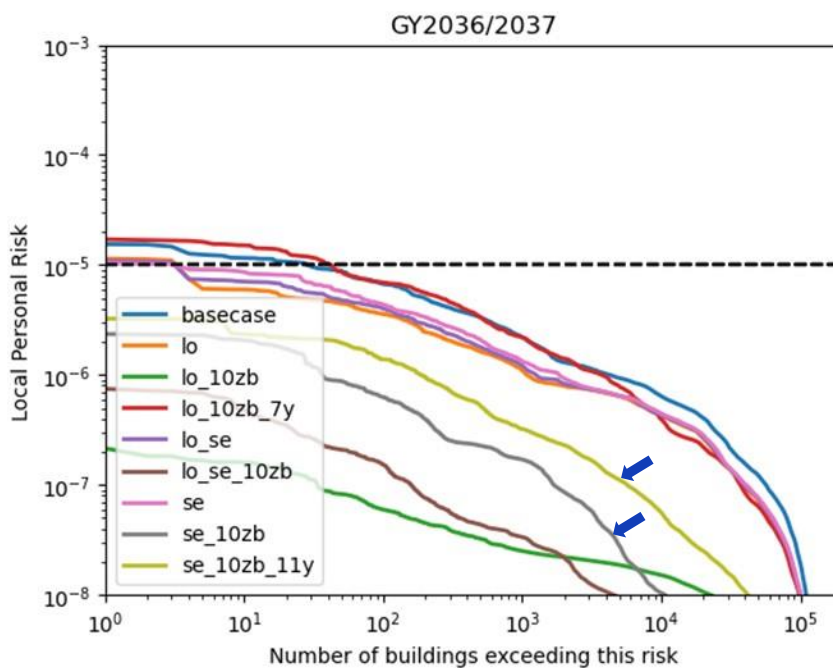
Figure 27 Risk exposure plot for GY 2036/2037. Note the increase of in risk for the se_10zb_11y case, where nitrogen injection ceases on the 1 October 2036. Despite the increase in risk, all buildings conform to the safety norm for this case.

4.5 Discussion and conclusions

Here, we have specifically investigated the potential positive effects of N_2 injection in the Groningen gas field on seismic event rate, seismic hazard, and seismic risk. We looked at two total volume scenarios to get a sense for the general response to different amounts of N_2 injection, and different spatial distributions, all under the assumption that the only effect of injection is on the gas pressure distribution, and that locally increasing the gas pressure leads to less seismicity at that location.

It is important to note that the seismic source model used in this study was developed with gas production in mind, and was calibrated on seismicity generated by gas production. As a result, the results obtained for different injection scenarios are automatically less well constrained. The source model may not include all physical mechanisms that are relevant in an injection scenario, and the model parameters are calibrated on a dataset that was collected when no gas injection was taking place. Nonetheless, these results give us first order indications on the effects of different quantities of N_2 injection, and the effects of the spatial distribution of that injection. In particular, they suggest that the potential positive effects of large-scale N_2 injection on both seismicity rate (the number of earthquakes per unit time) and seismic risk (the probability of loss of life due to seismicity) can be substantial compared to the 'no injection' base case.

For injection volume rates informed by estimated current N_2 production capacity (e.g. the LO scenario, in which 1x the annual nitrogen production capacity of the Zuidbroek II facility is injected in the Loppersum cluster) we see significant effects, both in terms of seismicity (Appendix A, Figure 29), hazard (Figure 22), and risk (Figure 25). For example, the number of buildings exposed to a risk level above the Meijdam norm (LPR $>10^{-5}$ y^{-1}) goes down from ~500 to ~200 after 1 year of injection, and to ~50 after 6 years of injection.

For the LO_10ZB scenario (inject 10 times the annual nitrogen production capacity of the Zuidbroek II facility in the Loppersum cluster), we see that the expected number of earthquakes of M1.5 and above goes down to zero after 7 years of injection (Figure 18). In the base case (no N_2 injection), the expected number of events does not reach zero at the end of our simulations (gas year 2053/2054) (Appendix A, Figure 28). For the LO_10ZB scenario, the number of buildings exposed to a risk level above the Meijdam norm (LPR $>10^{-5}$ y^{-1}) goes down to 3 after only 1 year of injection, while in the base case the number of exposed buildings remains ~500 (Figure 25; the blue line is hidden under the curves for the SE scenarios).

Injection scenarios that (partially) inject the nitrogen in the South-East clusters have less pronounced effects on seismicity, hazard, and risk on the short term, but potentially offer advantages on the longer term, since they reduce spatial gas pressure variability, and therefore are associated with less pressure equilibration once gas injection eventually ceases. In general, the injection scenarios modelled in this study are indicative of the approximate types of behaviour that can be expected under the set of modelling assumptions outlined at the beginning of this chapter. The scenarios represent broad classes of injection-related choices, mainly the injection volume/rate and spatial distribution of the injected N_2.

5 Explore seismic source model adjustments

5.1 Introduction

In this chapter, we investigate changes that can be made to the current seismic source model to include the potentially destabilizing (seismicity enhancing) effects related to nitrogen injection. Nitrogen injection causes pressure increase and temperature decrease in the reservoir. Although in general, induced seismicity can be caused by injection (e.g. fracking, wastewater disposal, Enhanced Geothermal Systems), in this case we do not expect significant effects of the pressure increase due to nitrogen injection on seismicity for the following reasons:

〉 The Groningen reservoir rock is very permeable, leading to modest near-well pore pressure increase when injecting (i.e. the near well pressure is reasonably well represented by the large-scale reservoir simulations). In fact, in our simulations, the bottom hole pressure of injection wells and the grid block average pressure of grid blocks with an injection well differ less than 0.1 MPa (1 bar). We therefore do not expect local failure around the well due to the pressure increase.

〉 In the stress field of the Groningen gas field, pressure increase is expected to stabilize the faults.

〉 Injection would be mainly aimed at stopping pressure decrease, rather than substantially increasing pore pressures compared to their present state. Mild pore pressure increase is already seen in some parts of the Groningen gas field for years. In these areas, seismicity is largely absent, suggesting that the current source model actually captures the reservoir response to moderate pore pressure increase rather well.

On the other hand, reservoir cooling would be associated with a decrease in horizontal stress and associated destabilization of fault. We therefore focus our efforts on adjusting the theoretical framework to deal with temperature changes.

The current source model is based on linear poroelasticity. We explore the theoretical foundations of linear poroelasticity with thermal effects in conjunction with its implementation on the model chain, to further examine their combined impact on induced seismicity.

5.2 Description of adjustments

Theory of linear poroelasticity combined with thermal effects: Linear poroelasticity describes the behavior of fluid-saturated porous materials under small deformation. It is based on principles such as conservation of mass, which ensures fluid balance within the pores, and conservation of momentum, which considers the balance of internal and external forces. The effective stress, according to Terzaghi's principle, is defined as the total stress minus the pore fluid pressure. Constitutive relations in this theory link stress σ and strain ε in the material, taking into account the interplay between the solid matrix and fluid pressure P_p.

The theory sets the basis for understanding more complex phenomena when additional factors like thermal effects are included. When thermal effects are incorporated, the theory extends to linear thermo-poroelasticity, addressing the thermal expansion/contraction of the solid matrix due to spatio-temporal variations in the temperature. Thus, the system of equations in index notation describing linear poroelasticity combined with thermal effects reads (Fjaer et al. 2008)

$$\sigma_{ij} = \frac{Ev}{(1+v)(1-2v)}\varepsilon_{vol}\delta_{ij} + \frac{E}{1+v}\varepsilon_{ij} + \alpha P_p \delta_{ij} + \frac{E}{1-2v}\alpha_T \Delta T \delta_{ij} \tag{1}$$

Where E, v, α, and α_T are the Young modulus, Poisson's ration, Biot's coefficient and linear thermal expansion coefficient, respectively. In the context of the model chain framework, ΔT is an input variable obtained from reservoir simulations that accounts for the spatio-temporal variations in the temperature field as fluid injection/production occur.

Uniaxial Strain Conditions

The seismic source model is based on uniaxial strain conditions, where strain is applied only in the vertical direction. This approach simplifies the material's response by focusing the analysis on stress and strain relations along the horizontal plane. Consequently, Equation (1) is rewritten to reflect changes in vertical and horizontal stresses as follows:

$$E\varepsilon_H = \Delta\sigma_H - v(\sigma_h + \sigma_v) - (1-2v)\alpha\Delta P_p - E\alpha_T\Delta T \tag{2.a}$$
$$E\varepsilon_h = \Delta\sigma_h - v(\sigma_H + \sigma_v) - (1-2v)\alpha\Delta P_p - E\alpha_T\Delta T \tag{2.b}$$
$$E\varepsilon_v = \Delta\sigma_v - v(\sigma_H + \sigma_h) - (1-2v)\alpha\Delta P_p - E\alpha_T\Delta T \tag{2.c}$$

With $\varepsilon_H = \varepsilon_h = 0$ under uniaxial strain conditions, the system simplifies further

$$\Delta\sigma_H = \Delta\sigma_h = \frac{1-2v}{1-v}\alpha\Delta P_p + \frac{H(1-2v)(1+v)}{(1-v)^2}\alpha_T\Delta T \tag{3.a}$$
$$\varepsilon_v = -\frac{1}{H}\alpha\Delta P_p - \frac{(v+1)}{(1-v)}\alpha_T\Delta T \tag{3.b}$$

Here, we assume $\Delta\sigma_v = 0$, because the vertical stress remains constant due to the constant weight of the overburden layers. For convenience, Equation (3.a) and (3.b) are expressed in terms of the uniaxial compaction modulus H. The uniaxial compaction modulus H is a measure of the material's stiffness under uniaxial strain conditions. The formula for the uniaxial compaction modulus H in terms of Poisson's ratio v and Young's modulus E is derived from the relationship between stress and strain under uniaxial conditions:

$$H = \frac{E}{(1-2v)(1+v)} \tag{4}$$

This relation comes from the generalized Hooke's Law and reflects the effect of Poisson's ratio on volumetric strain under uniaxial loading.

In the context of the source model framework, the uniaxial compaction modulus is a spatially varying model parameter. In other words, the amount of strain for a given amount of pore pressure change is not spatially constant, due to the spatial heterogeneity of the reservoir rock's material properties. We deem it likely that this implies that the reservoir rock would also not respond homogeneously to a given change in temperature. Here, we relate the sensitivity of the vertical strain to temperature change (given by α_T) to the uniaxial compaction modulus H.

An important feature to pay attention to is the relationship between the material stiffness E and the thermal expansion coefficient α_T. Generally, the stiffer the material, the less it expands or contracts with temperature changes. This trend is primarily due to stronger atomic or molecular bonds in stiffer materials, which resist deformation under both mechanical and thermal stresses. According to Le Bourhis (2014), there exists an inverse relationship between the thermal expansion coefficient (α_T) and Young's modulus (E). This relationship is expressed in terms of the uniaxial compaction coefficient as follows:

$$\alpha_T = \frac{a_T}{H} \tag{5}$$

where a_T is a new model parameter that has to be calibrated within the seismic source model. A prior range for this parameter could be defined based on the known range of α_T in Rotliegend sandstone rocks, and the range of values for H that are used in the current implementation of the seismic source model. Further calibration of the parameter a_T would have to be based on observations of either seismicity (or lack thereof) or subsidence, in combination with actual cold fluid injection and non-isothermal reservoir modelling.

5.3 Potential for further work

The updated source model could be implemented in the TNO Model Chain for Groningen, although the specifics depend on a number of factors:

〉 First of all, the currently derived method for including the effects of temperature change depends on a linearly elastic reservoir model. The model currently used for hazard and risk assessments (pSDRSA 2023) is in fact linearly elastic, but TNO has recommended including a non-linear rate-type compaction branch in the source model. Adding temperature effects to the rate-type implementation would be non-trivial.

〉 The calibration framework would have to deal with an additional parameter (a_T). We do not foresee that this would result in computational difficulties, even for the current 'brute-force' grid evaluation that is used for characterization of the parameter space.

〉 The model would have to be provided with a temperature forecast. These can be provided by reservoir simulators like Eclipse. To ensure that near-well effects are captured, it may be necessary to perform local grid refinement on the flow grids around the wells. Including a non-regular grid in the source model would require an additional update of the source model and some parts of the hazard and risk chain.

All in all, it appears feasible to update the linearly elastic source model to include temperature effects. Such a model could be calibrated in theory, although in practice this would require actual nitrogen injection (or at the very least temperature changes) to be performed. However, as stated above, we expect that the prior range of the new model parameter a_T can be relatively well-constrained based on existing data, suggesting that it may be possible to capture a range of expected outcomes in terms of seismicity to be calculated without further calibration.

5.4   Conclusions

We have discussed the theoretical basis for expanding the current linearly elastic seismic source model. Rather than assuming a single value for the thermal expansion coefficient, we have explored the connection between the thermal expansion coefficient and the uniaxial compaction modulus to include the expected spatially heterogenous impact of temperature on strains throughout the gas field. We expect that these alterations can be implemented in the TNO Model chain for Groningen, although not for more complicated compaction models such as rate-type compaction. Once implemented, forecasts that include the effect of temperature change could be produced, although they would necessarily be based on prior assumptions for the new model parameter a_T until this parameter can be calibrated on observed seismicity (or lack thereof) in combination with actual induced temperature changes in the reservoir.

6 Conclusions and recommendations

KEM-24b aimed to address the following research questions:

1. What can be learned from examples of fluid (including gas) injection in reservoirs similar to the Groningen reservoir?
2. Which injection scenarios for mitigating seismicity could be applied after production has stopped?
3. How can the existing Groningen SHRA (Seismic Hazard and Risk Assessment) model chain be adapted to include fluid injection?
4. What is the potential beneficial effect of fluid injection on the overall seismicity, seismic hazard and seismic risk?

Based on a literature review, we conclude that large-scale injection aimed at reducing seismicity in a previously heavily depleted gas field has not been done elsewhere. We judge that the closest analogous cases to the Groningen case (in terms of pressure history, expected possible geomechanical failure mechanisms, injection depth, and reservoir properties) are Dutch Underground Gas Storage (UGS) facilities. However, the relevance of these analogue cases for the Groningen case is limited, since UGS facilities are cyclically pressurized to pressures much higher than the depletion pressure and then depressurized again when the gas is produced. This is different from possible nitrogen injection in Groningen, where the goal would simply be to stop local pressure decrease wherever this is likely to result in seismicity, rather than large-scale re-pressurization as seen in UGS operations.

In this study, we specifically investigated the beneficial effects on seismic event rate, seismic hazard, and seismic risk associated with re-pressurization by N_2 injection in the Groningen gas field. We looked at two volume scenarios (1ZB and 10ZB) to get a sense for the general response to different amounts of N_2 injection, and different spatial distributions, all under the assumption that the only effect of injection is on the gas pressure distribution, and that locally increasing the gas pressure leads to less seismic activity at that location.

It is important to note that the seismic source model of the existing Groningen SHRA (Seismic Hazard and Risk Assessment) model chain used in this study was developed with gas *production* in mind, and was calibrated on seismicity generated by gas production. As a result, the results obtained for different *injection* scenarios are automatically less well constrained. The source model does not include all physical mechanisms that may be relevant in an injection scenario, especially those associated with temperature changes, and the model parameters are calibrated on a dataset that was collected when no gas injection was taking place. Nonetheless, we argue that this study should provide first order indications on the effects of different quantities of N_2 injection, and the effects of spatial distribution.

The model experiments suggest that, if gas volumes similar to the capacity of the Zuidbroek II nitrogen generation facility were available for large-scale injection, the positive effects on both seismicity rate (the number of earthquakes per unit time) and seismic risk (the probability of loss of life due to seismicity) could be substantial already after a single year of injection, when compared to the 'no injection' base case. In one scenario, the number of buildings exposed to a risk level above the Meijdam norm is reduced from approximately 500 after 1 year without injection to approximately 200 after 1 year of gas injection. Without injection this takes about 5 years. The effectiveness of injection depends on both the injection location and the total injected volume. The variability of seismic hazard and risk results between scenarios with the same amount of injected gas shows that there is room for optimization of spatial and temporal distribution of gas injection over the available wells. Further exploring this aspect was not part of the scope of this project. We have also not explored how a long-term injection strategy could be developed that includes eventually ending the N_2 injection. Such an 'exit-strategy' is clearly needed, as infinite injection in unfeasible from many perspectives, including physical considerations.

Although the current analyses only highlight positive effects of injection, we have discussed the theoretical basis for expanding the current seismic source model. We have explored the connection between the thermal expansion coefficient and the uniaxial compaction modulus to include the expected spatially heterogenous impact of temperature on strains throughout the gas field. We expect that these alterations can be implemented in the TNO Model chain for Groningen, although not (at least not in their current form) for more complicated compaction models such as rate-type compaction. Once implemented, forecasts that include the effect of temperature change could be produced, although they would necessarily be based on prior assumptions until the updated model can be calibrated with (lack of) observed seismicity during actual N_2 injection.

The results of this study suggest a number of possible further steps that could answer issues of both scientific and possibly practical interest:

- By incorporating the alterations suggested for the source model, it would be possible to study reservoir cooling effects as an additional driver of seismicity to the model.
- If the expected reductions in seismicity are judged to be valuable from either societal or economic perspective, the feasibility of the N_2 injection scenario's to minimize seismicity and seismic risk should be investigated in more detail. This would require collecting more detailed information about expected trends and fluctuations in the availability of N_2, and about the potential availability of wells and other infrastructure for transport and injection of N_2.
- Optimization of injection strategies can be done by numerical procedures that take costs and seismic risk into account as objectives (see e.g., Candela et al., 2022). Limitations posed by the available surface infrastructure could be included as constraints. Such an optimization exercise should consider how to adjust injection schemes to both decrease seismicity as rapidly as possible, while also reaching spatial pressure equilibrium within an acceptable timeframe.
- The usefulness of such follow-up activities should be based on an assessment of potential societal benefits, as could be done in a (Societal-)Cost-Benefit-Analysis (MKBA in Dutch).

References

Bommer, J.J., Stafford, P.J., Ruigrok, E., Rodriguez-Marek, A., Mtinalexis, M., Kruiver, P.P., Edwards, B., Dost, B., Van Elk, J. (2022) Ground-motion prediction models for induced earthquakes in the Groningen gas field, the Netherlands. J Seismol 26, 1157–118 https://doi.org/10.1007/s10950-022-10120-w

Bois, A.P., Mohajerani, M., Dousi, N. and Harms, S. (2013). Inducing earthquake by injecting water in a gas field: water-weakening effect. Society of Petroleum Engineers. http://doi.org/10.2118/166430-MS.

Buijze, L., Van Bijsterveldt, L., Cremer, H., Paap, B., Veldkamp, J.G., Wassing, B., Van Wees, J.-D., Van Yperen, G., Ter Heege, J., and Jaarsma, B., (2019). Review of induced seismicity in geothermal systems worldwide and implications for geothermal systems in the Netherlands. Netherlands Journal of Geosciences. 98. http://doi.org/10.1017/njg.2019.6.

Buijze L, Veldkamp H, Wassing B. (2023). Comparison of hydrocarbon and geothermal energy production in the Netherlands: reservoir characteristics, pressure and temperature changes, and implications for fault reactivation. *Netherlands Journal of Geosciences*;102:e7. http://doi.org/10.1017/njg.2023.6

Candela, T., C. Goncalves Machado, O. Leeuwenburgh, J. Ter Heege (2022). A physics-informed optimization workflow to manage injection while constraining induced seismicity: The Oklahoma case, Frontiers in Earth Science, 10:1053951. https://doi.org/10.3389/feart.2022.1053951

Cesca, S., Stich, D., Grigoli, F. *et al.* (2021). Seismicity at the Castor gas reservoir driven by pore pressure diffusion and asperities loading. *Nat Commun* 12, 4783. https://doi.org/10.1038/s41467-021-24949-1.

Cesca, S., Stich, D., Grigoli, F. *et al.* (2022). Reply to: Multiple induced seismicity mechanisms at Castor underground gas storage illustrate the need for thorough monitoring. *Nat Commun* 13, 3445 (2022). https://doi.org/10.1038/s41467-022-30904-5.

Cheng Y., W. Liu, T. Xu, Y. Zhang, X. Zhang, Y. Xing, B. Feng, Y. Xia, (2023). Seismicity induced by geological CO_2 storage: A review,Earth-Science Reviews, Volume 239, https://doi.org/10.1016/j.earscirev.2023.104369.

Commissie Meijdam (2015). Eindadvies Handelingsperspectief voor Groningen

Crowley, H., Pinho, R., Van Elk, J., Uilenreef, J., (2019) Probabilistic damage assessment of buildings due to induced seismicity. Bull. of Earthquake Eng. Volume 17, 4495-4516. https://doi.org/10.1007/s10518-018-0462-1

Davies, R., Foulger, G., Bindley, A., Styles, P. (2013). Induced seismicity and hydraulic fracturing for recovery of hydrocarbons. Mar Pet Geol 45:171–185.

Draganov, D., Naranjo, D., Polychronopoulou, K., and Weemstra, C. (2023). The potential of probabilistic moment-tensor inversions for the characterization of geothermal reservoirs in urban environments, EGU General Assembly 2023, Vienna, Austria, 24–28 Apr 2023, EGU23-14534, https://doi.org/10.5194/egusphere-egu23-14534.

Ellsworth, W. L. (2013). Science 341, 1225942, https://doi.org/10.1126/science.1225942.

Evans, K. F., A. Zappone, T. Kraft, N. Deichmann, F. Moia, (2012). A survey of the induced seismic responses to fluid injection in geothermal and CO_2 reservoirs in Europe. Geothermics 41, 30–54, https://doi.org/10.1016/j.geothermics.2011.08.002.

Foulger, G.R., Wilson, M.P., Gluyas, J.G., Julian, B.R., Davies, R.J. (2018). Global review of human-induced earthquakes. Earth Sci Rev. https://doi.org/10.1016/j.earscirev.2017.07.008.

Fugro (2022a). Effect of pressure maintenance by fluid injection on seismic risk (KEM24/IUC202003010) Umbrella Report A | 1020-169309.R01 01 | 30 September 2022.

Fugro (2022b). Effect of pressure maintenance by fluid injection on seismic hazard, Hazard analysis Report | KEM-24 Report C 172147-REP01-FNV_SHA_KEM24 03, September 2022.

Gasunie (1980). Physical properties of natural gas, NV Nederlandse Gasunie.

Grigoli, F. et al. (2017). Current challenges in monitoring, discrimination, and management of induced seismicity related to underground industrial activities: a European perspective. *Rev. Geophysics* 55, 310–340.

KEM (2022). KEM-24 Research review, evaluation and interpretation of "Effect of pressure maintenance by fluid injection on seismic risk".

KEM-19 (2022). KEM-19 Evaluation of post-abandonment fluid migration and ground motion risks in subsurface exploitation operations in the Netherlands – Phase 1, 1 July, 2022.

Kivi, I. R., Boyet, A., Wu, H., Walter, L., Hanson-Hedgecock, S., Parisio, F., and Vilarrasa, V. (2023). Global physics-based database of injection-induced seismicity, Earth Syst. Sci. Data, 15, 3163–3182, https://doi.org/10.5194/essd-15-3163-2023.

Mandal, R., Lui, S.K.Y. (2022). Interdependent effects of fluid injection parameters on triggered aseismic slip and seismicity. *Sci Rep* 12, 20922. https://doi.org/10.1038/s41598-022-25239-6

McGarr, A. (2014). Maximum magnitude earthquakes induced by fluid injection. J Geophys Res Solid Earth 119:1008–1019. https://doi.org/10.1002/2013JB010597.

Mijnlieff, H.F (2020). Introduction to the geothermal play and reservoir geology of the Netherlands. *Netherlands Journal of Geosciences*. 2020;99:e2. http://doi.org/10.1017/njg.2020.2.

Muntendam-Bos A.G., Hoedeman G., Polychronopoulou K., Draganov D., Weemstra C., van der Zee W., Bakker R.R., and Roest H. (2022). An overview of induced seismicity in the Netherlands. Netherlands Journal of Geosciences, Volume 101, e1. https://doi.org/10.1017/njg.2021.14

NAM (2016). Groningen Pressure Maintenance (GPM) study – Progress report, February 2016.

NAM (2020). Seismic Hazard and Risk Assessment Groningen Field update for Production Profile GTS – raming 2020 March 2020, EP202003201727

NAM (2023a). Seismic threat assessment for Schoonebeek-Zechstein water injection. Report: EP202304200850, April 2023.

NAM (2023b). Groningen Dynamic Model update 2023. Report: EP202306200914.

Rubinstein, J.L. and Mahani, A.B. (2015). Myths and Facts on wastewater injection, hydraulic fracturing, enhanced oil recovery, and induced seismicity. Seismol Res Lett 86(4):1060–1067

Shapiro, S. A. and Dinske, C., 2009. Fluid-induced seismicity: pressure diffusion and hydraulic fracturing. Geophysical Prospecting 57: 301–310. https://doi.org/10.1111/j.1365-2478.2008.00770.x.

SodM (2023). Risico's voor mens en milieu door afvalstromen rondom injectielocatie Borgsweer, 30 mei 2023.

Suckale J. (2009). Induced seismicity in hydrocarbon fields. Adv Geophys 51:55–106.

TNO (2014). Literature review on injection-related induced seismicity and its relevance to nitrogen injection. TNO project report 2014 R11761, December 2014.

TNO (2015a). Injection-Related Induced Seismicity and its relevance to Nitrogen Injection: Description of Dutch field cases. TNO report 2015 R10906, November 2015.

TNO (2015b). Injection Related Induced Seismicity and its relevance to Nitrogen Injection: Modeling of geomechanical effects of injection on fault stability. TNO report 2015 R11259, November 2015.

TNO (2015c). Injection Related Induced Seismicity and its relevance to Nitrogen Injection: Main findings, recommendations and general guidelines. TNO report R11648, December 2015.

TNO (2022) Probabilistic Seismic Hazard and Risk Analysis in the TNO Model Chain Groningen. TNO 2022 R11052.

TNO (2023). [in Dutch] Publieke Seismische Dreigings- en Risicoanalyse Groningen gasveld 2023. TNO 2023 R10682.

TNO (2023b): https://github.com/TNO/SHRA-Groningen-seismic-source-model

TNO (2023c): https://github.com/TNO/SHRA-Groningen-hazard-risk-models

Vilarrasa, V., De Simone, S., Carrera, J. & Villaseñor, A. (2022). Multiple induced seismicity mechanisms at Castor underground gas storage illustrate the need for thorough monitoring. *Nat. Commun.*, https://doi.org/10.1038/s41467-022-30903-6.

Vörös R, Baisch S. (2022). Induced seismicity and seismic risk management – a showcase from the Californië geothermal field (the Netherlands). *Netherlands Journal of Geosciences*. 2022;101:e15. doi:10.1017/njg.2022.12

Warpinski, N.R., Du, J., Zimmer, U. (2012). Measurements of hydraulic-fracture-induced seismicity in gas shales. SPE Prod Oper 27:240–252.

Zang, A., Oye, V., Jousset, P., Deichmann, N., Gritto, R., McGarr, A., Majer, E., Bruhn D. (2014). Analysis of induced seismicity in geothermal reservoirs—an overview. Anal Induc Seism Geotherm Oper 52:6–21. https://doi.org/10.1016/j.geothermics.2014.06.005.996.

Zang, A., Zimmermann, G., Hofmann, H. *et al.* (2019). How to Reduce Fluid-Injection-Induced Seismicity. *Rock Mech Rock Eng* **52**, 475–493. https://doi.org/10.1007/s00603-018-1467-4.

Appendix A: Seismic hazard and risk assessment figures

Here we provide all figures related to the seismic hazard and risk assessment performed for all scenarios.
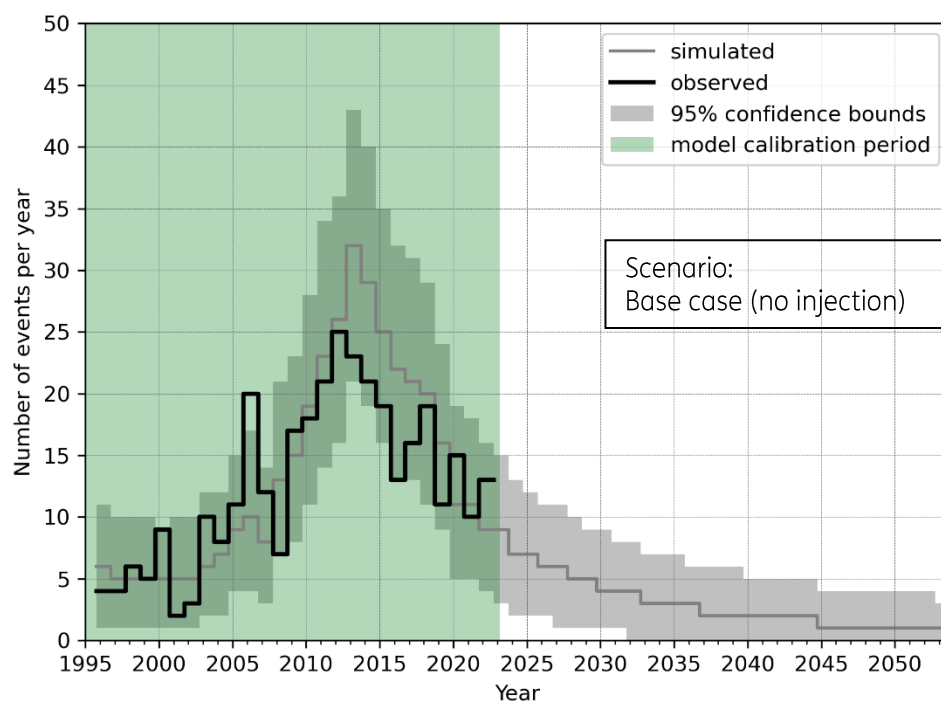
Figure 28: Number of events per year in the Groningen field of M1.5 and above. Base case (no N_2 injection). The solid grey line is the modelled expected number of events, the grey area gives the 95% confidence bounds per year. The solid black line is the data and the green area is the period over which the model is calibrated.
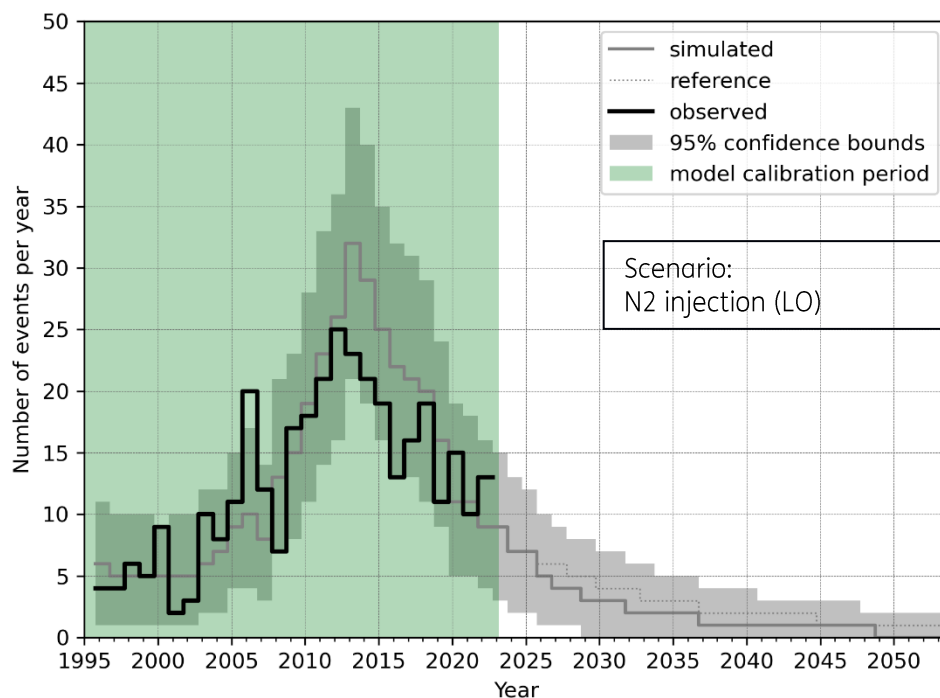
Figure 29: As Figure 28, except for the LO scenario. The dotted reference line represents the base case for comparison.
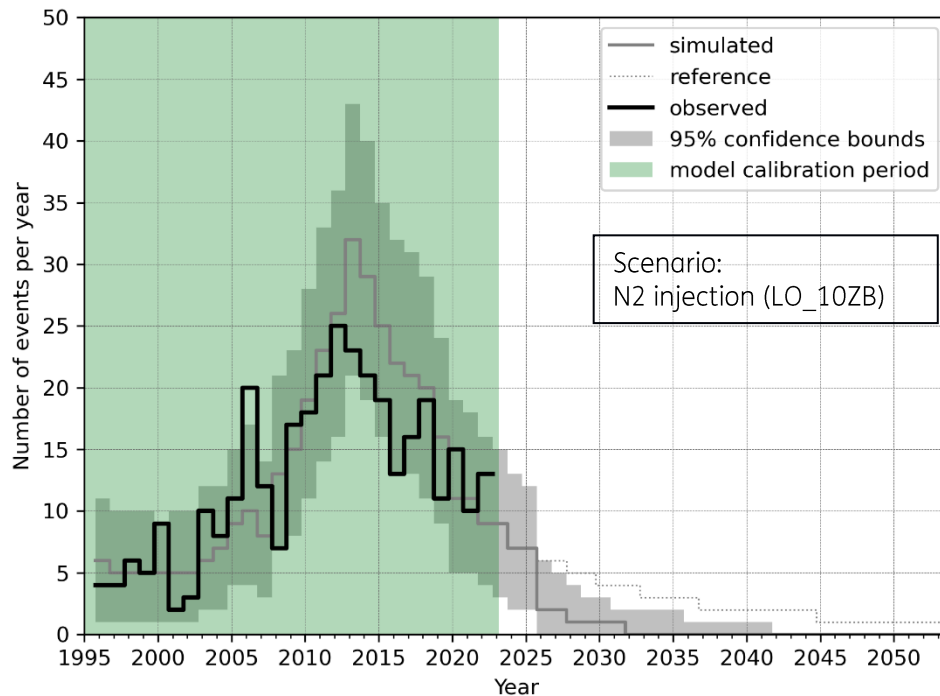
Figure 30: As Figure 28, except for the LO_10ZB scenario. The dotted reference line represents the base case for comparison.
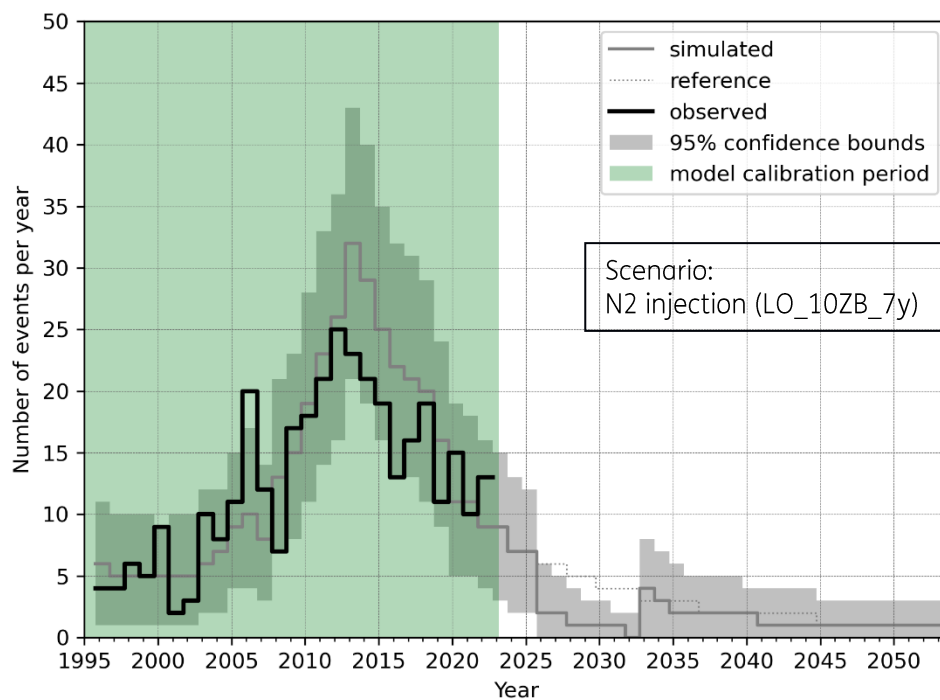
Figure 31: As Figure 28, except for the LO_10ZB_7y scenario. The dotted reference line represents the base case for comparison.
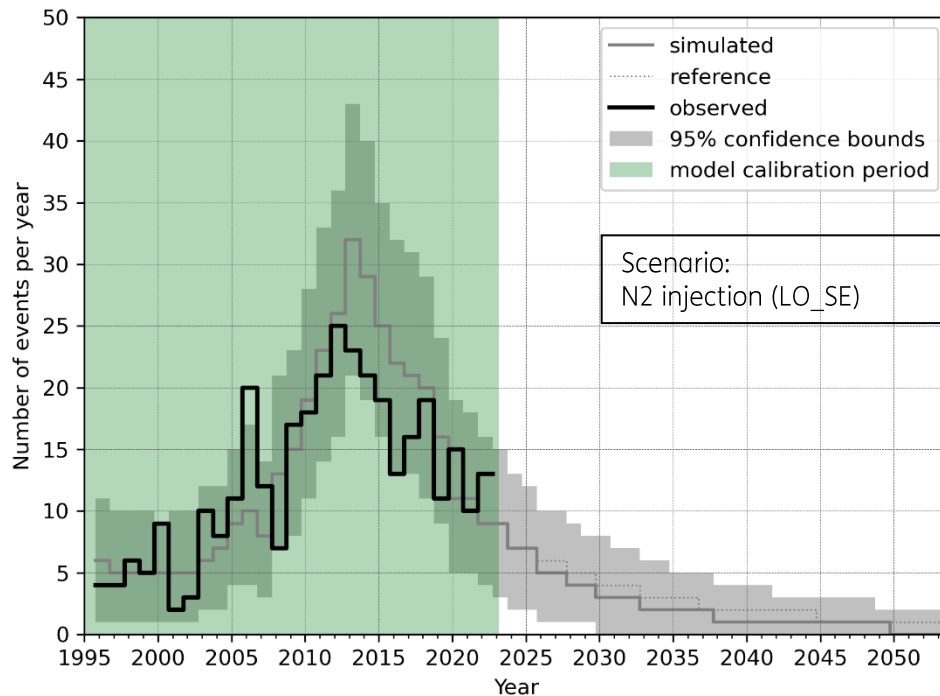
Figure 32: As Figure 28, except for the LO_SE scenario. The dotted reference line represents the base case for comparison.
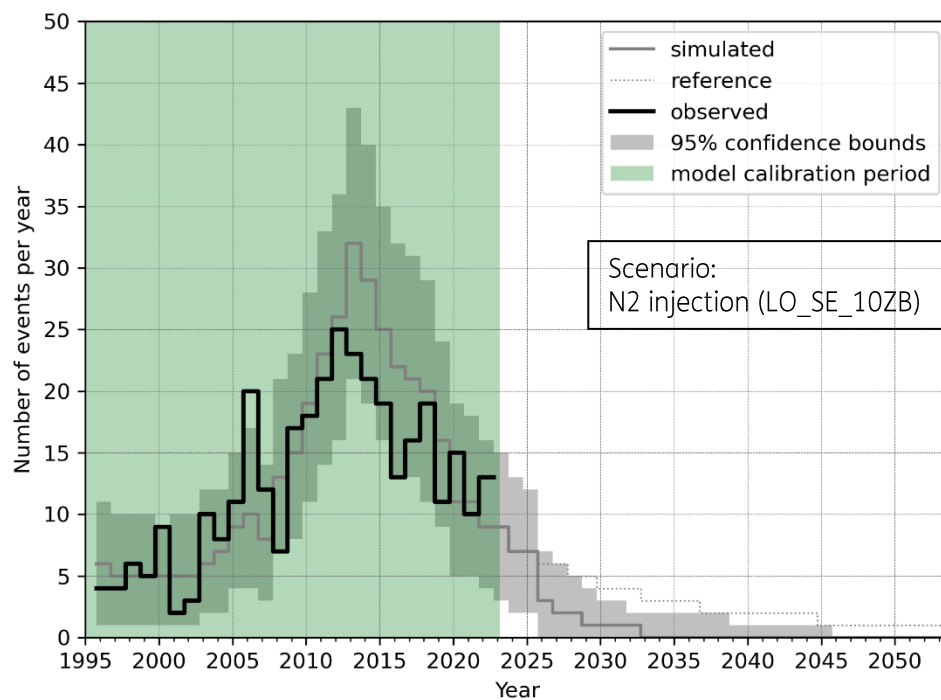
Figure 33: As Figure 28, except for the LO_SE_10ZB scenario. The dotted reference line represents the base case for comparison.
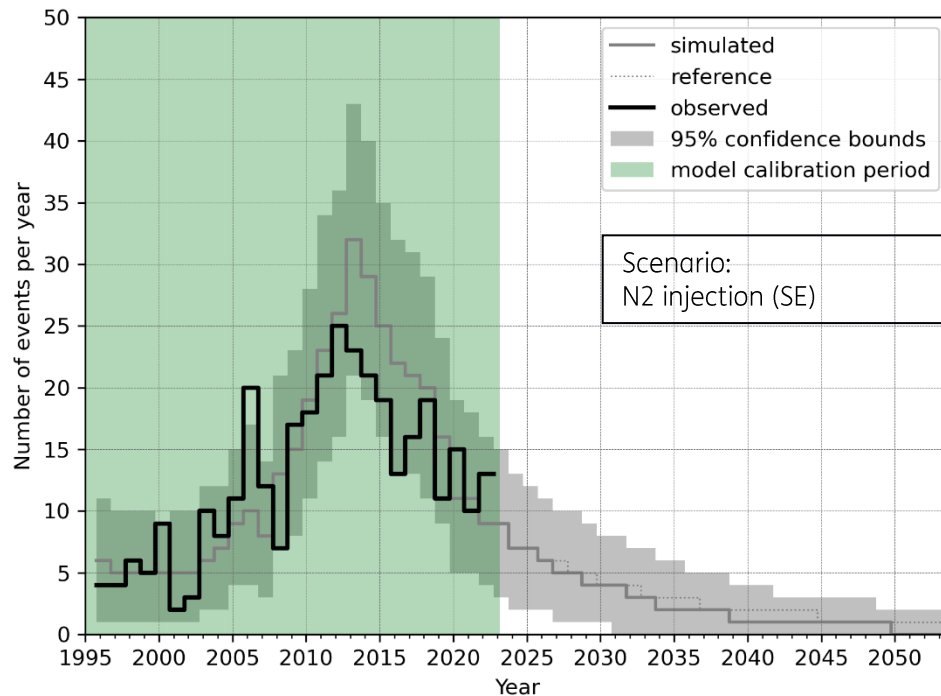
Figure 34: As Figure 28, except for the SE scenario. The dotted reference line represents the base case for comparison.
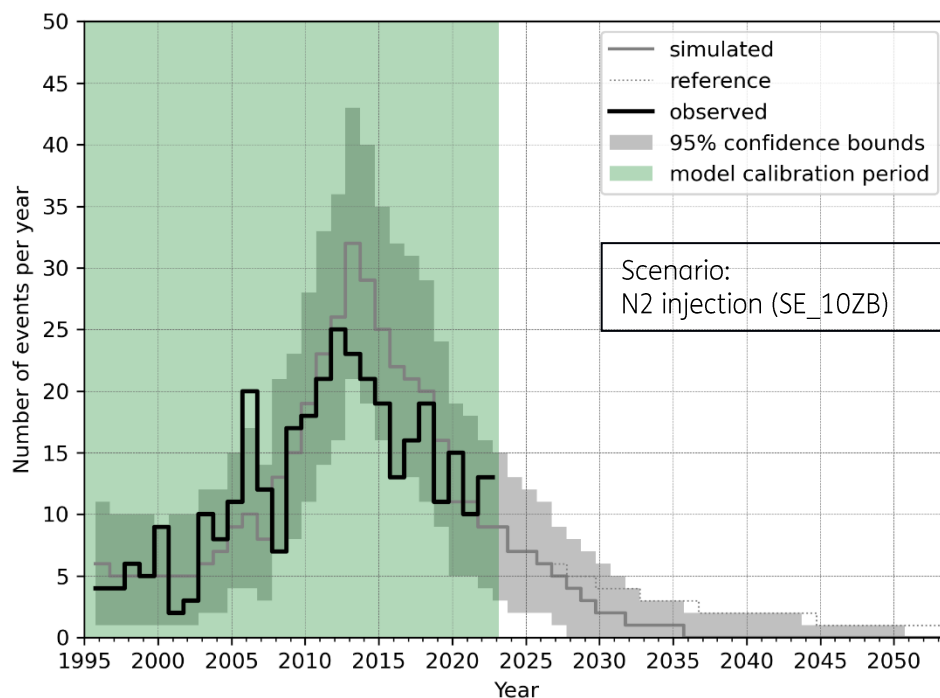
Figure 35: As Figure 28, except for the SE_10ZB scenario. The dotted reference line represents the base case for comparison.
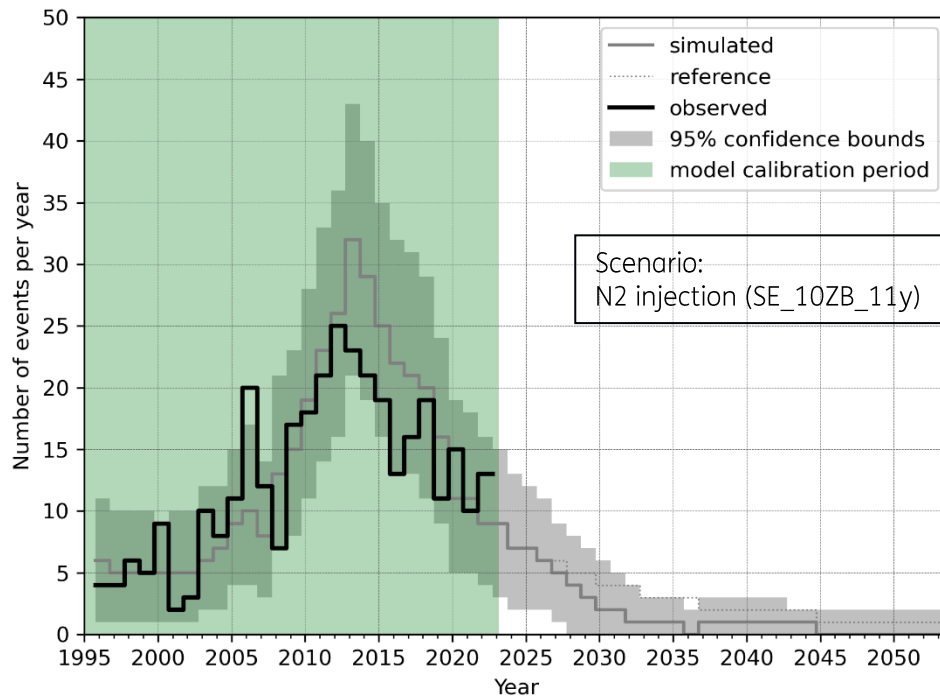
Figure 36: As Figure 28, except for the SE_10ZB_11y scenario. The dotted reference line represents the base case for comparison.
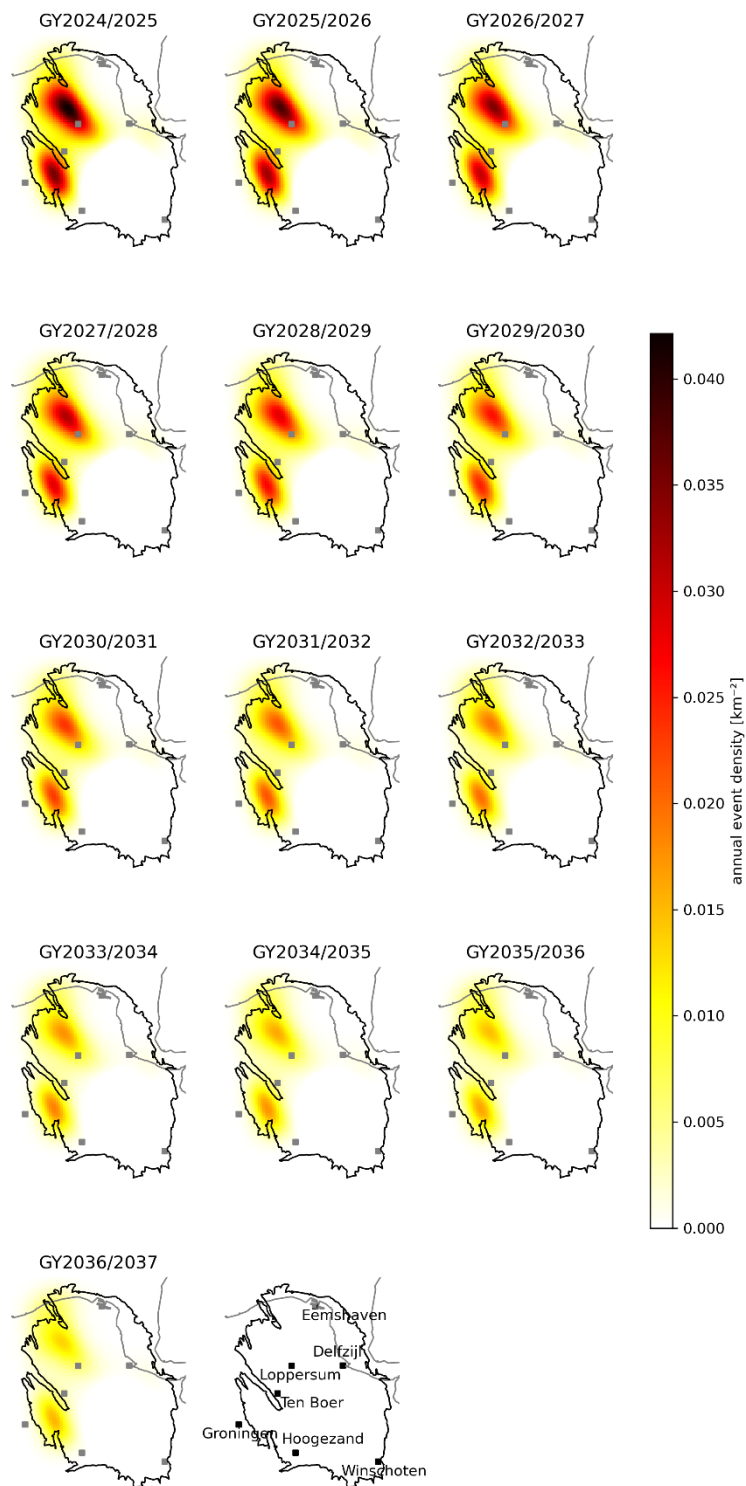
Figure 37: Annual spatial distribution of the seismicity for GY2024/2025 until GY2036/2037. The colour represents the annual expected number of events per square kilometre. Base case (no N_2 injection).
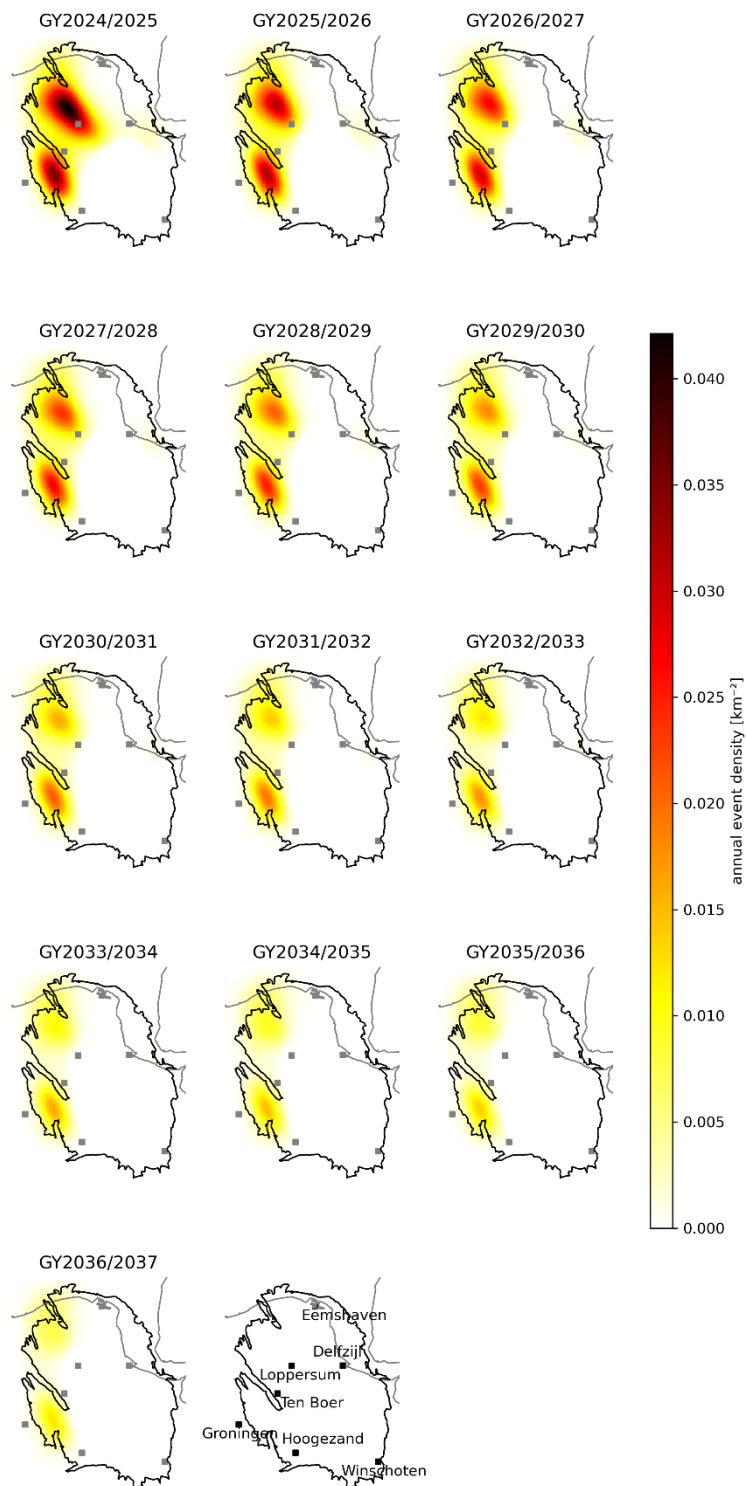
Figure 38: As Figure 37, except for the LO scenario
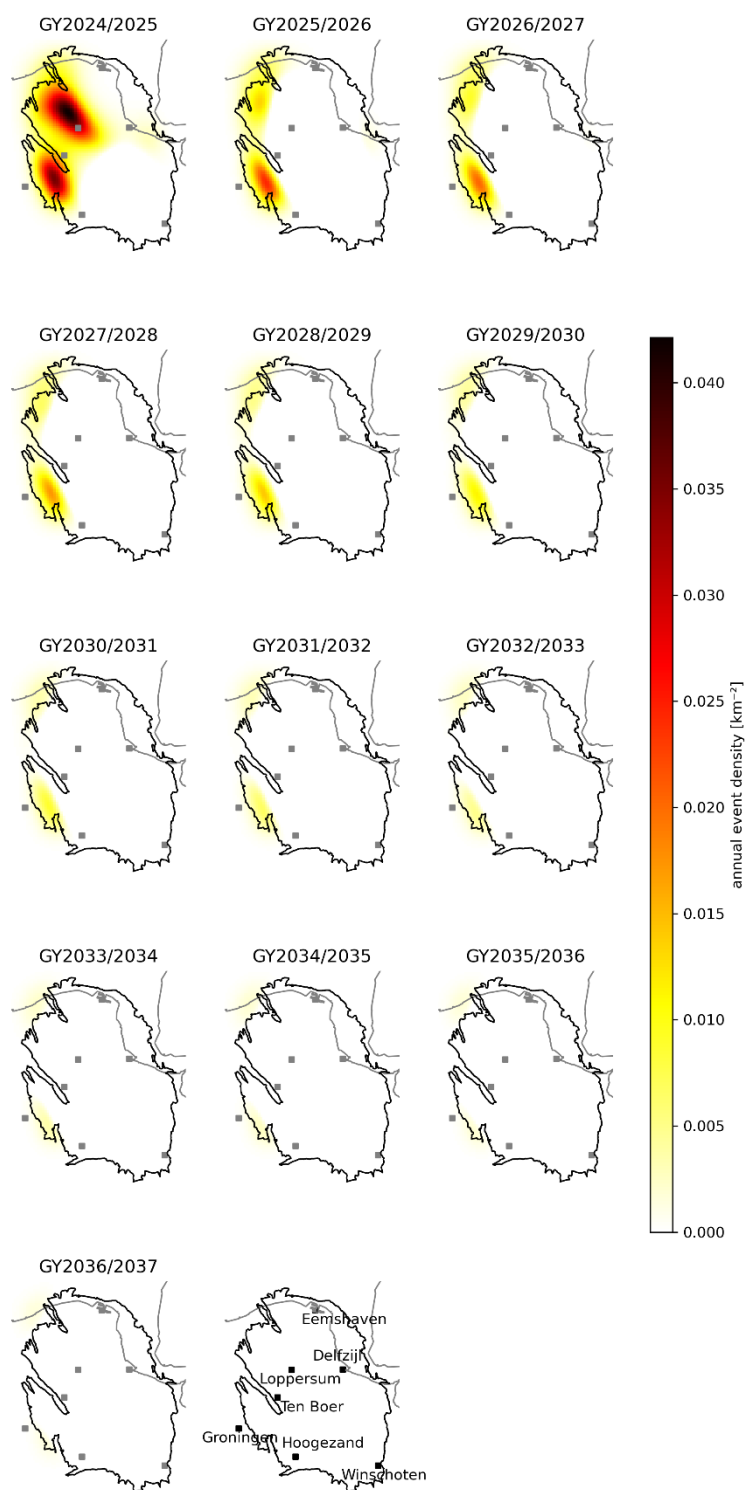
Figure 39: As Figure 37, except for the LO_10ZB scenario
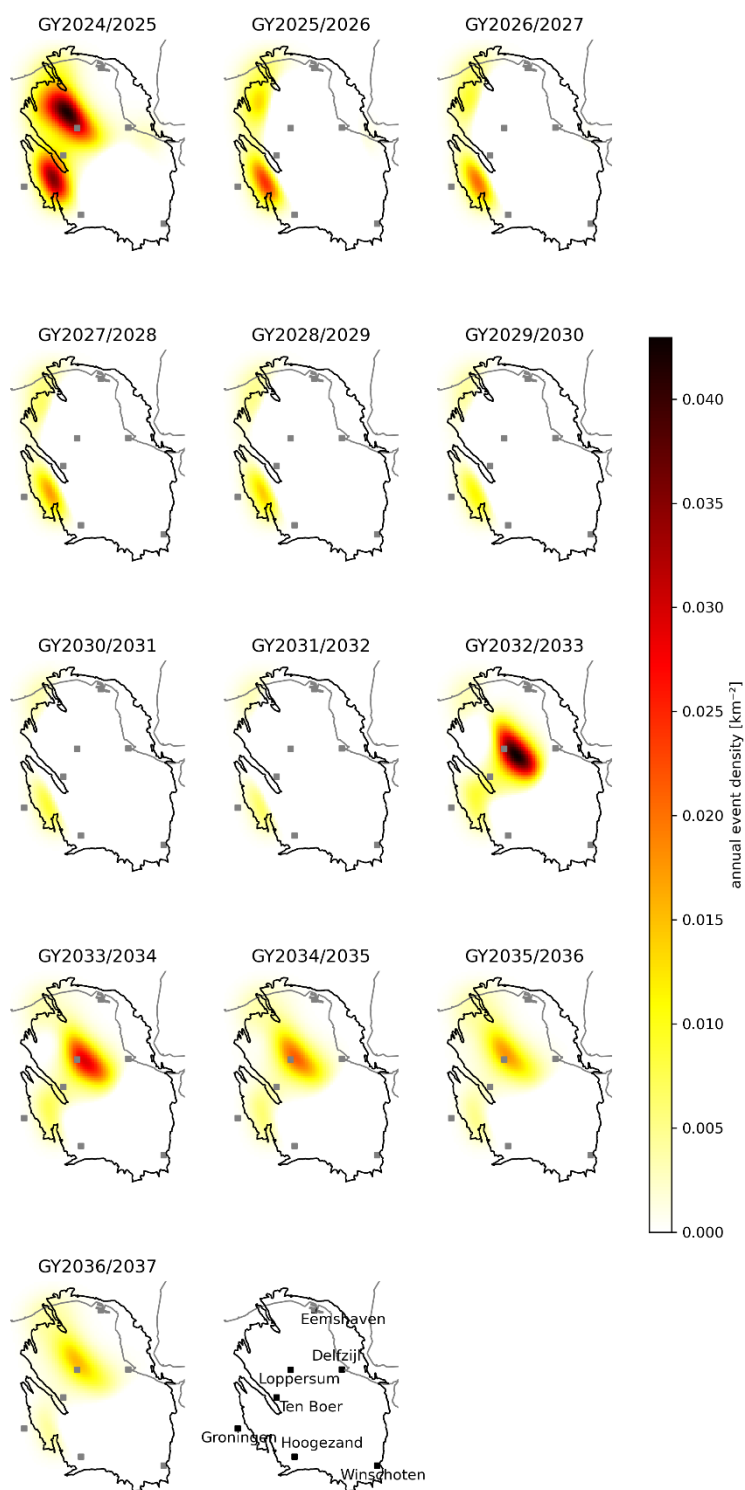
Figure 40: As Figure 37, except for the LO_10ZB_7y scenario
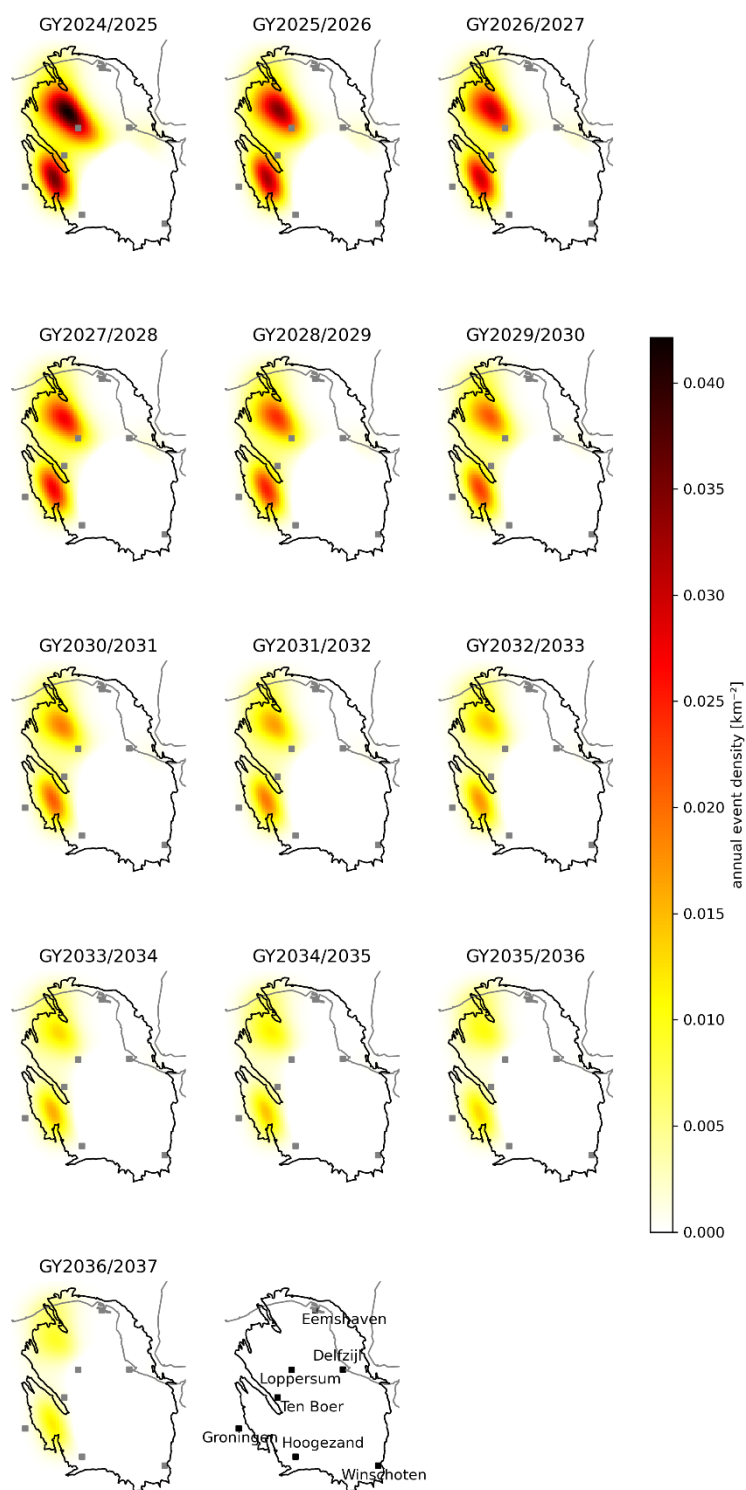
Figure 41: As Figure 37, except for the LO_SE scenario
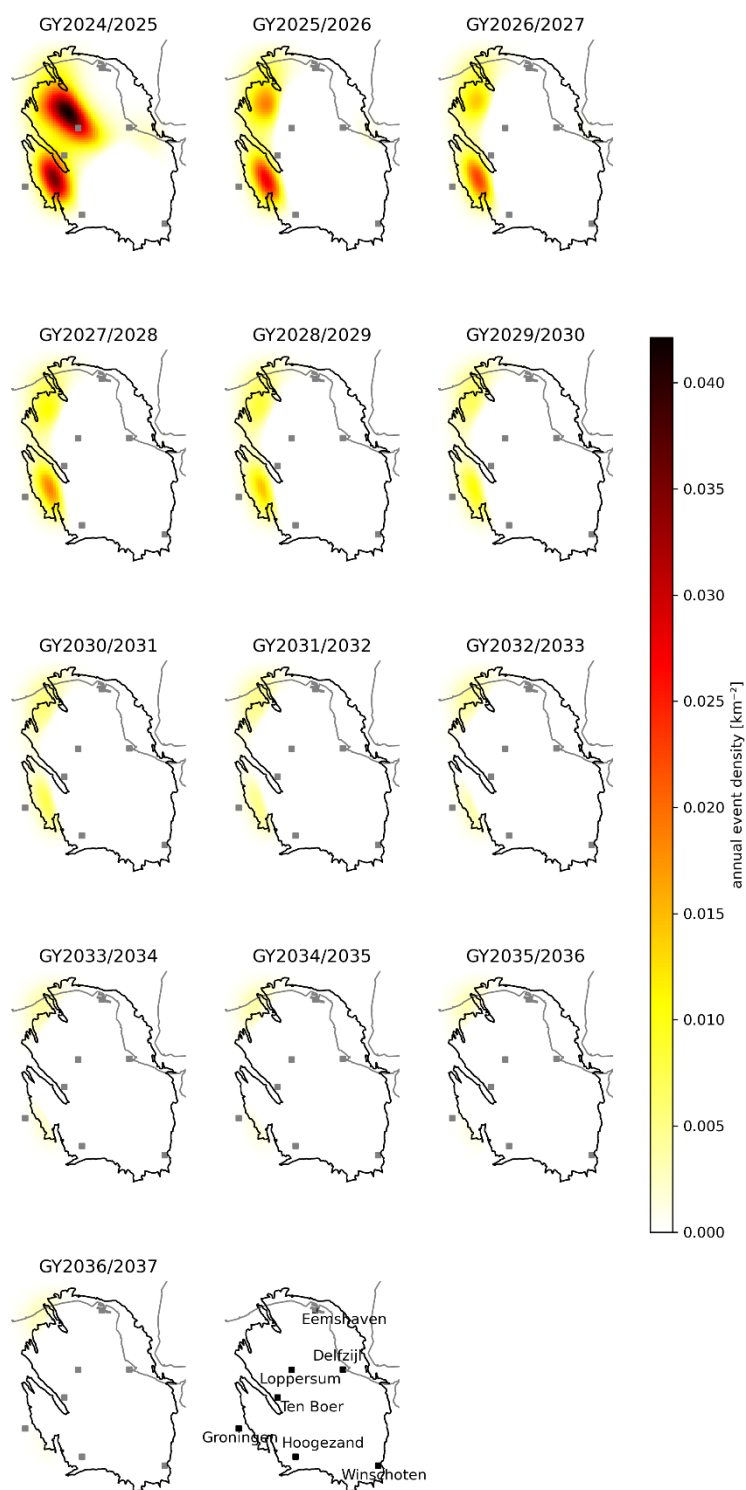
Figure 42: As Figure 37, except for the LO_SE_10ZB scenario
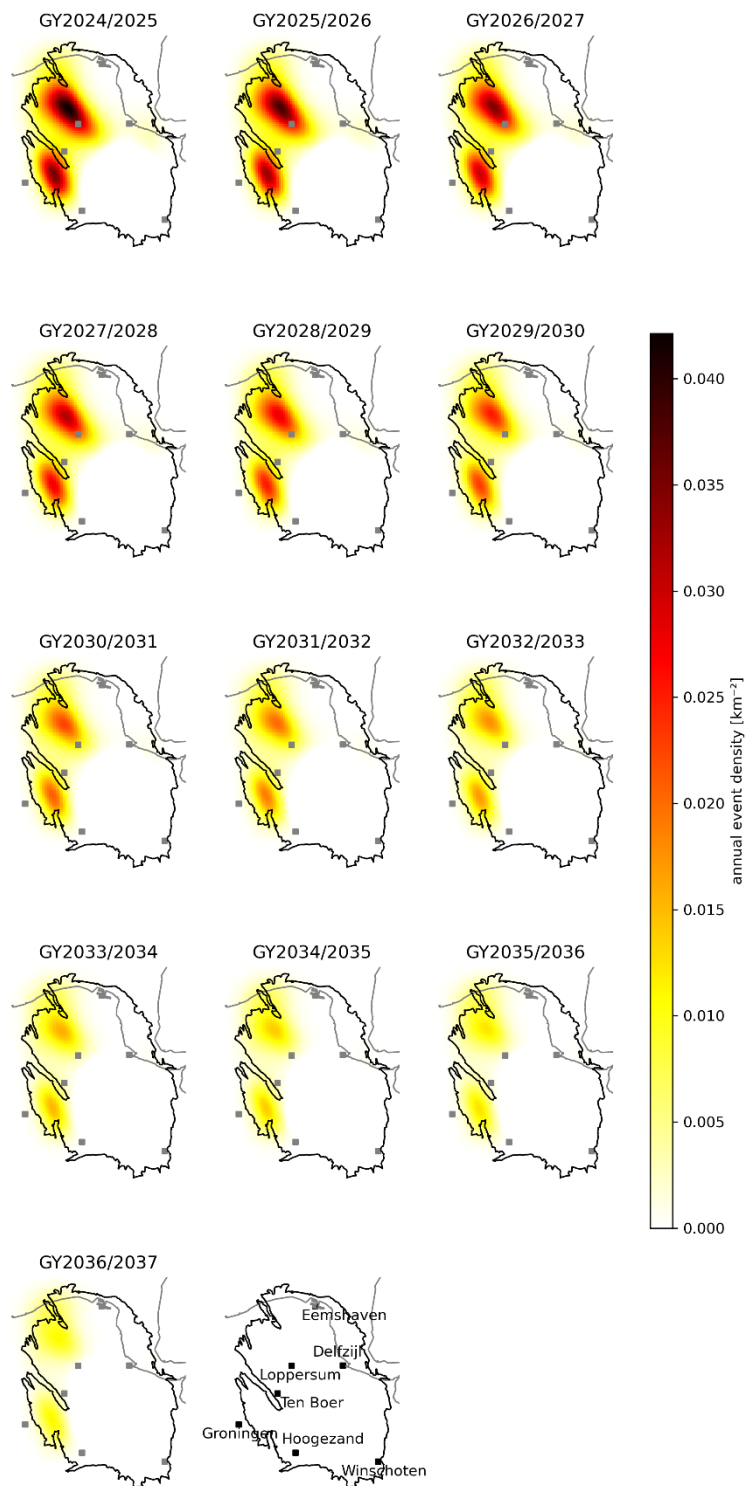
Figure 43: As Figure 37, except for the SE scenario
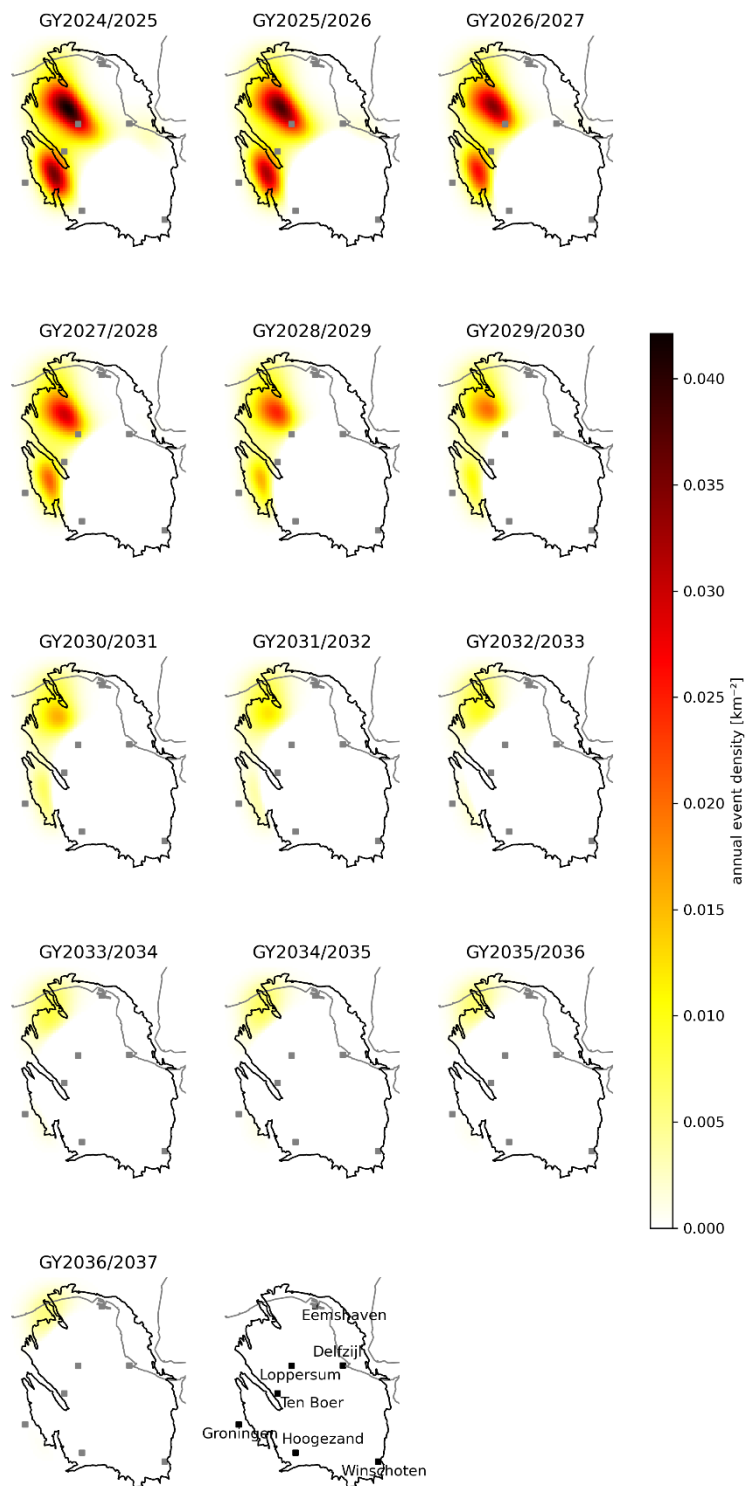
Figure 44: As Figure 37, except for the SE_10ZB scenario
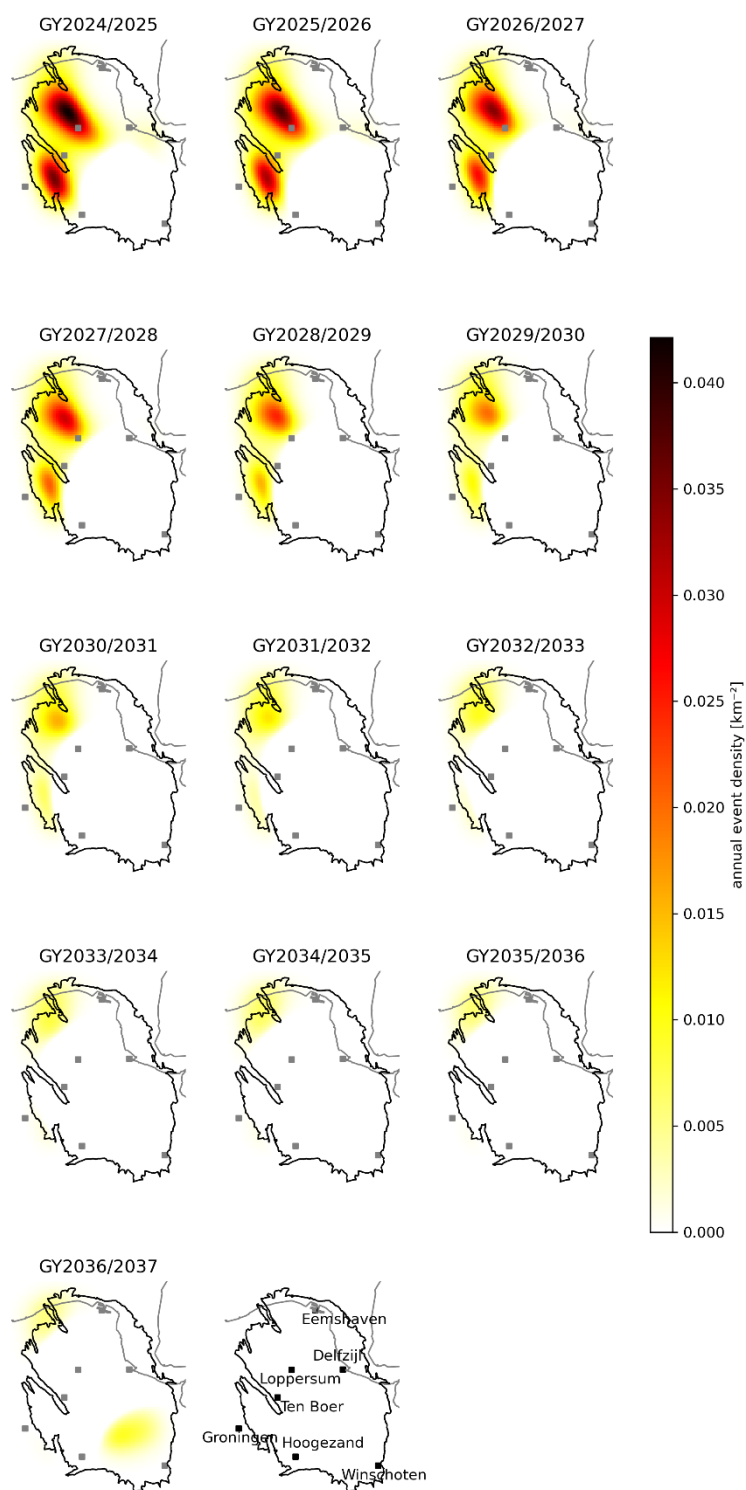
Figure 45: As Figure 37, except for the SE_10ZB_11y scenario

Sa[0.01] return period: 475 years
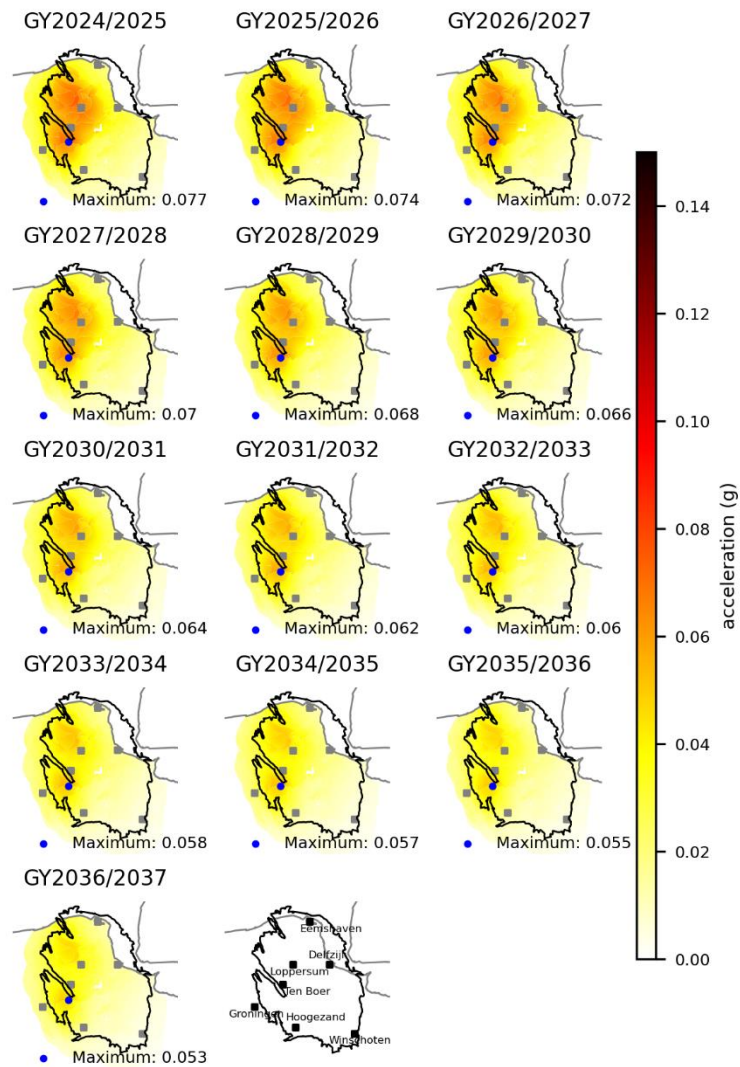
Figure 46: Peak Ground Acceleration (pseudo-spectral acceleration at 0.01 s) hazard map for a 475 return period (10% probability of exceedance in 50 years). The blue dot indicates the position of the largest hazard for each year. Base case (no N_2 injection).
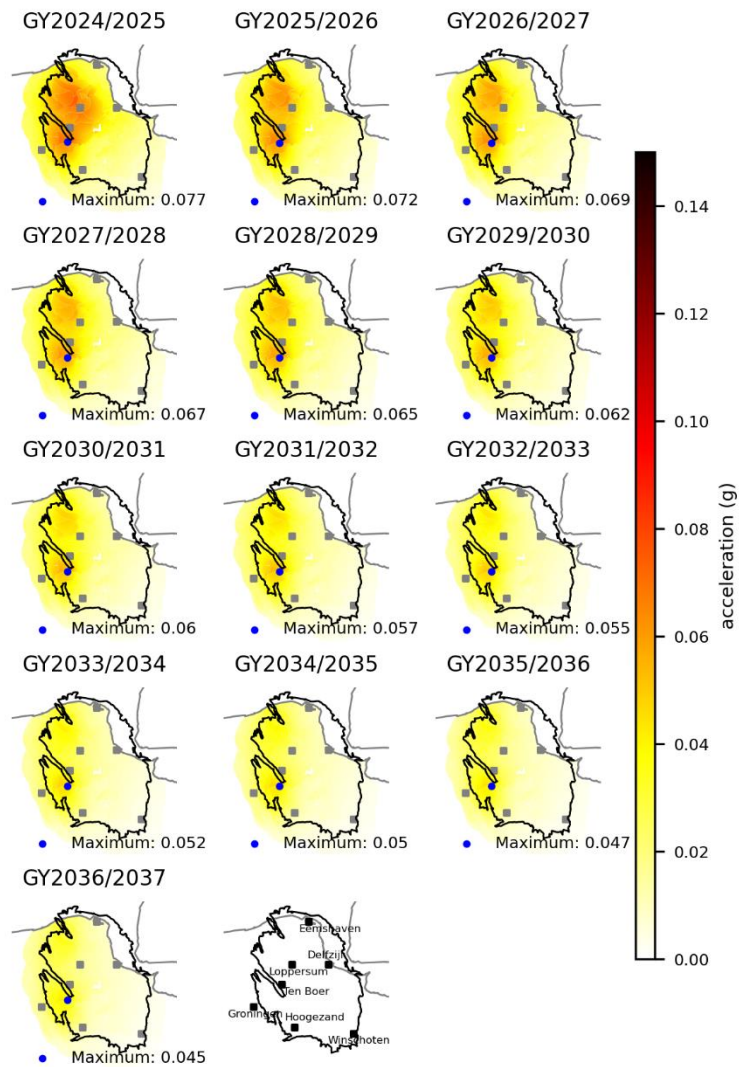
Figure 47: As Figure 46, except for the LO scenario
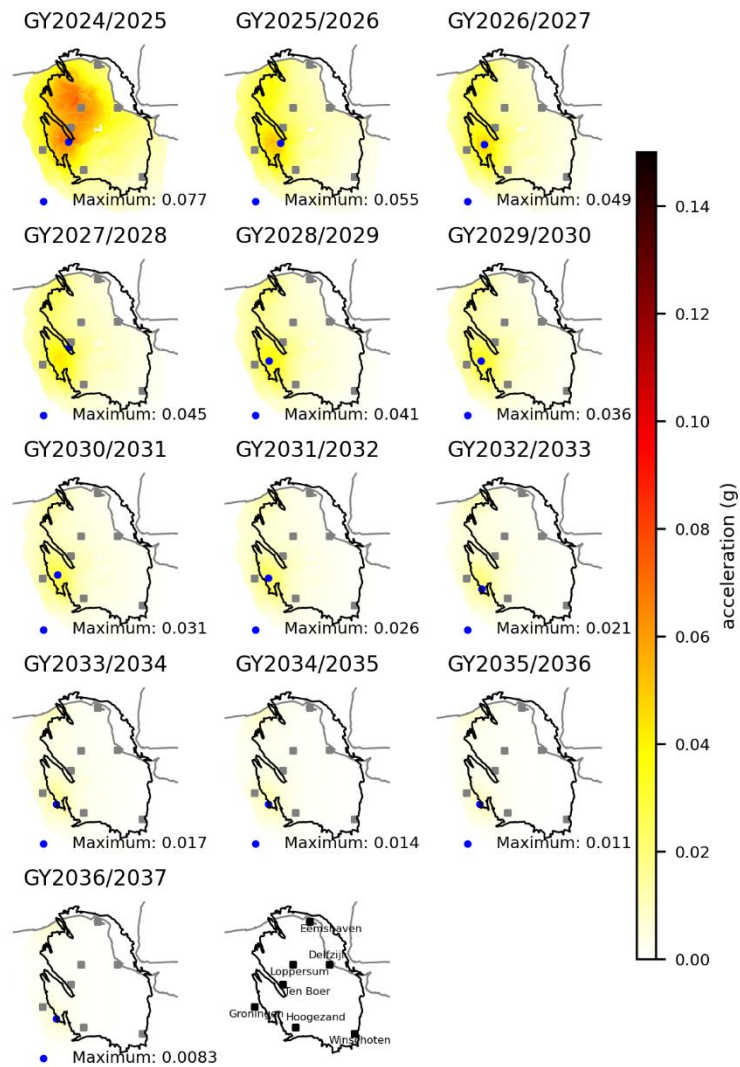
Figure 48: As Figure 46, except for the LO_10ZB scenario
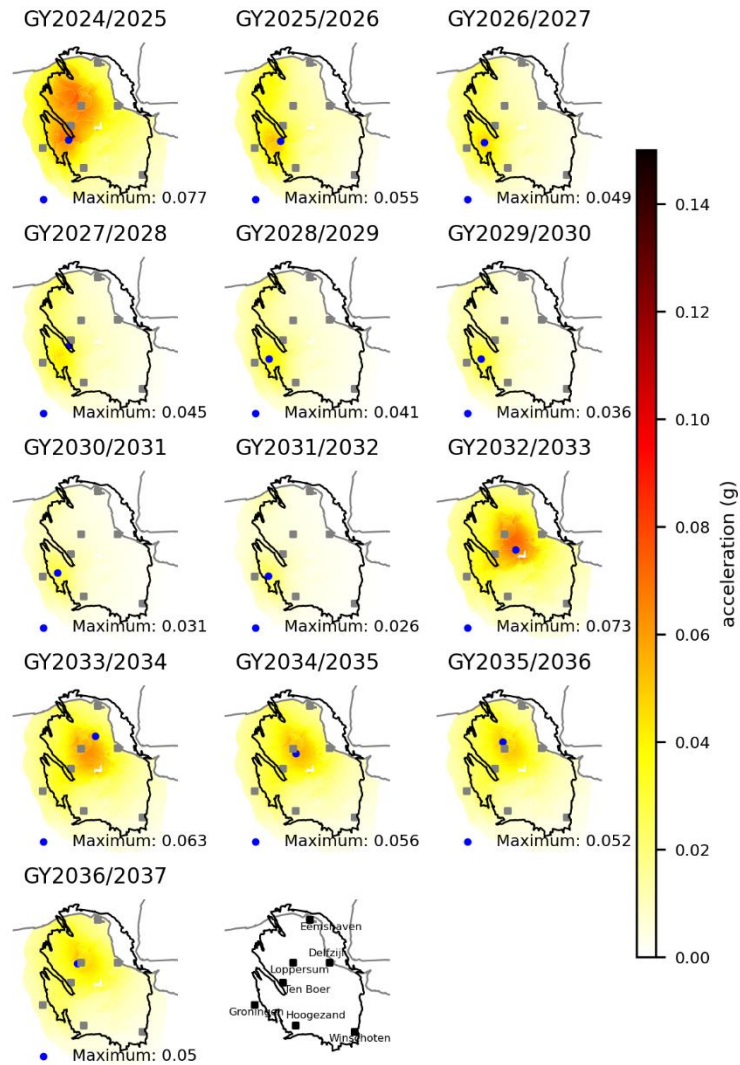
Figure 49: As Figure 46, except for the LO_10ZB_7y scenario

Sa[0.01] return period: 475 years
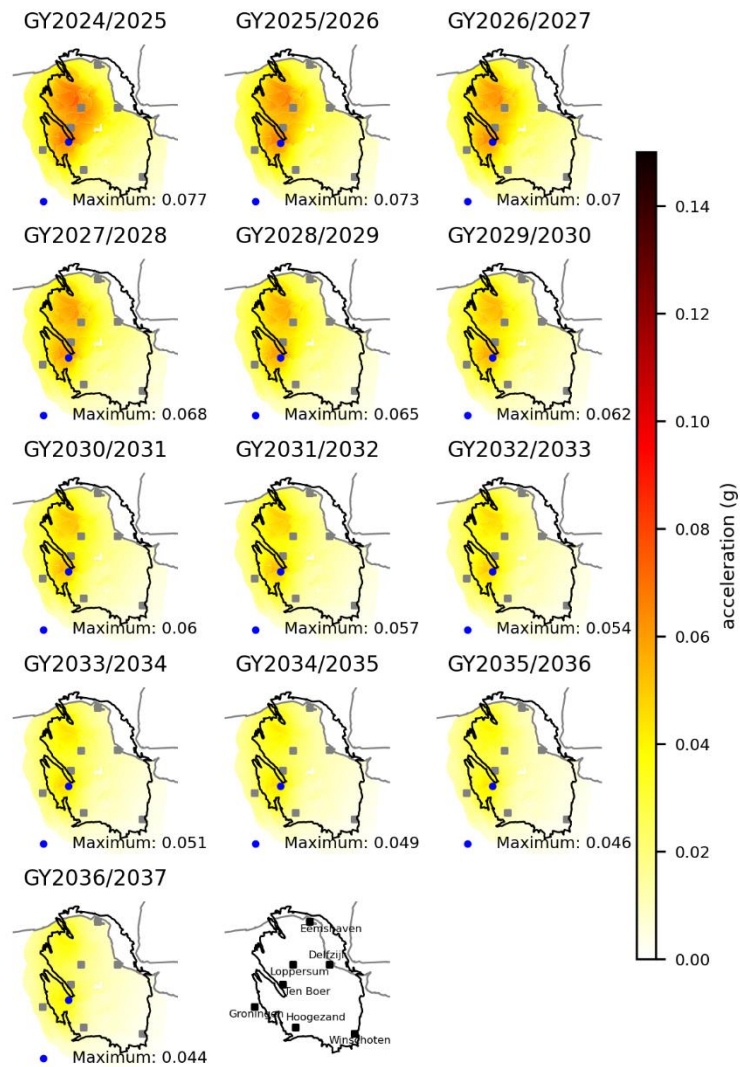
Figure 50: As Figure 46, except for the LO_SE scenario
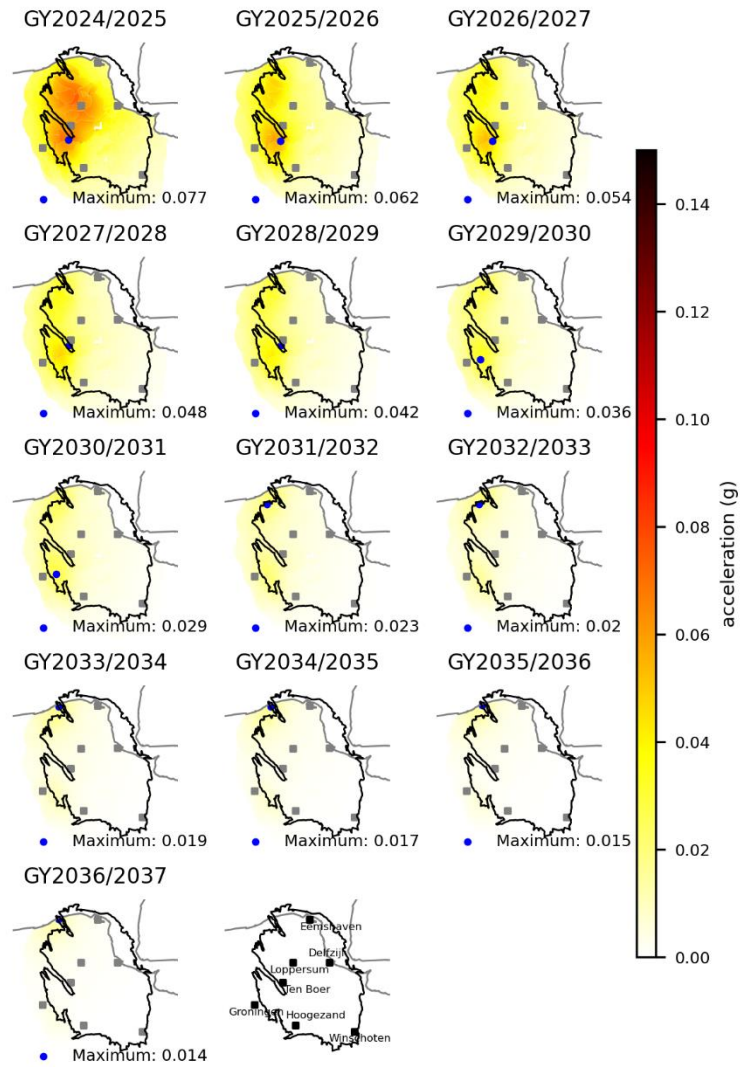
Figure 51: As Figure 46, except for the LO_SE_10ZB scenario
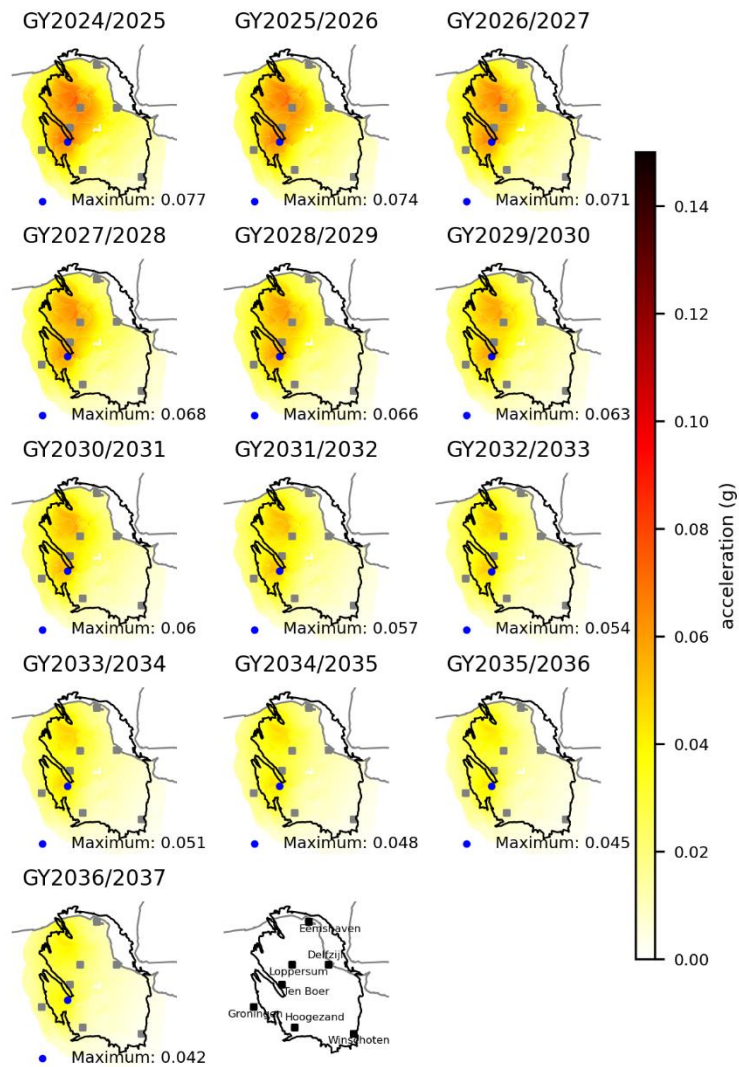
Figure 52: As Figure 46, except for the SE scenario
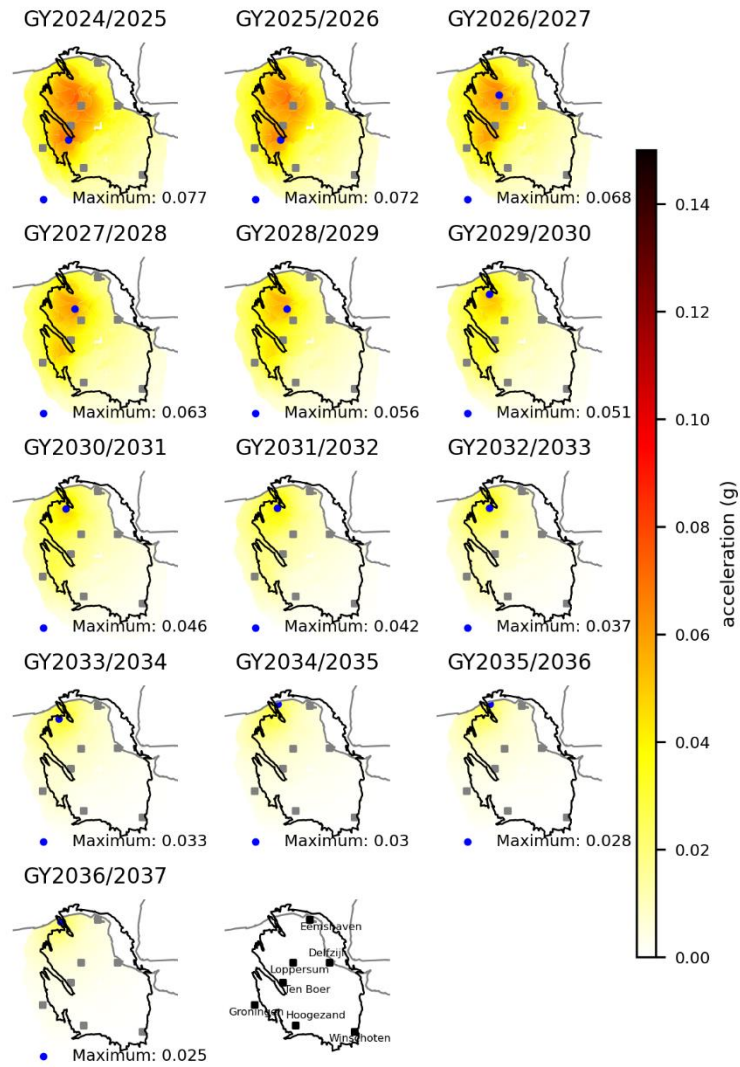
Figure 53: As Figure 46, except for the SE_10ZB scenario
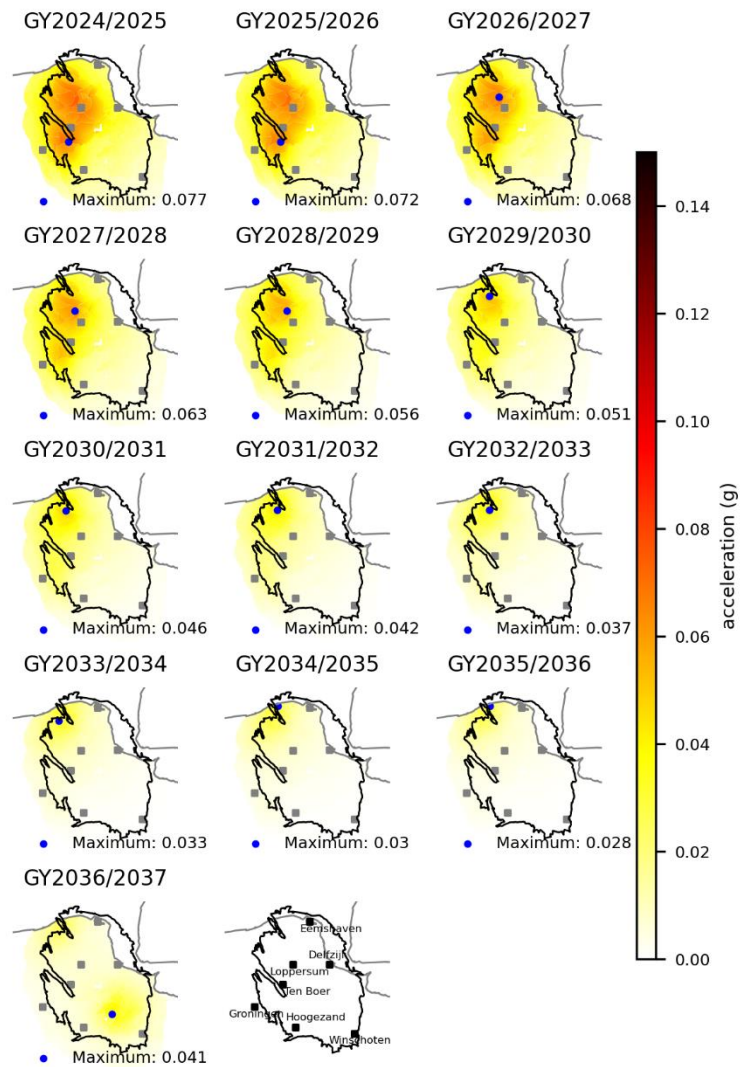
Figure 54: As Figure 46, except for the SE_10ZB_11y scenario
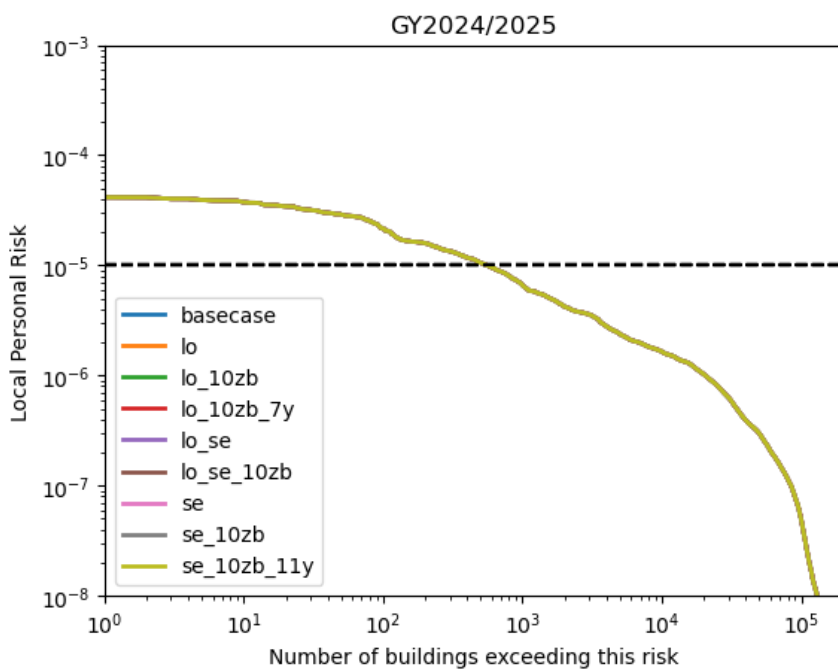
Figure 55: Risk exposure plot. Shows how many buildings (on the x-axis) are exposed to a given local personal risk (y-axis). Shows all scenarios considered for GY 2024/2025. Since N_2 injection starts on the 1st of October 2025 in all scenarios (1st day of gas year 2025/2026), the risk exposure is identical for all scenarios. Approximately 500 buildings exceed the Meijdam norm ($10^{-5}\,y^{-1}$) for all scenarios.
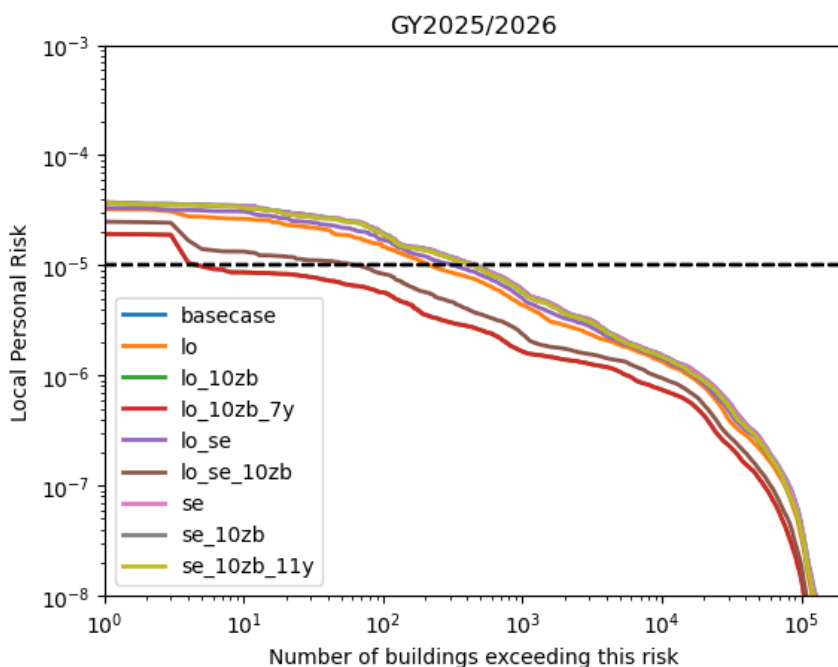
Figure 56: Risk exposure plot for GY 2025/2026. The risk profile decreases compared to previous year for all scenarios (including the base case), but with different amounts. For the scenarios where 10x the Zuidbroek II capacity of N_2 production is injected in the clusters around Loppersum, the number of buildings not conforming to the safety norm goes down to 3 buildings.
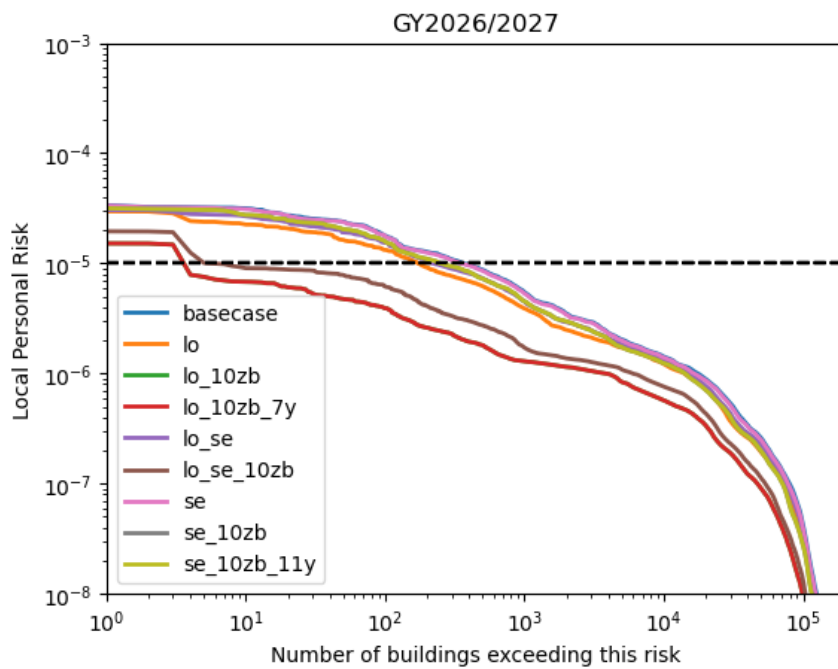
Figure 57: Risk exposure plot for GY 2026/2027. The risk profile decreases compared to last year for all scenarios (including the base case), but with different amounts.
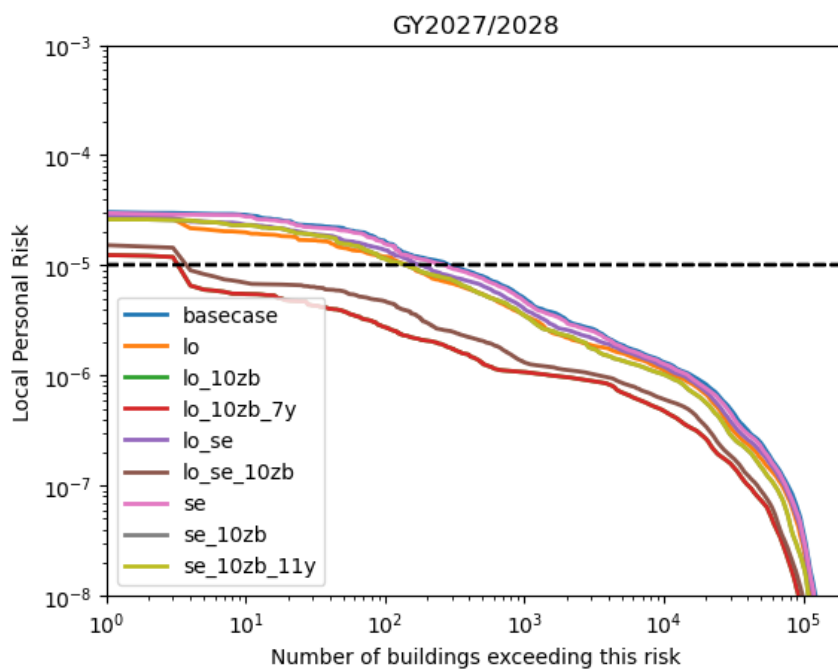

Figure 58: Risk exposure plot for GY 2027/2028. The risk profile decreases compared to last year for all scenarios (including the base case), but with different amounts.
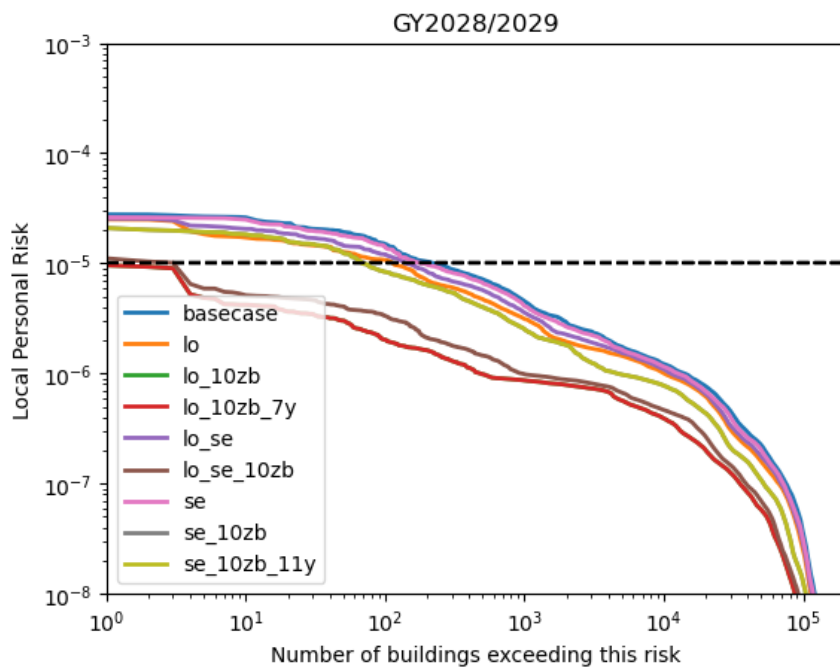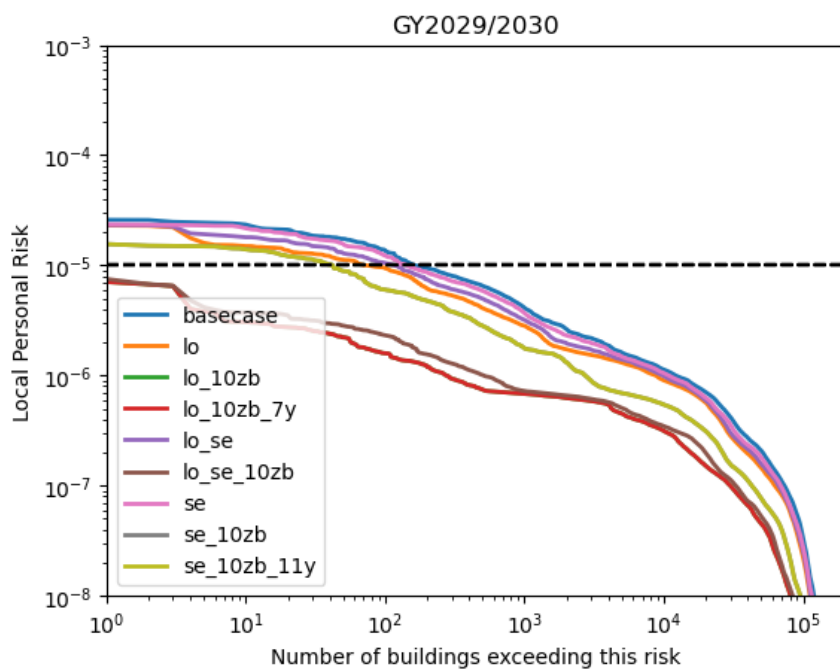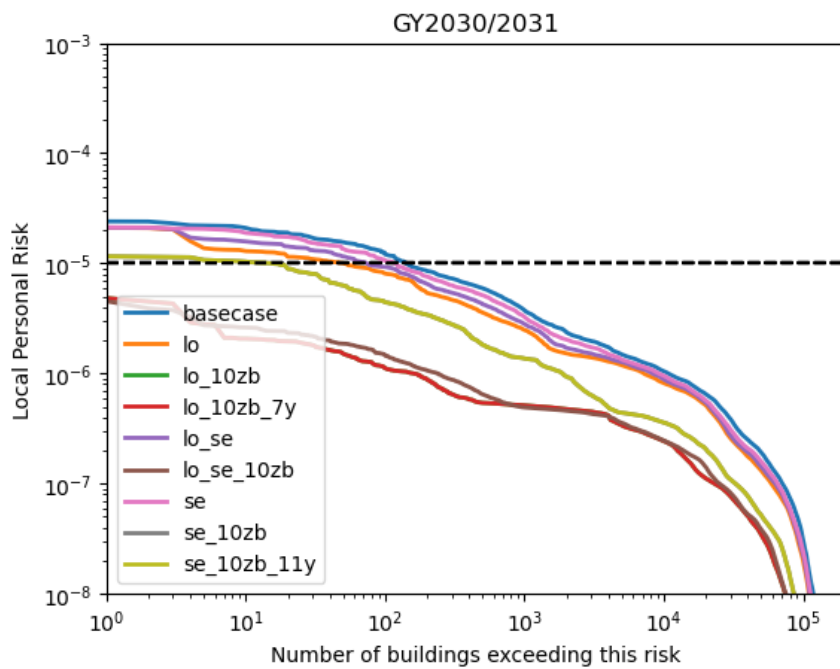
Figure 59: Risk exposure plot for GY 2028/2029. The risk profile decreases compared to last year for all scenarios (including the base case), but with different amounts.

Figure 60: Risk exposure plot for GY 2029/2030. The risk profile decreases compared to last year for all scenarios (including the base case), but with different amounts.

Figure 61: Risk exposure plot for GY 2030/2031. The risk profile decreases compared to last year for all scenarios (including the base case), but with different amounts.
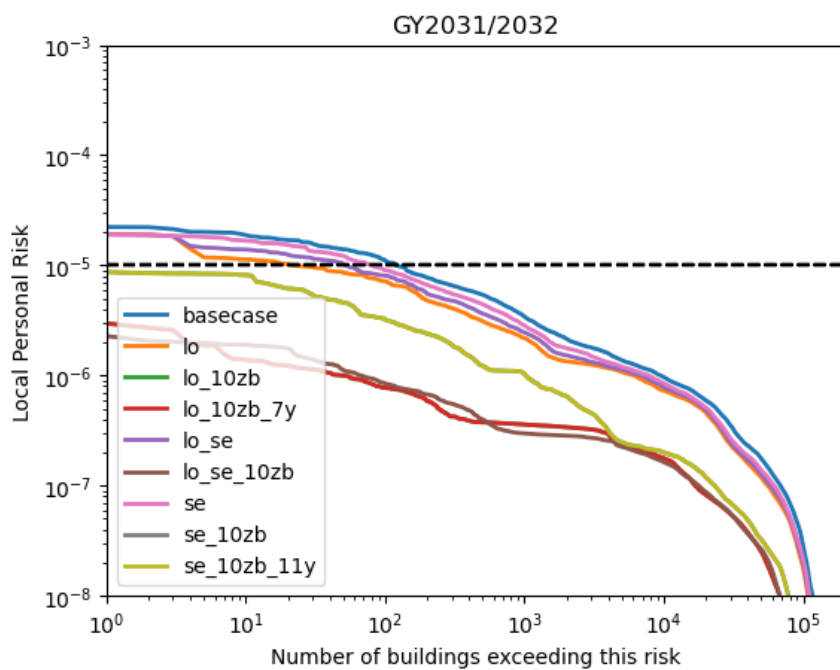

Figure 62: Risk exposure plot for GY 2031/2032. The risk profile decreases compared to last year for all scenarios (including the base case), but with different amounts.
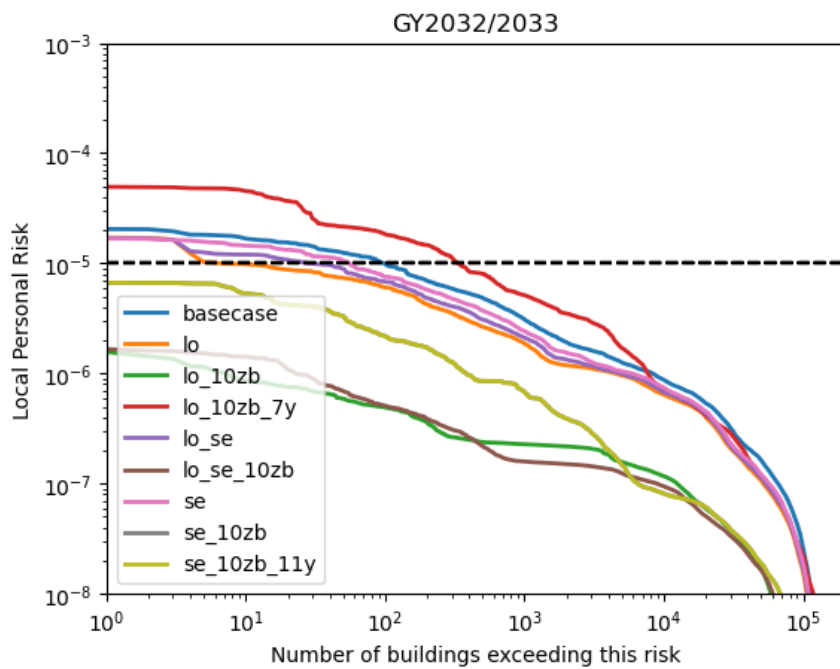
Figure 63: Risk exposure plot for GY 2032/2033. Note the large increase in risk for the lo_10zb_7y case, where nitrogen injection ceases on the 1 October 2032.
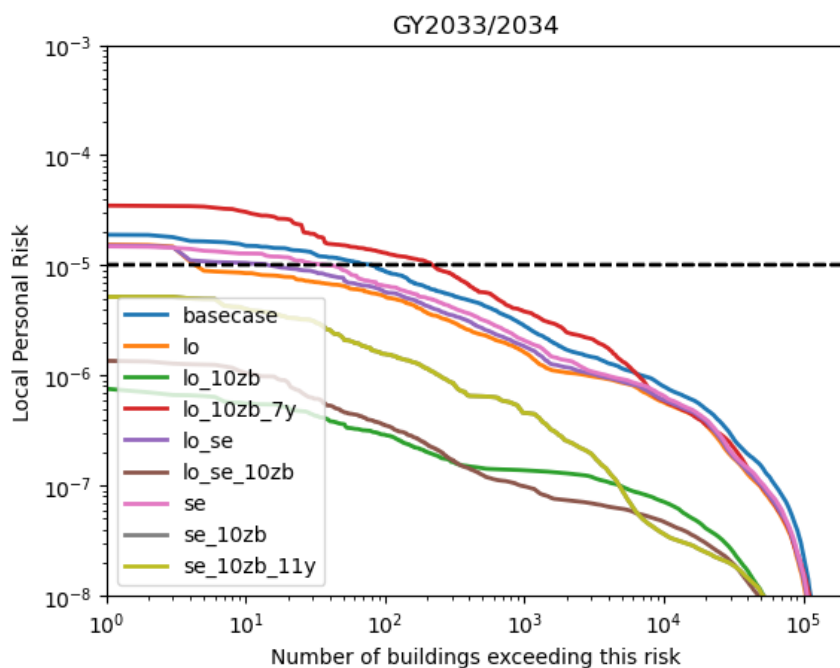

Figure 64 Risk exposure plot for GY 2033/2034. The risk profile decreases compared to last year for all scenarios (including the base case), but with different amounts.

Figure 65 Risk exposure plot for GY 2034/2035. The risk profile decreases compared to last year for all scenarios (including the base case), but with different amounts.

Figure 66: Risk exposure plot for GY 2035/2036. The risk profile decreases compared to last year for all scenarios (including the base case), but with different amounts.
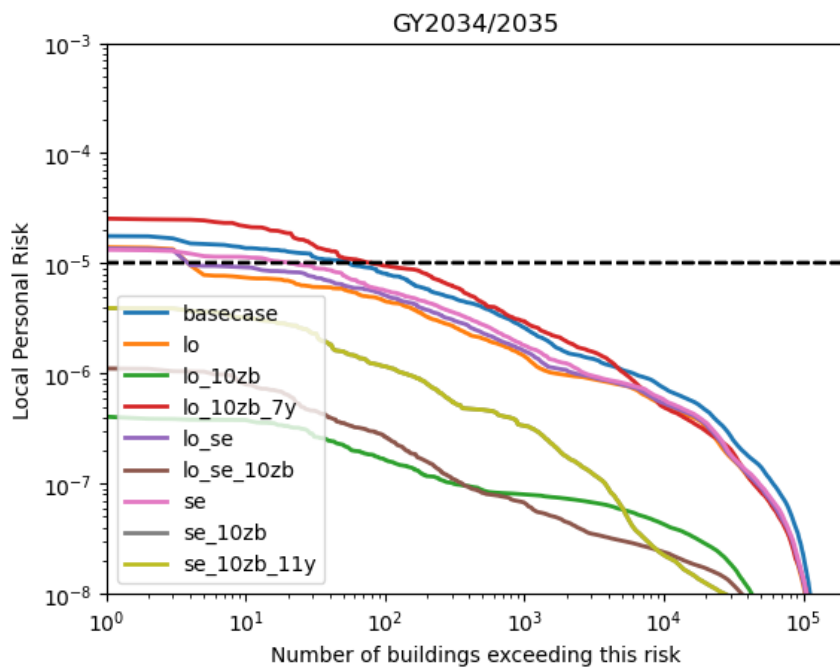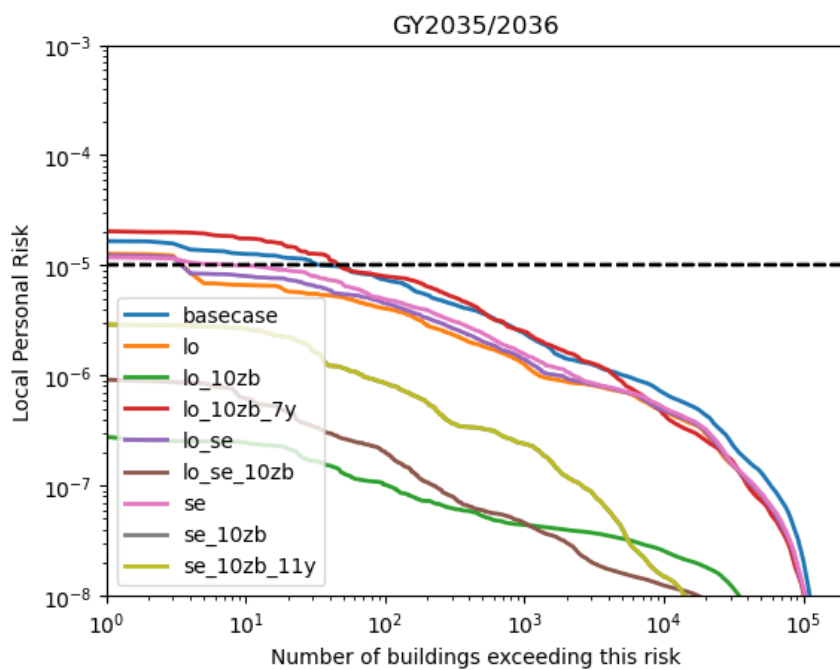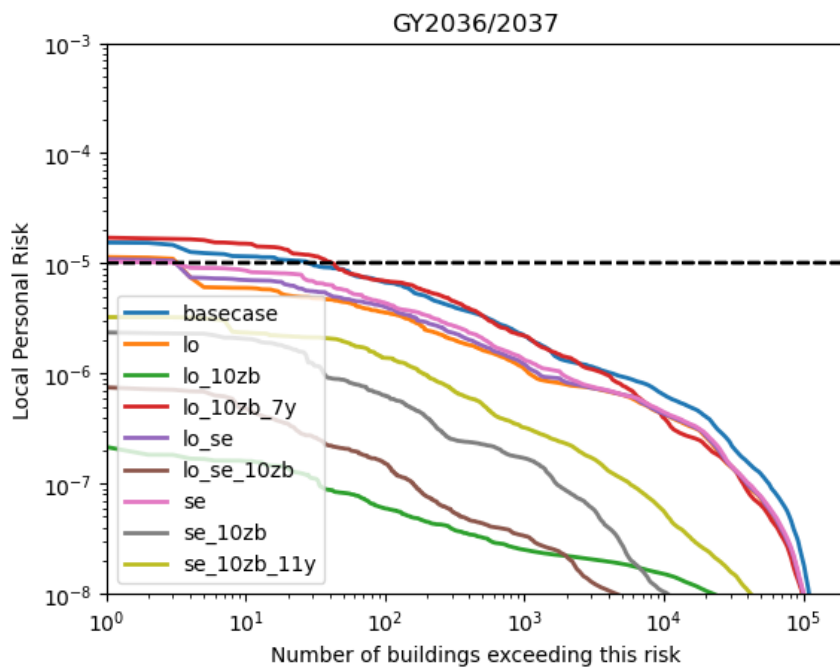
Figure 67 Risk exposure plot for GY 2036/2037. Note the increase of in risk for the se_10zb_11y case, where nitrogen injection ceases on the 1 October 2036. Despite the increase in risk, all buildings conform to the safety norm for this case.

Appendix B: Derivation of source model equations including fault offsets

In the main body of this report, we propose a method for including thermoelastic stresses. Here we show that this method can be applied in the full source model framework, which includes fault offsets as an 'amplification' term for stresses.

Following the Bourne & Oates (2017) conventions, contractive strains and compressive stresses are negative, pore pressure depletion is negative. In this context, it is sensible to define cooling as a negative temperature change. For an isotropic, homogeneous, linear, poro-thermo-elastic medium, the incremental total stress relationship with bulk strain may be written as:

$$\Delta\sigma_{ij} = \frac{E}{(1+\nu)}\left[\Delta\varepsilon_{ij} + \frac{\nu}{1-2\nu}\Delta\varepsilon_{kk}\delta_{ij}\right] - \alpha\Delta P\delta_{ij} - \frac{E}{1-2\nu}\alpha_T\Delta T\delta_{ij}$$

Following Bourne & Oates (2017) section 2.3.2 we get an expression for the vertically averaged strain tensor:

$$\bar{\varepsilon}_{ij} = \begin{pmatrix} \lambda_1 & 0 & 0 \\ 0 & 0 & 0 \\ 0 & 0 & \lambda_3 \end{pmatrix}$$

with

$$\lambda_{1,3} = \frac{\bar{\varepsilon}_{zz}}{2}\left(1 \pm \sqrt{1+\Gamma^2}\right)$$

where

$$\pm : \begin{cases} - & for\ \lambda_1 \\ + & for\ \lambda_3 \end{cases}$$

and Γ is the geometric gradient of the reservoir, which is large at faults.

Using this definition of the strain, we can write an expression for the change in the vertically averaged largest principle total stress σ_1 and the change in the smallest principle total stress σ_3:

$$\Delta\bar{\sigma}_{1,3} = \frac{E}{(1+\nu)}\left[\frac{1 \pm (1-2\nu)\sqrt{1+\Gamma^2}}{2(1-2\nu)}\right]\bar{\varepsilon}_{zz} - \left(\alpha\Delta P + \frac{E}{1-2\nu}\alpha_T\Delta T\right)$$

where

$$\bar{\varepsilon}_{zz} = \frac{1}{E}\frac{(1+\nu)(1-2\nu)}{1-\nu}\alpha\Delta P + \frac{1+\nu}{1-\nu}\alpha_T\Delta T$$

And therefore

$$\alpha \Delta P + \frac{E}{1 - 2\nu} \alpha_T \Delta T = \frac{\bar{\varepsilon}_{zz} E (1 - \nu)}{(1 - 2\nu)(1 + \nu)}$$

This allows us to write the stress changes in terms of $\bar{\varepsilon}_{zz}$:

$$\Delta \bar{\sigma}_{1,3} = \frac{E}{(1 + \nu)} \left[\frac{1 \pm (1 - 2\nu)\sqrt{1 + \Gamma^2}}{2(1 - 2\nu)} \right] \bar{\varepsilon}_{zz} - \frac{\bar{\varepsilon}_{zz} E (1 - \nu)}{(1 - 2\nu)(1 + \nu)}$$

$$\Delta \bar{\sigma}_{1,3} = \bar{\varepsilon}_{zz} E \left\{ \left[\frac{1 \pm (1 - 2\nu)\sqrt{1 + \Gamma^2}}{2(1 - 2\nu)(1 + \nu)} \right] - \frac{(1 - \nu)}{(1 - 2\nu)(1 + \nu)} \right\}$$

This shows that the poro-elastic and thermo-elastic effects on the stress are fully encoded in the vertical strain signal.

For completeness, we'll derive the the incremental maximum shear and mean total normal stresses developed within the thin sheet, after which we can make use of the Bourne and Oates framework for the rest of the source model:

$$\Delta \tau = \frac{1}{2} (\Delta \sigma_1 - \Delta \sigma_3)$$

$$\Delta \sigma_n = \frac{1}{2} (\Delta \sigma_1 + \Delta \sigma_3)$$

$$\Delta \tau = \frac{1}{2} \left(\bar{\varepsilon}_{zz} E \left\{ \left[\frac{1 - (1 - 2\nu)\sqrt{1 + \Gamma^2}}{2(1 - 2\nu)(1 + \nu)} \right] - \frac{(1 - \nu)}{(1 - 2\nu)(1 + \nu)} \right\} \right. $$
$$\left. - \bar{\varepsilon}_{zz} E \left\{ \left[\frac{1 + (1 - 2\nu)\sqrt{1 + \Gamma^2}}{2(1 - 2\nu)(1 + \nu)} \right] + \frac{(1 - \nu)}{(1 - 2\nu)(1 + \nu)} \right\} \right)$$

$$\Delta \tau = \frac{1}{2} \left(\bar{\varepsilon}_{zz} E \left[\frac{1 - (1 - 2\nu)\sqrt{1 + \Gamma^2}}{2(1 - 2\nu)(1 + \nu)} \right] - \bar{\varepsilon}_{zz} E \left[\frac{1 + (1 - 2\nu)\sqrt{1 + \Gamma^2}}{2(1 - 2\nu)(1 + \nu)} \right] \right)$$

$$\Delta \tau = - \bar{\varepsilon}_{zz} E \frac{\sqrt{1 + \Gamma^2}}{2(1 + \nu)}$$

$$\Delta \tau = -\sqrt{1 + \Gamma^2} \gamma H \bar{\varepsilon}_{zz}$$

where

$$\gamma = \frac{1 - 2\nu}{2(1 - \nu)} \text{ and } H = \frac{E}{(1 - 2\nu)(1 + \nu)}$$

And similarly for $\Delta \sigma_n$:

$$\Delta \sigma_n = \frac{1}{2} \left(\bar{\varepsilon}_{zz} E \left\{ \left[\frac{1 - (1 - 2\nu)\sqrt{1 + \Gamma^2}}{2(1 - 2\nu)(1 + \nu)} \right] - \frac{(1 - \nu)}{(1 - 2\nu)(1 + \nu)} \right\} \right.$$
$$\left. + \bar{\varepsilon}_{zz} E \left\{ \left[\frac{1 + (1 - 2\nu)\sqrt{1 + \Gamma^2}}{2(1 - 2\nu)(1 + \nu)} \right] - \frac{(1 - \nu)}{(1 - 2\nu)(1 + \nu)} \right\} \right)$$

$$\Delta\sigma_n = \frac{1}{2}\left(\bar{\varepsilon}_{zz}E\left(\left[\frac{2}{2(1-2v)(1+v)}\right] - \frac{2(1-v)}{(1-2v)(1+v)}\right)\right)$$

$$\Delta\sigma_n = \bar{\varepsilon}_{zz}E\left(\left[\frac{1}{2(1-2v)(1+v)}\right] - \frac{2(1-v)}{2(1-2v)(1+v)}\right)$$

$$\Delta\sigma_n = \bar{\varepsilon}_{zz}E\left(\frac{-(1-2v)}{2(1-2v)(1+v)}\right)$$

$$\Delta\sigma_n = -\frac{\bar{\varepsilon}_{zz}E}{2(1+v)}$$

$$\Delta\sigma_n = -\gamma H\bar{\varepsilon}_{zz}$$

These expressions are identical to the ones obtained by Bourne & Oates (2017), but have now explicitly included the thermal component in the vertically averaged vertical strain throughout the derivation.

Signature

Authorization release

Y.A. Schavemaker MSc
Research manager